2014-01-21

Time-Dependent and Cracking Analysis of Prestressed Concrete Curved Bridges Constructed in Stages

Ford, Russell

UNIVERSITY OF CALGARY

Time-Dependent and Cracking Analysis of Prestressed Concrete Curved Bridges Constructed in Stages

by

Russell Ford

A THESIS

SUBMITTED TO THE FACULTY OF GRADUATE STUDIES

IN PARTIAL FULFILMENT OF THE REQUIREMENTS FOR THE

DEGREE OF MASTER OF SCIENCE

DEPARTMENT OF CIVIL ENGINEERING

CALGARY, ALBERTA

JANUARY, 2014

ABSTRACT

Concrete structures are ubiquitous. Serviceability analysis of structures has become critical. Engineers need simple tools that follow structural codes and facilitate manipulation of design parameters.

Literature is available for structural response, including cracking and time-dependent effects, of segmentally constructed straight elements. This thesis takes that work and extends it to include biaxial bending and torsion. Using existing curved element formulation, a model is developed for uniaxial elements with varying cross section, prestressing, and external loading.

Verification against existing problems in two and three dimensions is performed. Demonstration of the model's capability is included, showing problems from the literature and a real world highway bridge in Calgary, Alberta. A parametric study to examine the effects of changing the prestressing to meet design code criteria for fatigue analysis is included. Real design code loading requirements are used, and the designer can see how the structure responds to changing parameters.

ACKNOWLEDGEMENTS

First, the author would like to thank Dr. Mamdouh El-Badry for his support and encouragement. His high standards and mentorship throughout the author's academic career have been instrumental in guiding and shaping his work.

Also, many of the other professors at the University of Calgary were instrumental in starting and feeding the author's passion for structural engineering. They include Dr. Nigel Shrive, Dr. John Newhook, and Dr. Tom Brown. The author was priviledged to have had the opportunity to learn structural mechanics from Dr. Amin Ghali.

The help and advice from fellow students was invaluable. A sincere thank you to Mark Hagel, Timm Stein, Kyle Schonknecht, Rainer Herzinger, and Gerd Birkle is long overdue.

Finally, and most importantly, this work would not have been possible without the patience, support, and understanding of my wife Melissa Ford and the rest of my family.

TABLE OF CONTENTS

TABLE OF FIGURES

LIST OF TABLES

LIST OF SYMBOLS

A	=	cross sectional area of section
A_{ry}, A_{rz}	=	reduced area for shear
A_{ns}, A_{ps}	=	non prestressed or prestressed steel area
$[A]_u$	=	matrix of forces at each section from unit displacements at nodal ends
A	=	cumulative angle change in tendon for prestress friction loss
α	=	shape factor for shear
B_y, B_z	=	first moment of area
β	=	tension stiffening coefficent for cracked sections
c	=	depth of cracked zone in section (uniaxial bending only)
$[d]$	=	section stiffness matrix
$[d]_m$	=	mean section stiffness matrix
$\{D\}$	=	vector of nodal displacements
d	=	prestress anchor set loss

E_c = modulus of elasticity of concrete

$E_c(t,t_0)$ = age adjusted modulus for concrete between t_0 and t

E_{ns}, E_{ps} = modulus of elasticity of steel

ε_c, ε_{cu} = strain in concrete (ultimate)

$\varepsilon_{cs}(t,t_0)$ = shrinkage in concrete between t_0 and t

ε_{cs0} = ultimate shrinkage in concrete

$\{\varepsilon\}$ = vector of strains on section

$\{\varepsilon\}_1$ = vector of strains on section, assuming cracking never took place

$\{\varepsilon\}_2$ = vector of strains on section, cracked state

$\{\varepsilon\}_m$ = mean strain in a cracked section

$\Delta\varepsilon_c(t,t_0)$ = change in strain in concrete between time t_0 and t

$\Delta\varepsilon_{cf}(t,t_0)$ = total free strain in concrete between t_0 and t

$\{\Delta\varepsilon_f\}(t,t_0)$ = total free strain in section between t_0 and t

f_c' = ultimate compressive stress in concrete

f_{ct} = ultimate tensile stress in concrete

f_{cm} = mean compressive strength of concrete

$\{F^*\}$ = vector of forces in local coordinate system

$\{F(t)\}$ = fixed end forces at time t

$\{\Delta F(t_2,t_1)\}$ = change in fixed end forces between time t_1 and t_2

$\phi(t,t_0)$ = creep coefficient for concrete between t_0 and t

ϕ_d = ultimate creep from delayed elastic strain

ϕ_f = ultimate creep flow

G_c = shear modulus of elasticity (age adjusted)

$G_c(t,t_0)$ = shear modulus of elasticity (age adjusted)

h_0 = notional thickness of section

H = stiffness transformation matrix

I_{yy}, I_{zz}, I_{yz} = moment of inertia

J = torsion constant

k = linear coefficient for prestress friction loss

λ_t = unit vector in direction of prestress tendon

M_y, M_z = bending moment on section

μ = wobble coefficient for prestress friction loss

N = normal force on section

n = modular ratio

$\{n\}$ = principal normal vector for calculating prestress effect

$N_i(\xi)$ = shape function for Lagrange interpolation

ν = poisson's ratio

O_1, O_2 = notation for element ends

$\Delta P(t,t_0)$ = change in prestress force between t_0 and t

Q = shearing force on section

$q(\xi)$ = distributed load (varies along element axis)

$[R(\xi_2, \xi_1)]$ = equilibrating matrix at section 2 for a load applied at section 1

s = length along tendon for prestress friction loss calculation

$[S]$ = stiffness matrix

$S_i(\xi)$ = spline function for spline interpolation

σ_c = stress in concrete

σ_{c1max} = maximum concrete stress in an uncracked section

$\Delta\sigma(t,t_0)$ = change of stress between t0 and t

$\Delta\sigma_{pr}(t,t_0)$ = prestress relaxation under constant stress

$\Delta\sigma_{pr}(t,t_0)$ = reduced prestress relaxation

T = twisting moment on section

$[T(\xi_i)]$ = coordinate system transformation matrix at section i

τ_{yz} = shear stress on section in yz plane

wi = weight coefficient for gaussian quadrature calculation

Ω = coefficient for calculation of prestress loss reduction factor

$\chi(t,t_0)$ = aging coefficient for concrete between t_0 and t

$\chi_r(t,t_0)$ = intrinsic prestress loss factor

y_{ps}^*, z_{ps}^* = location of prestress tendon in section (local coordinate system)

ψ_y, ψ_z = curvature

ζ = interpolation coefficient for cracked sections

Chapter One: **INTRODUCTION**

1.1 General

It is arguable that no single material is more prevalent in modern structural engineering than concrete. Portland cement structures form the backbone of our civil infrastructure, particularly post WWII. Whether in the bridges we drive on, the buildings we work in, or the reservoirs that contain our drinking water, concrete has proven to be an efficient, economic, and versatile material. The last 50 years of research and experience in the concrete industry have led to important developments. Prestressed concrete construction is at the forefront of these advancements, especially when considering the modern highway bridge system.

Concrete is not without its inherent problems. Over time and under sustained stress, concrete creeps. This magnifies the initial elastic deformation by a substantial factor ranging from 2 to 4. Concrete exposed to a dry environment or a very humid one will, respectively, lose or gain moisture and deform accordingly. The effects of these processes, known respectively as shrinkage or swelling, can be very significant in some climates. In addition to these problems, prestressing steel subjected to very high stress will relax, resulting in loss of compression on the concrete. All of these time-dependent phenomena can dramatically change the state of stress and strain in concrete over time. Failure to consider these phenomena in the design phase can lead to problems later in the structure's life with cracking of concrete, corrosion of steel, and excessive deflection. These problems can significantly reduce the service lifespan of the structure, resulting in

excessive cost to governments in the form of repairs and rehabilitation. As the majority of concrete structures in North America are still relatively young, the accumulation of maintenance costs in government budgets will soon begin to restrict new construction if design for serviceability and durability as well as strength does not become commonplace.

Analysis of the serviceability of concrete structures often requires an approach that is different from ultimate state analysis. While design for strength allows a margin for conservatism, the overestimation of serviceability parameters can lead to problems with camber, deflection, and formwork adjustment. Accuracy is important.

Another factor complicating the design and analysis of prestressed concrete structures is the construction process. Modern construction demands short aggressive schedules. Concrete is often mixed to develop rapid strength gain and early stripping of formwork. As a result, the load and support mechanisms for a structure can change over time as members and components are added and removed. Since the properties of concrete change over time as well, it is likely that the stresses at some point during erection will exceed those the structure will experience in service. It is for these reasons that a complete and proper time-dependent analysis is an essential tool in the design and analysis of prestressed concrete structures.

1.2 Objectives and Scope

For quite some time, computational methods have been used in structural analysis. Over the past several decades, modeling of concrete bridges has changed from assemblies of

simple straight elements to complex finite element methods that account for the nonlinear behaviour of the materials used in construction. These advanced models can accurately predict the response of structures near connections, and can determine displacements and stresses as structures undergo significant deformation.

Most structural design in practice, however, does not require or warrant such advanced methods of analysis. Practicing structural engineers frequently require a capable tool that can rapidly determine the effect of changing parameters. How does the reinforcing ratio in a span affect the midspan displacement? How effective will the reinforcement be in controlling cracks and limiting their width? What happens if the prestressing force is decreased or increased by a certain percentage? The complexity of most finite element software makes it difficult for the average user to see the path from input to output clearly. What is needed is a tool for the analysis of real world concrete structures that takes into account the most significant facets of the analysis, but that remains simple and straightforward enough that the results can be understood and interpreted by the user. Integration with existing design codes is also important.

To fulfill these criteria, a one-dimensional space frame element provides a good approach. The fundamentals of basic beam theory are familiar to practicing structural engineers.

The most fundamental element for space frame analysis was suggested by Timoshenko and Gere (1961). Significant improvements were introduced by several authors including Surana (1979), culminating in Jirousek and Bouberguig (1979), who introduced an

isoparametric element suitable for representing macro elements in bridges. Maher (1985) used the Jirousek element to develop a method to optimise the prestressing profile and magnitude in bridges to minimize stresses from torsion and bending.

Debaiky (1997) improved on Maher's work by including time dependent effects from creep and shrinkage in the analysis, and including non-prestressed steel. The method of calculation of creep and shrinkage has been studied at length. The basis of the analysis remained the isoparametric Jirousek element. Debaiky's element remains a good element for elastic calculations.

Time dependent effects in concrete have long been a subject of study. Trost and Marsh (1967) showed that superposition was a valid solution approach. Bazant and Wu (1972) demonstrated how a simplified aging coefficient could be used to account for gradually developing stress. Further research, such as Khalil (1979), was focused on numerical efficiency of creep calculations. In the late 1990's, major design codes were published with a full suite of calculations for predicting time dependent effects.

Ultimately, however, analysis of concrete structures must account for concrete cracking. The non-linearity introduced by concrete cracking complicates the analysis significantly. Several approaches have been used, including Ketchum (1985), who modeled the cross section as "pixels". Work by El-Badry (1988) includes a thorough procedure for analysing cracking in plane frames, including the effects of non-prestressed steel, prestressing, and time-dependent effects. The equations and degrees of freedom presented by El-Badry (1988) are simplified due to the planar nature of the analysis.

The objective of the work presented in this thesis is to develop a model that incorporates the detailed analysis at the section level presented by El-Badry (1988), which comprehensively includes all elements required in structural design codes, and to expand it into the third dimension where biaxial bending and torsion can be included as Maher (1985) and Debaiky (1997) have done. Multi-stage construction techniques of concrete bridges must be accounted for. The input should be simple enough that parameters can be easily adjusted to examine their effect.

The basic calculations underlying time-dependent analysis are not particularly complicated. The most difficult phases require solution of a system of equations. However, when structures have complex construction stages, or many members to be assembled or constructed, the quantity of computations becomes large enough to necessitate the use of a computer to sort the data and keep track of the results. Twenty years ago, this sort of analysis required large, powerful computers and very careful and efficient programming; today, the power and storage available in personal computers are more than sufficient to handle the task.

The model developed in this work handles non-prismatic, arbitrarily curved, cracked space frame elements that can be built up of several different materials and constructed in stages. The method can analyze structures for both instantaneous and time-dependent effects.

1.3 Organization of Thesis

It is best to consider the model under discussion in terms of the layers that it works on. The analysis is performed at 4 different levels, with each one requiring transitions to the one above and below it. At each level, there are displacements and forces which can be related using stiffness.

The primary level is that of the individual fibres in the material. The stress and strain interactions at this level are governed by the properties of the material. Chapter 2 covers how they are related and how they are calculated, where the phenomena governing serviceability of concrete structures are discussed.

The second level of the model is the cross-section of the element. A section is formed by the intersection of the element with a plane whose normal lies along the tangent of the element's longitudinal axis. Geometry governs the interactions at this level; the relevant properties, for example, are the second moment of area and the area of the section. The displacements are the strain and the curvatures, and the forces are the internal forces or stress resultants. Chapter 3 deals with the analysis of a section under instantaneous and time-dependent effects.

Multiple sections define an element. The beam elements in the model are single axis members that connect two points in space. The displacements in question are those at the ends of the element; the forces are the member-end forces. Analysis of elements is covered in detail in Chapter 4, including the calculation of stiffness and fixed-end forces.

There is much attention paid to the manner in which the member's orientation is calculated and how these calculations affect the results.

The final level in the model is the analysis at the structure level. The structure is simply an assemblage of elements, but also takes into account the boundary conditions and the construction stages. The displacements are the global values at each individual node, and the forces are the reactions that keep the structure as a whole in equilibrium. Chapter 5 deals with the analysis of the structure.

Chapter 6 contains examples that use either closed-form solutions or existing computer programs to verify the validity and accuracy of the model. It also includes demonstration of the model's capabilities on new problems.

It should be noted here that much of the implementation of the algorithms and procedures outlined herein require a fairly good background in numerical methods. While the usage of these techniques is presented here, the theory and reasoning behind their development is published elsewhere.

Chapter 7 presents a summary of the research, the conclusions drawn, and recommendations for future work.

Chapter Two: **BEHAVIOUR OF MATERIALS**

2.1 General

Modern bridges are complex heterogeneous structures, made of several different materials. For the sake of simplicity, and for the purposes of this work, only concrete, prestressed, and non-prestressed steel are considered. In order to calculate the response of a cross section, the response of each of the materials must first be taken into account.

2.2 Concrete

Studies into the behaviour of concrete are numerous. Neville (1997) is a very thorough and comprehensive reference for all properties of concrete, including compressive and tensile strength.

Given the segmental nature of the structures under consideration here, the analysis must account for concrete that is loaded very early after curing as well as that which has been in place for some time. Different materials may be used for the deck and girder of a bridge, for example. We must differentiate between precast and cast-in-place material as well.

2.2.1 Stress and Strain

Concrete behaves in a non-linear fashion. This is caused by two factors: the first and most obvious is that concrete's weak tensile strength causes it to crack, and the second is

that as the stress exceeds roughly $0.5f_c'$, the stiffness decreases significantly and more strain is experienced. This is shown in Figure 2.1 below.

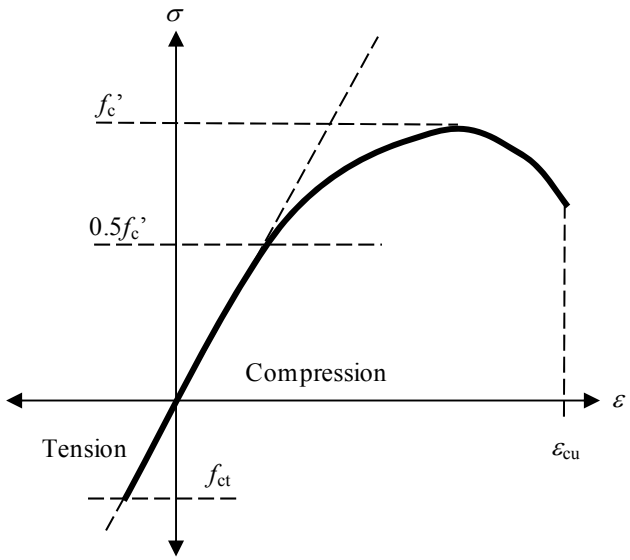

Figure 2.1: Stress-Strain Relationship for Concrete

As the figure shows, the stress-strain relationship is approximately linear in the range of 0 to $0.5f_c'$. The effect of tension in the concrete is discussed later.

2.2.2 Creep

Suppose that at some time t_0, a concrete specimen is subjected to initial stress $\sigma_c(t_0)$. Assuming that the response of the specimen is in the elastic range, instantaneous strain will develop:

$$\varepsilon_c(t_0) = \frac{\sigma_c(t_0)}{E_c(t_0)} \tag{2.1}$$

If the stress $\sigma_c(t_0)$ is sustained to a later time t, strain due to creep of concrete will develop. The amount of creep that will develop is influenced primarily by the following factors (Neville, 1997):

1. The age of concrete at loading – the earlier the load is applied, the higher the creep that is experienced over the same duration of loading.

2. Duration of loading – intuitively, the longer the load acts, the more creep develops.

3. Stress Intensity – more stress gives more creep. This relationship is linear up to stress equal to 0.4 to 0.6 f_c'.

4. Compressive Strength – An increase in concrete strength provides a decrease in creep.

5. Aggregate Content – Increasing aggregate volume decreases cement content by volume and results in lower creep.

6. Notional Thickness – The more surface area exposed for a given volume, the higher creep will be.

7. Relative Humidity – Lower humidity means higher moisture loss and higher creep.

8. Ambient Temperature – Creep generally increases proportional to temperature in the range of 10°C – 60°C.

Based on these factors and experimental data, several researchers have developed models to predict creep. As early as 1965, England and Illston presented creep functions which included elastic, delayed recoverable, and irrecoverable components. Work by Selna (1969) and Scanlon and Murray (1974) improved their work to provide simple equations that only required storage of the previous 2 intervals. Bazant and Wu (1973) and Kabir (1976) improved these equations to require only the previous interval to be stored. Khalil (1979) includes a good summary of this approach, which employs a Dirichlet series and least-squares curve fitting to determine the salient coefficients. This approach is presented and discussed later in this chapter.

The change in strain due to creep, denoted $\Delta\varepsilon_c(t,t_0)$, can be calculated by

$$\Delta\varepsilon_c(t,t_0) = \phi(t,t_0)\,\varepsilon_c(t_0) \tag{2.2}$$

where $\phi(t,t_0)$ denotes the factor of increase of strain that would occur, if free to do so, between t_0 and t for a stress applied at t_0. Note that this is only the increase in strain between t_0 and t; it does not include the instantaneous effects. The total strain, $\varepsilon_c(t)$, instantaneous plus creep, at time t will be given as:

$$\varepsilon_c(t) = \varepsilon_c(t_0) + \Delta\varepsilon(t,t_0) = \sigma_c(t_0)\frac{1+\phi(t,t_0)}{E_c(t_0)} \tag{2.3}$$

Creep essentially has two components: an irrecoverable component, and delayed elastic strain, which can be recovered once the stress is removed (Neville, 1997). The former has no limit, and is dependent on age at loading and duration of load; the latter has a limit which is reached very quickly and is only dependent on load duration (and not age at loading).

2.2.2.1 Aging Coefficient

All stress applied to concrete has creep associated with it. This problem is iterative; the restraint of creep (by nonprestressed steel, for example) causes stress to develop, which in turn causes creep. The problem this presents is that these creep-restraint stresses are not applied instantaneously; they develop gradually over time. There is no single time of loading associated with them. As such, their effect at a later time is less than if the full increment were applied instantaneously. Figure 2.2 shows the effect of a stress increment applied in one instant compared to one developed gradually.

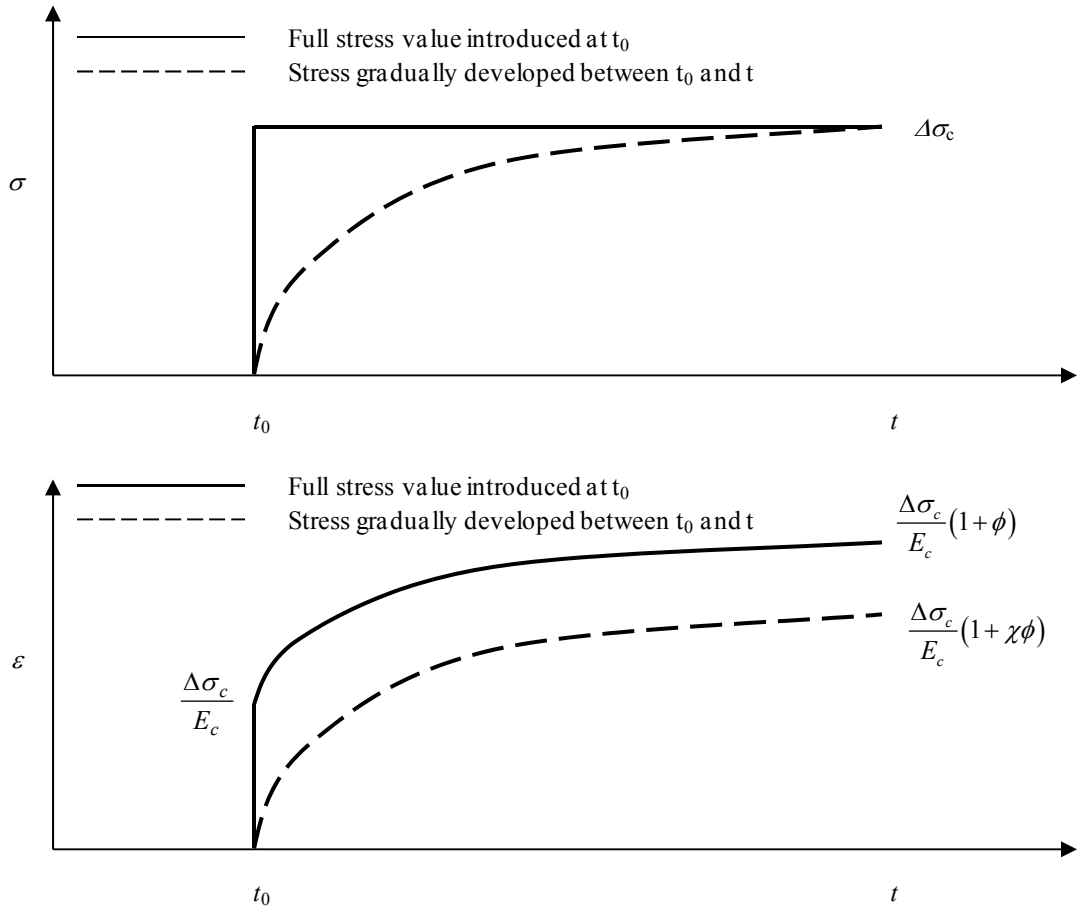

Figure 2.2: Strain due to Instantaneous vs. Gradually Developed Stress

The total strain at time t due to instantaneously applied and gradually developing stress can be calculated as:

$$\varepsilon_c(t) = \sigma_c(t_0)\frac{1+\phi(t,t_0)}{E_c(t_0)} + \int_0^{\Delta\sigma_c(t)} \frac{1+\phi(t,\tau)}{E_c(\tau)} d\sigma_c(\tau) \tag{2.4}$$

While accurate, this is overly complicated and is not suitable for simple use. The integral can be evaluated numerically in a step-by-step fashion with suitably small increments of

stress and time to find the overall effect. In any case, the amount of strain which will occur from a gradually introduced stress is less than that which would develop if it were applied all at once. It is possible to introduce a coefficient, $\chi(t,t_0)$, such that

$$\int_0^{\Delta\sigma_c(t)} \frac{1+\phi(t,\tau)}{E_c(\tau)} d\sigma_c(\tau) = \Delta\sigma_c(t) \frac{1+\chi(t,t_0)\phi(t,t_0)}{E_c(t_0)} \tag{2.5}$$

This coefficient is called the "aging coefficient" and was introduced by Trost and Marsh (1967) and later improved by Bazant (1972). It typically has values in the range of 0.7-0.9. Using the aging coefficient, a new modulus can be calculated that takes into account the gradual development of creep:

$$\overline{E_c}(t,t_0) = \frac{E_c(t_0)}{1+\chi\phi(t,t_0)} \tag{2.6}$$

$\overline{E_c}(t,t_0)$ is known as the "age-adjusted modulus of elasticity" and can be used to find the strain that occurs due to a gradually developing stress between t_0 and t. The total strain at time t is simply

$$\varepsilon_c(t) = \varepsilon_c(t_0) + \Delta\varepsilon_c(t,t_0) = \frac{\sigma_c(t_0)}{E_c(t_0)} + \frac{\Delta\sigma_c(t,t_0)}{\overline{E_c}(t,t_0)} \tag{2.7}$$

For the current model with an arbitrary number of timesteps, it is necessary to calculate the total free strain due to creep which occurs as a result of the stress history. The change in strain (if free to occur) between time t_i and t_{i+1} is

$$\Delta\varepsilon_c\left(t_{i+1},t_i\right)=\sum_{j=0}^{i}\left(\varepsilon_c\left(t_j\right)+\frac{\Delta\sigma_c\left(t_{j+1},t_j\right)}{E_c\left(t_j\right)}\right)\left(\phi\left(t_{i+1},t_j\right)-\phi\left(t_i,t_j\right)\right) \tag{2.8}$$

where the term $\Delta\sigma_c\left(t_{i+1},t_i\right)$ is nil for the summation when j=i.

2.2.2.2 Stress History

The biggest problem with the method presented above is that it requires the entire stress history to be stored in order to calculate the free strain. This is not desirable as the storage requirement can become large. While current microcomputer technology has advanced to the point where memory storage is not generally a concern, efficiency in computing is always desirable.

A Dirichlet series can be used to model the creep curves. The properties of the series are used to simplify the integrations involved in the calculations and come up with a formulation that does not require storage of stress history.

The creep function proposed by Khalil (1979) is of the form

$$\phi\left(t,t_0\right)=\phi_f F\left(t,t_0\right)+\phi_d D\left(t-t_0\right) \tag{2.9}$$

where ϕ_f is the ultimate creep flow, and ϕ_d is the ultimate delayed elastic strain. The functions F and D implement the Dirichlet series:

$$F\left(t,t_0\right)=\sum_{i=1}^{n}a_i e^{-\lambda_i t_0}\left(1-e^{-\lambda_i\left(t-t_0\right)}\right) \tag{2.10}$$

$$D(t-t_0)=\sum_{i=1}^{n} b_i\left(1-e^{-\gamma_i(t-t_0)}\right) \tag{2.11}$$

The summations in (2.10) and (2.11) must be carried out over a predefined number of terms; Khalil (1979) suggests that 4 are sufficient. The terms a_i, b_i, λ_i, and γ_i are constants that determine the shape of the curve; their calculation is presented below.

The CEB-FIP 1978 code that Khalil used to derive his creep formulation was changed in 1990. The new code does not differentiate between creep flow and delayed elastic strain. As a result, the model will only use the creep flow formulation as it includes terms for both the age at loading and the duration of the load.

Without replicating his work here, Khalil (1979) uses the properties of the Dirichlet series to derive an expression for the free strain that occurs in the j^{th} interval because of creep:

$$\Delta\varepsilon_f\left(t_{j+1},t_j\right)_d=\sum_{i=1}^{n} A_{ij}\left(1-e^{-\lambda_i\Delta t_j}\right) \tag{2.12}$$

$$A_{ij}=A_{i,j-1}e^{-\lambda_i\Delta t_{j-1}}+\phi_f\frac{\sigma\left(t_j\right)}{E_c\left(t_j\right)}a_{ij}e^{-\lambda_i\tau_j} \tag{2.13}$$

For example, in interval 1,

$$A_{i1}=\phi_f\frac{\sigma\left(t_1\right)}{E_c\left(t_1\right)}a_{i1}e^{-\lambda_i\tau_1} \tag{2.14}$$

Then, for interval 2,

$$A_{i2} = A_{i1} e^{-\lambda_i \Delta t_1} + \phi_f \frac{\sigma(t_2)}{E_c(t_2)} a_{i2} e^{-\lambda_i \tau_2} \tag{2.15}$$

Rather than carrying forward the stress history, only the A values need be stored (one per interval per Dirichlet series term). It is worth noting that full stress history storage is not overly intensive unless many time stages and elements are necessary in the analysis.

2.2.2.3 Determination of Coefficients

Selna's Dirichlet series method for creep coefficients requires calculation of several parameters; namely, a_i, b_i, λ_i, and γ_i. Khalil (1979) suggests that the CEB code be used for generating the curves as it is the only code which recognizes the two distinct components of strain. For each age at loading, τ_i, the following matrix equation can be written:

$$\begin{bmatrix} e^{-\lambda_1 \tau_i}\left(1-e^{-\lambda_1(t_1-\tau_i)}\right) & \cdots & e^{-\lambda_4 \tau_i}\left(1-e^{-\lambda_4(t_1-\tau_i)}\right) \\ e^{-\lambda_1 \tau_i}\left(1-e^{-\lambda_1(t_2-\tau_i)}\right) & & e^{-\lambda_4 \tau_i}\left(1-e^{-\lambda_4(t_2-\tau_i)}\right) \\ \vdots & & \vdots \\ e^{-\lambda_1 \tau_i}\left(1-e^{-\lambda_1(t_m-\tau_i)}\right) & \cdots & e^{-\lambda_4 \tau_i}\left(1-e^{-\lambda_4(t_m-\tau_i)}\right) \end{bmatrix} \begin{Bmatrix} a_{1i} \\ a_{2i} \\ \vdots \\ a_{ni} \end{Bmatrix} = \begin{Bmatrix} F(t_1,\tau_i) \\ F(t_2,\tau_i) \\ \vdots \\ F(t_m,\tau_i) \end{Bmatrix} \tag{2.16}$$

where n is the number of Dirichlet series terms (to reiterate, Khalil (1979) suggests that 4 is sufficient), m is the number of observation times, and a_{ji} is the coefficient for the j^{th} term in the series for τ_i age at loading.

System (2.16) is overdetermined; there are more equations than there are unknowns. The non-linearity that results from the λ_i's makes the solution difficult; repeating the procedure for sets of λ and choosing those that result in the best least squares fit is the right approach. For this model, Khalil (1979) has suggested values for the coefficients.

To find the a_i's, a least squares approach is used.

$$\begin{aligned} [S]_{m\times n}\{a\}_{n\times 1} &= \{F\}_{m\times 1} \\ \left([S]^T[S]\right)_{n\times n}\{a\}_{n\times 1} &= \left([S]^T\{F\}\right)_{n\times 1} \\ \{a\}_{n\times 1} &= \left([S]^T[S]\right)^{-1}_{n\times n}\left([S]^T\{F\}\right)_{n\times 1} \\ \{a\} &= \left([S]^T[S]\right)^{-1}[S]^T\{F\} \end{aligned} \tag{2.17}$$

The error in the terms for the i^{th} age at loading can be calculated as

$$E_i = \sum_{j=1}^{m}\left(\phi\left(t_j,\tau_i\right) - \sum_{k=1}^{n} a_{ki} e^{-\lambda_k \tau_i}\left(1 - e^{-\lambda_k\left(t_j-\tau_i\right)}\right)\right)^2 \tag{2.18}$$

Adding all of the errors from each age at loading gives a value for the total error which can be used to compare different sets of λ_i's. Optimal values for the normal temperature range are shown in Table 2.1.

Table 2.1: Values for lambda in Dirichlet Series

i	1	2	3	4
λ_i	0.1	0.02	0.003	0.0004

Given the relatively low cost of computer storage and memory, storing the entire strain and stress history are not problematic. The user is given the option of either method.

2.2.3 Shrinkage

Concrete placed in a dry environment will lose moisture over time, causing shrinkage. Likewise, concrete submerged in water will absorb moisture over time and swell. In either case, the phenomenon is independent of the state of stress of the material (unlike creep). The analysis for shrinkage and swelling is the same; the material, if unrestrained, will undergo a free strain. It is assumed in the model that this effect is uniform throughout the section (see 3.9.1). This free strain that will occur in an unrestrained specimen between some time t_0 and a later time t is denoted $\varepsilon_{cs}(t,t_0)$. Its value is positive if the concrete swells and negative if it shrinks.

The shrinkage that develops over time gradually increases towards an ultimate value. The shrinkage function can be expressed as

$$\varepsilon_{cs}\left(t,t_s\right)=\varepsilon_{cs0}\beta\left(t-t_s\right) \tag{2.19}$$

where ε_{cs0} is the ultimate shrinkage, which is a function of the relative humidity and the notional thickness, and $\beta(t)$ is the time function. t_s is the time that the specimen is subjected to the humidity gradient.

In a fashion similar to creep, the shrinkage that takes place between t_i and t_{i+1} can be calculated by subtraction:

$$\varepsilon_{cs}\left(t_{i+1},t_i\right)=\varepsilon_{cs}\left(t_{i+1},t_s\right)-\varepsilon_{cs}\left(t_i,t_s\right) \tag{2.20}$$

2.2.4 Total Free Strain due to Creep and Shrinkage

To calculate the stress required to restrain creep amd shrinkage over time, the total free strain that would occur in the interval must be calculated.

$$\Delta\varepsilon_f\left(t,t_0\right)=\varepsilon\left(t_0\right)\phi\left(t,t_0\right)+\varepsilon_{cs}\left(t,t_0\right) \tag{2.21}$$

In a step-by-step in time analysis, the free strain is required between time t_i and t_{i+1} for loads applied at time t_0. The creep occuring in this interval can be found by subtracting the creep that has already occurred ($\phi(t_i,t_0)$) from the creep which would occur up to t_{i+1} ($\phi(t_{i+1}, t_0)$). Since this works only for loads applied at t_0, a summation must be done for all previous loading steps. Mathematically,

$$\Delta\varepsilon_f\left(t,t_0\right)=\sum_{j=0}^{i}\varepsilon\left(t_j\right)\left(\phi\left(t_{i+1},t_j\right)-\phi\left(t_i,t_j\right)\right) \tag{2.22}$$

where $\varepsilon(t_j)$ is the strain that occurs due to instantaneous loading at t_j. There is a problem with this formulation, however. Time-dependent effects that have occurred in all previous intervals will have introduced stress which also needs to be accounted for. The stress developing between t_i and t_{i+1} will have the same effect as if it were introduced at some intermediate time closer to t_i. Conservatively, assume that it occurred at t_i. This simplifies the calculation and eliminates the need for more creep coefficients. An "equivalent instantaneous strain" can be calculated which represents an effective strain at

t_0 due to the stress developed between t_0 and t. The modulus of elasticity of the concrete is $E_c(t_0)$.

$$\Delta\varepsilon_{equiv}\left(t_0\right)=\frac{\Delta\sigma_c\left(t,t_0\right)}{E_c\left(t_0\right)} \tag{2.23}$$

Dealing with shrinkage is a much simpler proposition since it is independent of stress. The six-element strain vector will have all elements zero except for the first.

The final equation for free strain due to creep and shrinkage is

$$\Delta\varepsilon_f\left(t_{i+1},t_i\right)_{free}=\sum_{j=0}^{i}\left(\varepsilon\left(t_j\right)+\frac{\Delta\sigma\left(t_{j+1},t_j\right)}{E_c\left(t_j\right)}\right)\left(\phi\left(t_{i+1},t_j\right)-\phi\left(t_i,t_j\right)\right)+\Delta\varepsilon_{cs}\left(t_{i+1},t_i\right) \tag{2.24}$$

Note that the $\Delta\sigma$ term in the above equation is zero for (t_{i+1}, t_i). Alternatively, equation (2.13) can be used as it does not require storage of the stress history for the section.

Once the free strain is known, it is possible to calculate the forces which, when applied to the concrete, would prevent that strain from occurring. Since the forces in question develop gradually between t_i and t_{i+1}, the age-adjusted modulus of elasticity is required.

$$\overline{E_c}\left(t,t_0\right)=\frac{E_c\left(t_0\right)}{1+\chi\phi\left(t,t_0\right)} \tag{2.25}$$

2.2.5 Structural Concrete Codes

Two major publications are recognized as the basis for time dependent effects in concrete design and analysis. They are the ACI Committee 209 (1998), Prediction of Creep,

Shrinkage, and Temperature Effects, and the Comité Euro-International du Beton – Federation Internationale de la Precontrainte (CEB-FIP) Model Code for Concrete Structures (MC-90). Ghali, Favre, and El-Badry (2011) contains a summary of the equations and touches on two European codes as well.

Other codes, such as CSA A23.3-04 (2004), provide greatly simplified expressions for the calculation of time dependent effects in concrete. These equations, while quick and simple, do not account for the complex nature of segmental construction or staged prestressing effects. Furthermore, these simplified codes allow for more thorough analysis in lieu of their use.

In practice, the CEB-FIP and ACI codes should generally be used as they are recognized as the standard for analysis and design. The program developed by the author to support this work allows the user to select either code or input values themselves.

2.3 Relaxation of Prestressing Steel

Suppose that a steel cable is stretched between two fixed points in such a way that the stress is high. Over time, the stress will decrease as the tendon relaxes. This drop in stress is called "intrinsic relaxation", and can be calculated by (Ghali, Favre, and El-Badry, 2011)

$$\frac{\Delta\sigma_{pr}\left(t,t_0\right)}{\sigma_{p0}} = -\frac{\log\left(t-t_0\right)}{10}\left(\frac{\sigma_{p0}}{f_{py}} - 0.55\right) \tag{2.26}$$

where f_{py} is the yield stress of the tendon, which is the stress at a strain of 0.01. t and t_0 are measured in hours.

If that same cable is embedded in a concrete specimen, the situation changes. The stress exerted on the concrete by the cable will cause creep, and shrinkage will occur as well. Both of these phenomena serve to decrease the level of stress in the cable and therefore the rate of prestress loss. The value for loss used in prestressed concrete should be less than the full value obtained from a constant length test. This is accounted for by using a coefficient χ_r less than 1, such that

$$\Delta\bar{\sigma}_{pr} = \chi_r \Delta\sigma_{pr} \tag{2.27}$$

where $\Delta\bar{\sigma}_{pr}$ is the reduced relaxation, which accounts for creep and shrinkage. It is this value that should be used in the analysis of prestress loss.

The coefficient χ_r is tabulated in the literature; Ghali, Favre, and El-Badry (2011) express it as a function of two quantities: the value λ, which is the ratio of the initial stress in the tendon to the tensile strength of the prestressing steel, and the value Ω, the ratio of the difference between the total losses from all effects and the intrinsic loss to the initial stress. If the total prestress loss is only the intrinsic value, the value of Ω is 0.0. Mathematically,

$$\Omega = \frac{\Delta\sigma_{pr} - \Delta\sigma_{ps}}{\sigma_{p0}} \qquad \lambda = \frac{\sigma_{p0}}{f_{pu}} \tag{2.28}$$

Obviously, the value of the total loss is not known before the value of χ_r is calculated. Iteration must be used to find the value. An initial value can be estimated, then the analysis will indicate a new value. This can be repeated until the change in the value from the previously obtained result is small. Table 2.2 gives reduced relaxation coefficients for different values of λ and Ω (Ghali et al., 2011)

Table 2.2: Reduced Relaxation Coefficient

Ω	λ					
	0.55	0.60	0.65	0.70	0.75	0.80
0.0	1.000	1.000	1.000	1.000	1.000	1.000
0.1	0.6492	0.6978	0.7282	0.7490	0.7642	0.7757
0.2	0.4168	0.4820	0.5259	0.5573	0.5806	0.5987
0.3	0.2824	0.3393	0.3832	0.4166	0.4425	0.4630
0.4	0.2118	0.2546	0.2897	0.3188	0.3429	0.3627
0.5	0.1694	0.2037	0.2318	0.2551	0.2748	0.2917

2.4 Summary

Equations have been developed to predict the stress and strain in the components of a structure at the fibre level, using both engineering principles and existing design codes. Considerations have been made for numerical efficiency.

The next step is to consider the resultant of these effects, or the displacements and forces at the section level under both external loading and time dependent effects.

Chapter Three: **ANALYSIS OF A SECTION**

Analysis of stress and strain is pivotal to serviceability analysis of concrete structures. Since deformations of a structure are a direct result of strain, the analysis of stress and strain in a cross-section is at the foundation of serviceability. Serviceability analysis is complicated by several factors. Over time, creep and shrinkage of concrete and relaxation of prestressing tendons causes redistribution of stress within the section. Since the structures considered here are built in stages, the addition of concrete parts over time can also have a dramatic effect on the development and distribution of time-dependent stresses. Once the stress at any point in the concrete exceeds the tensile capacity, cracking occurs. This causes changes in the properties of a section and can lead to large increases in strains. In statically determinate systems, the displacements will increase. In statically indeterminate structures, the change in stiffness resulting from cracking can cause redistribution of stress and change in the member end forces. These changes cause variation in the status of cracking, leading to a system which requires non-linear analysis to solve.

The calculation of stress is essential because structural codes limit service stress levels in concrete. If fatigue loading is a concern, the range of stress in the structure is an important factor in the design. When cracking takes place, the increase in steel strain can be used to calculate an estimate of the crack width. This can be compared to code requirements for serviceability. Most importantly, strains can be used to calculate the

displacements and flexibility of a member, which allows for a full displacement method analysis of a structure.

This chapter is focused on the calculation of stress and strain in a cross section, due to both instantaneous and time-dependent effects. The displacement method is used.

3.1 Section Definition

For the purpose of this analysis, a cross section is composed of any number of precast or cast-in-place concrete parts, with any number of prestressed or non-prestressed steel bars. Prestressing can be pre- or post-tensioned; for post-tensioning, both bonded and unbonded tendons can be considered. Tendons can be added as unbonded and then bonded at a later time. Since curved 3-dimensional beam elements are modeled, sections need not be symmetric about any axis, though the calculation of certain parameters (namely the shear centre location and the torsion constant) are substantially more difficult for irregular section shapes. This is explored in greater detail below.

3.2 Assumptions

Before the analysis procedure is presented, it is essential to review the assumptions that are introduced.

1. Concrete exhibits an elastic stress-strain relationship as long as the stress is below roughly 0.4-0.5f_c' (Ghali, Favre, and El-Badry, 2011). It is assumed here that service stress levels are in this range. In addition, it is assumed that the strains in the steel layers are below yielding. Given these conditions, it is possible to

superimpose strains and stresses from different intervals. This superposition must be modified to account for nonlinearity due to cracking; see section 3.8.

2. Plane sections remain plane, and no warping occurs. As Maher (1985) and Debaiky (1997) point out, this has been established to be acceptable for the type of sections and span to length ratios generally used in bridge design.

3. The strains in the steel (both prestressed and nonprestressed) and concrete are compatible – no slippage of the bond occurs. The tension stiffening effect that results from bond damage is accounted for by mean strain interpolation; see 3.10 for details. This means that the calculation of stresses and strains between a crack and the distance required to regain full bond are incorrectly predicted, but this is acceptable for the purposes set out here.

4. The shearing strain (twisting/shearing) and normal strain (axial/bending) equations are independent.

5. For unbonded tendons, no strain compatibility exists between the concrete and the steel. Bonded tendons have full strain compatibility. Friction loss and anchor slip are accounted for in the analysis.

Given these assumptions, a planar stress distribution will result from the application of internal forces.

3.3 Coordinate System

Elements in the model are simple beam-type elements with a single arbitrarily curved axis. Sections are provided at any point on the axis. The plane of the cross section is assumed to be perpendicular to the axis of the element. The local coordinate system for the section consists of three orthogonal axes: the x-axis is directly out of the section, while the y- and z- axes are contained in the plane. The system is easily defined by three unit vectors (λ_x^*, λ_y^*, λ_z^*) whose components are measured in the global coordinate system.

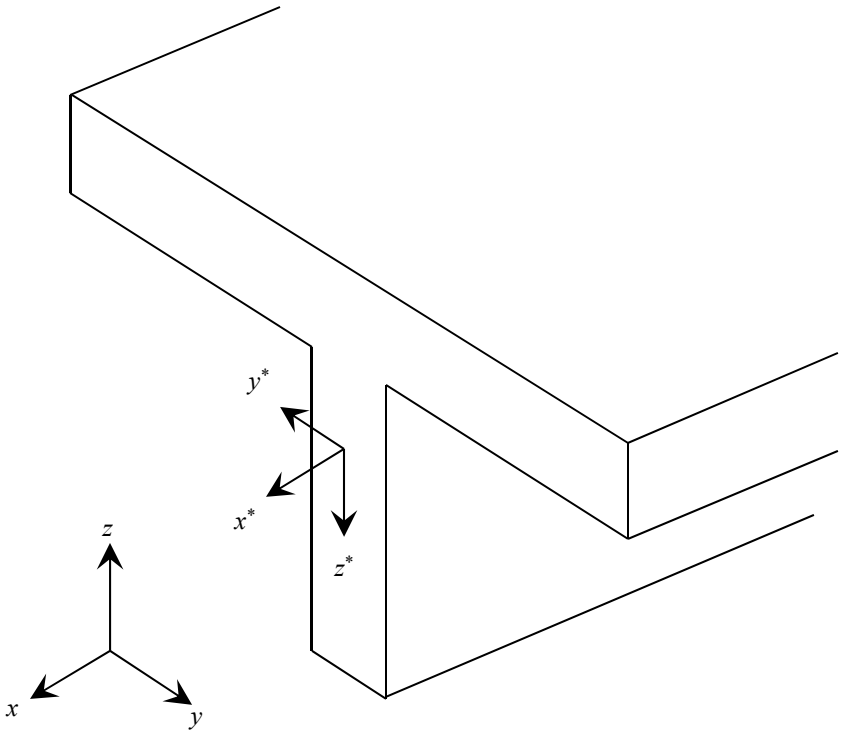

Figure 3.1: Local Coordinate System

This is the same system used by Jirousek and Bouberguig (1979) and Maher (1985).

3.4 Strains

With the coordinate system in place, the strains can be defined. It warrants explanation first that since the model accounts for shear deformations, it is necessary to define the rotation of the section as a separate displacement field. For a beam where shear deformations are ignored,

$$\theta_y^* = -\frac{dw^*}{dx^*}$$
$$\theta_z^* = \frac{dv^*}{dx^*} \tag{3.1}$$

However, if shear deformations are included, the total slope of the beam is the sum of the rotation and the shearing strain:

$$\frac{dw^*}{dx^*} = \gamma_z - \theta_y^*$$
$$\frac{dv^*}{dx^*} = \gamma_y + \theta_z^* \tag{3.2}$$

This is the distinguishing property of the beam element proposed by Timoshenko (1961) and will be used in this analysis. With this in mind, the strains used in the model can be defined:

$$\{\varepsilon\} = \begin{Bmatrix} \varepsilon_O \\ \gamma_y \\ \gamma_z \\ \theta \\ \psi_y \\ \psi_z \end{Bmatrix} = \begin{Bmatrix} \dfrac{du^*}{dx^*} \\ \dfrac{dv^*}{dx^*} - \theta_z^* \\ \dfrac{dw^*}{dx^*} + \theta_y^* \\ \dfrac{d\theta_x^*}{dx^*} \\ \dfrac{d\theta_z^*}{dx^*} \\ \dfrac{d\theta_y^*}{dx^*} \end{Bmatrix} \tag{3.3}$$

3.5 Applied Forces

There are six stress resultants in three dimensions – three forces and three moments. They can be defined as follows:

$$\{F^*\} = \begin{Bmatrix} N \\ Q_y^* \\ Q_z^* \\ T \\ M_y^* \\ M_z^* \end{Bmatrix} = \begin{Bmatrix} \int \sigma_x dA \\ \int \tau_{xy} dA \\ \int \tau_{xz} dA \\ \int \left(\tau_{xz} y - \tau_{xy} z \right) dA \\ \int \sigma_x z dA \\ -\int \sigma_x y dA \end{Bmatrix} \tag{3.4}$$

Note that the model only uses three stresses – the normal stress σ_x and the two in-plane shearing stresses τ_{yz} and τ_{zy}.

3.6 Section Properties

Conventional analysis equations for a cross-section generally use properties calculated about the centroid. Centroidal properties allow for simple calculation of strains based on internal forces.

$$\varepsilon_O = \frac{N}{EA} \qquad \psi_y = \frac{M_y}{EI_{yy}} \qquad \psi_z = \frac{M_z}{EI_{zz}} \qquad \gamma_y = \frac{V_y}{GA_{ry}} \qquad \gamma_z = \frac{V_z}{GA_{rz}} \qquad \theta = \frac{T}{GJ_c} \tag{3.5}$$

In matrix form, this becomes

$$\left\{F^*\right\} = \left[d\right]\left\{\varepsilon\right\}$$

$$\begin{Bmatrix} N \\ V_y^* \\ V_z^* \\ T \\ M_y^* \\ M_z^* \end{Bmatrix} = \begin{bmatrix} EA & & & & & \\ & GA_{ry} & & & & \\ & & GA_{rz} & & & \\ & & & GJ & & \\ & & & & EI_{yy}^* & \\ & & & & & EI_{zz}^* \end{bmatrix} \begin{Bmatrix} \varepsilon_O \\ \gamma_y \\ \gamma_z \\ \theta \\ \psi_y \\ \psi_z \end{Bmatrix} \tag{3.6}$$

where the normal strains are about the centroid and the shearing strains are about the shear centre, and the axes y and z are principal axes for the section. The shear modulus, G, can be calculated using poisson's ratio.

The problem that this presents in the current procedure is that the centroid is not static; the addition of parts with time (eg: a cast-in-place deck on a precast girder), cracking of concrete, and time-dependent effects all cause a change in the location of the centroid. Furthermore, the shear centre is often not coincident with the centroid. To avoid these problems, Ghali, Favre, and El-Badry (2011) selected a general reference point in the cross section and calculated the properties about that point. While this does complicate the analysis somewhat in that the axial force and bending moment equations are no longer independent, it allows superposition of strains and stresses from intervals where the centroid is not located in the same place. The interdependence of the axial force and bending moment can be handled by the addition of two new properties: B, the first moment of area about the reference point, and I_{yz}, the product of inertia. The new equations are presented below in matrix form:

$$E\begin{pmatrix} A & B_y & B_z \\ B_y & I_{yy} & I_{yz} \\ B_z & I_{yz} & I_{zz} \end{pmatrix}\begin{Bmatrix} \varepsilon_O \\ \psi_y \\ \psi_z \end{Bmatrix} = \begin{Bmatrix} N \\ M_y \\ M_z \end{Bmatrix} \qquad \text{and} \qquad G\begin{pmatrix} A_{ry} & & \\ & A_{rz} & \\ A_{ry}z_s & -A_{rz}y_s & J \end{pmatrix}\begin{Bmatrix} \gamma_y \\ \gamma_z \\ \theta \end{Bmatrix} = \begin{Bmatrix} V_y \\ V_z \\ T \end{Bmatrix} \tag{3.7}$$

where y_s and z_s are the shear centre's location. Combining these two systems into one yields the elasticity relationship for the current model:

$$\begin{pmatrix} Q_{x'} \\ Q_{y'} \\ Q_{z'} \\ M_{x'} \\ M_{y'} \\ M_{z'} \end{pmatrix} = \begin{pmatrix} N \\ V_y \\ V_z \\ T \\ M_y \\ M_z \end{pmatrix} = \begin{bmatrix} EA & & & & EB_y & EB_z \\ & GA_{ry} & & -GA_{ry}z_s & & \\ & & GA_{rz} & GA_{rz}y_s & & \\ & -GA_{ry}z_s & GA_{rz}y_s & GJ & & \\ EB_y & & & & EI_y & EI_{yz} \\ EB_z & & & & EI_{yz} & EI_z \end{bmatrix} \begin{pmatrix} \varepsilon_0 \\ \gamma_y \\ \gamma_z \\ \theta \\ \psi_y \\ \psi_z \end{pmatrix} \tag{3.8}$$

where elements not shown are equal to zero. Note the independence of the twisting/shear and axial/bending equations. In finite element terminology, this forms the familiar relationship

$$\{\sigma\} = [d]\{\varepsilon\} \tag{3.9}$$

The path forward is clear – given the geometric arrangement of the cross section, the following properties must be determined:

- A, the cross sectional area
- B_y, B_z, the first moments of area
- I_{yy}, I_{zz}, the second moments of area
- I_{yz}, the product of moment of area
- A_{ry}, A_{rz}, the reduced (shear) areas

- J, the torsional constant
- y_s, z_s, the location of the shear centre

The following sections detail the determination of these properties for concrete, steel, and non-prestressed steel components. The discussion of the shear-related properties (A_r, J) is delegated to 3.6.3.

3.6.1 Concrete Parts

Several approaches have been used to model the effects of forces on a cross section. When nonlinear analysis due to cracking is considered, the traditional methods for property calculation are not always suitable.

Ketchum (1985) represented the cross section as a grid of square elements and developed equations for the properties and resultants assuming constant stress and strain in each one. This approach lends itself well to doing calculations at ultimate limit state, because the stress-strain relationship can be completely non-linear and not affect the complexity of the calculation. For serviceability analysis, every fibre is either behaving in a linear fashion, or has cracked and does not contribute to the stiffness. Properties can be calculated in the traditional fashion by ignoring all concrete in the tension zone once cracking has occurred.

El-Badry (1988) adopted this approach, and defined sections as a series of trapezoids by their thickness and width and the top and bottom. This works very well for planar

analysis because the neutral axis or tension zone boundary is always horizontal. The calculation of properties is simply a summation of the values for each trapezoid.

Given the arbitrary nature of the section definition, and the consideration of biaxial bending in the analysis, a procedure is required to calculate cross section properties of an arbitrary polygon.

Kawakami and Ghali (1996) showed how a concrete cross section of arbitrary geometry could be represented by a closed series of planar points, the outline of which defines the shape of the part. The polygons need not be regular, and can be concave. They are used to define concrete parts. Three examples are shown in Figure 3.2:

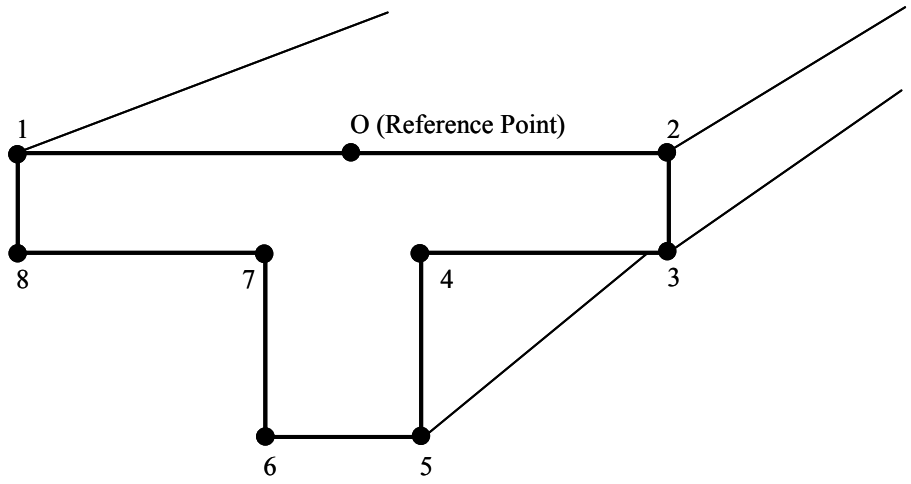

a) Simple T-Section

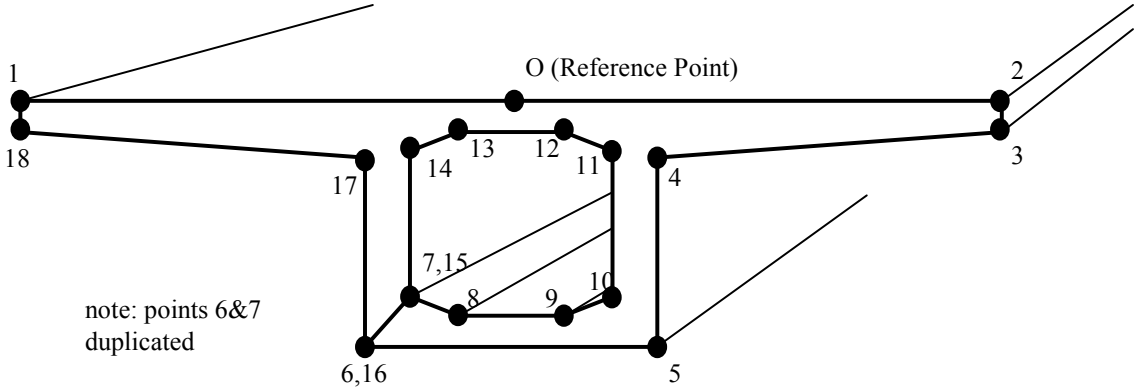

b) Complex Box Section

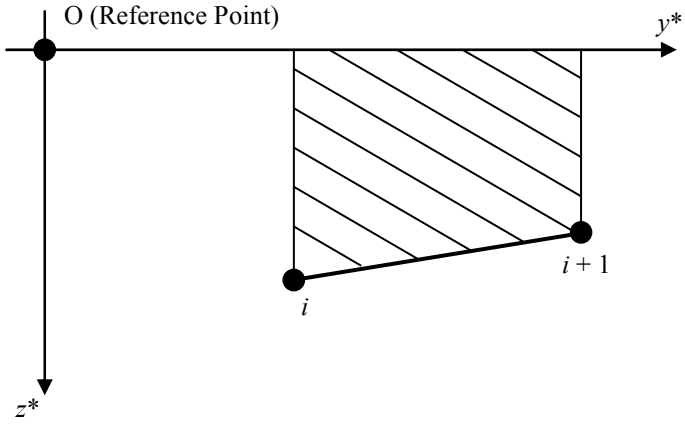

c) Elemental Trapezoid

Figure 3.2: Definition of Cross Section for Calculation of Properties

Figure 3.2a shows a simple T-beam cross section, defined by 8 points. As Kawakami and Ghali (1996) pointed out, a void like in Figure 3.2b can be accounted for by replicating some of the points. The void is actually outside of the polygon.

Kawakami and Ghali (1996) present a numerical method for the calculation of the integral $\int x^m y^n dA$ for any integers m and n.

The method is straightforward. As shown in Figure 3.2c above, any 2 points represent a trapezoidal shape. The integration dA can be expressed as the sum of the integrations carried out over each trapezoid.

$$H_{mn} = \int x^m y^n dA = \sum_{i=1}^{N} \Delta_i$$

$$\bar{x} = x - x_i$$

$$y = y_i + \frac{\Delta y_i}{\Delta x_i}\bar{x}$$

$$\Delta_i = \int_0^{\Delta x_i} \int_0^{y_i + \frac{\Delta y_i}{\Delta x_i}\bar{x}} \left(x_i + \bar{x}\right)^m y^n dy\, d\bar{x}$$

By integrating, simplifying, and using a binomial expansion for the appropriate terms, the final result becomes

$$\int x^m y^n dA = \sum_{i=1}^{N} \frac{1}{n+1} \left(\sum_{j=0}^{m} {}_m C_j x_i^{m-j} \Delta x_i^{j+1} \left(\sum_{k=0}^{n+1} {}_{n+1} C_k \frac{y_i^{n+1-k} \Delta y_i^{k}}{k+j+1} \right) \right) \qquad (3.10)$$

3.6.2 Steel Parts

Since biaxial bending is present in this analysis, it is not sufficient to show where a layer of bars is located. Each bar must be separately specified with its own x and y coordinates in the cross section, along with an area of steel. In practice, large amounts of reinforcing steel are used, and specifying the location of every bar would be very onerous. Alternatively, the modeller can simply specify the ratio of steel area to concrete area in the shape. Specifying the reinforcement ratio implies that the steel is distributed uniformly in the concrete. The geometric properties for the steel are simply equal to the reinforcement ratio multiplied by the properties for the concrete. The approach to use will vary depending on the problem to be considered.

For prestressing tendons, the tendons must be specified by location. The duct area can also be specified.

3.6.3 Superposition and Properties Related to Shear Stress

One major assumption necessary in the analysis is that the section property matrices can be superimposed, ie:

$$EI = \sum \left(EI\right)_i = E_{ref} \sum \frac{E_i}{E_{ref}} I_i = E_{ref} \sum \left(nI\right)_i \tag{3.11}$$

where n_i is the modular ratio or transformation factor for concrete or steel part i.

This works very well and is accurate for the normal strain properties because they are simple integrals dA, eg: $I_{yz} = \int yz\, dA$. However, the shearing matrix properties are not simple integrals. The reduced area is a rational function of two integrals, and the torsion constant requires a pre-assumed stress distribution or membrane analogy for calculation. In the case of thin-walled sections where the stress distribution through the wall can be assumed constant, simple closed-form equations are available. It is also possible to calculate the properties for standard solid sections such as rectangles or circles. It is possible to find the torsional constant for sections using numerical methods and either St. Venant's or Prandtl's approach, both of which involve the solution of a second-order partial differential equation.

For the torsional constant, J, there is a much simpler and perfectly acceptable approximation for the torsional constant using the second moments of area and the area (Oden and Ripperger, 1980):

$$J \approx \frac{0.025A^4}{I_x + I_y} \tag{3.12}$$

The reduced area, A_r, is a term that accounts for the non-uniform distribution of shear stress in the cross section. It can be calculated using the following (Ghali, Neville, and Brown, 2009):

$$A_r = \frac{I^2}{\int \frac{Q^2}{b^2} dA} \tag{3.13}$$

It is possible to express the reduced area as the normal area divided by a constant:

$$A_r = A/\alpha \qquad \alpha \geq 1$$

For simple rectangular shapes, the constant $\alpha = 1.2$. In order to simplify the analysis and handle changing cross-section geometry, the model assumes that the ratio A_r/A is constant for each section. It is possible to specify different values for A_{rx}/A and A_{ry}/A.

In the case of a composite section, superposition is assumed:

$$GJ = \sum_i GJ_i \tag{3.14}$$

This underestimates the torsional stiffness of composite sections.

It is critical to note that calculation of J using the method outlined in 3.8 for closed sections will not accurately calculate torsional stiffness. Using the membrane analogy, the height of the membrane along the enclosed surface is constant. The method above forces the height to be zero.

3.7 Cracking

Concrete is weak in tension. Under low tensile stress (often less than 10% of the compressive capacity), rupture occurs. While this may begin at the extreme fibre, the crack will propagate towards the neutral axis. At the same time as this occurs, the neutral axis shifts. In a completely unreinforced concrete section, this corresponds to failure of

the member as there is no part of the section which can take up the tension. When steel is present in the section, it will take the tension lost by the concrete and the section will go into a second state of equilibrium where the crack extends right to the point where the stress no longer exceeds f_{ct}. In practice, the tension zone's contribution is ignored and cracking is assumed to extend to the neutral axis. Therefore, to define the extent of cracking in the section, it is sufficient to find the new neutral axis orientation. For simple sections subjected to only an axial force and/or bending moment, it is possible to derive equations for the location and orientation of the neutral axis. When both an axial force and bending moment are present on a rectangular or T-section, a cubic equation can be found whose roots represent the cracked section depth (Ghali, Favre, and El-Badry, 2011). However, with arbitrary polygonal geometry and biaxial moments with normal force, this would be very complicated. Instead of deriving a closed-form solution to find the cracking depth, the current model uses an iterative algorithm described below. The following discussion will be carried out assuming uniaxial behaviour for illustration purpose.

It is worthwhile beforehand to discuss the effects of the internal forces on the cracked section properties. Again, the two equations to be satisfied are

$$\begin{aligned} N &= E\left(\varepsilon_0 A + \psi_y B_y\right) \\ M_y &= E\left(\varepsilon_0 B_y + \psi_y I_y\right) \end{aligned} \tag{3.15}$$

At any given load (N and M), there are two solutions to the system – one for the uncracked section, and one with all concrete in tension ignored.

The simplest case to analyze is the one where only axial force acts on a symmetric section with the reference point at the centroid (M_y=0, B_y=0). The above equations can be simplified to only include axial strain at the reference point and the area ($EA\varepsilon = N$). In this case, the area A is made up of the concrete and steel: $A = A_c + nA_s$, where A_c and A_s are the areas of concrete and steel respectively and n is a transformation factor equal to the ratio of the modulus of elasticity of steel to concrete. If cracking occurs in this case, all of the concrete will be removed, and the new area will simply be nA_s. As such, the N-ε diagram will be trilinear (see Figure 3.3).

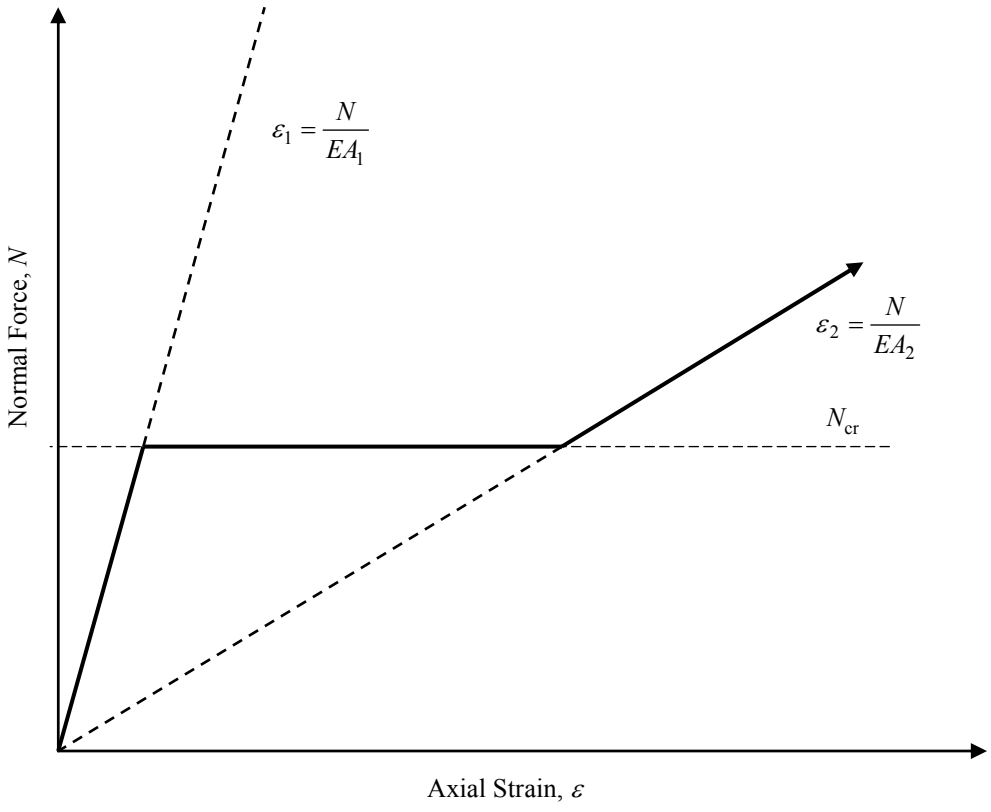

Figure 3.3: Normal Force vs. Axial Strain for RC Section

Slightly more complicated but essentially the same is the case of bending moment without axial force. Cracking will produce strain at the reference point now, because B becomes non-zero once cracking occurs. The moment-curvature relationship is simple, however: $M_y = E(\psi_y I_y)$. Again, a bilinear relationship is produced. Even though M continues to increase, the neutral axis remains in the same position. To see why this is the case, examine the equations above in matrix form.

$$E\begin{bmatrix} A & B_y \\ B_y & I_y \end{bmatrix}\begin{Bmatrix} \varepsilon_0 \\ \psi_y \end{Bmatrix} = \begin{Bmatrix} N \\ M_y \end{Bmatrix} \tag{3.16}$$

The location of the neutral axis relative to the reference point is simply $-\frac{\varepsilon_0}{\psi_y}$. The cracked section properties will only change if this ratio changes. If both N and M are magnified by the same factor, then both ε_0 and ψ will be as well, and the neutral axis will not move.

In bridge analysis, this is unlikely to be the case. Typically, the normal force comes from prestressing, while the bending moments come from imposed loads. This independence between N and M means that as load is applied to the section, the neutral axis moves and the section properties change. The moment-curvature relationship is no longer bilinear, even though the materials are elastic. For this reason, the calculation of crack depth for prestressed sections is handled using a parameter $e = M / N$ (Ghali, Favre, and El-Badry, 2011).

Biaxial bending further complicates matters, as the neutral axis can no longer be defined as simply a position relative to the reference point. The location and orientation are required. While this could be accomplished with an eccentricity in two directions, a direct computational approach is more suitable and is explained below.

3.8 Instantaneous Stress and Strain

At a given time t, a new set of forces are applied on the section. At the same time, new parts can be added or subtracted and prestressing can be applied. A step-by-step procedure is presented to calculate the instantaneous stress and strain that develops, taking into account the possibility of cracking in the section.

The state of internal forces on the section will control the geometric properties of the cracked section. For this reason, it is often necessary to take into account the pre-existing state of stress in the concrete when finding the properties.

El-Badry (1988) explains the process of decompression, where the new force to be applied on the section is partitioned into two parts: one which will bring the stress in the concrete to zero, and the part which remains from the original load. This method is advantageous because it can be used on sections which are precracked and those which are uncracked. Essentially, the section is unloaded, and the reverse of the effect required to do so is added to the applied force. Strains in the unloading stage use the current section properties, and the adjusted force is applied on the new cross section.

The forces which will remove all stress from the concrete can be found by

$$\{F\}_1 = -\frac{1}{E_c}[d]\{\sigma\}_c \tag{3.17}$$

where [*d*] is the 6x6 transformed matrix for the entire section (not just the concrete part), and $\{\sigma\}_c$ is the strain in the concrete part where cracking will occur. E_c is the modulus of elasticity of the concrete part being decompressed. Note that σ / E is not equal to the strain because of time-dependent effects.

El-Badry's analysis was undertaken on horizontally symmetric sections under uniaxial bending, and as a result, there are only three possibilities for any concrete part: uncracked (all points in compression or tension below f_{ct}), partially cracked (some points below f_{ct}, some above), or fully cracked (all points in tension above f_{ct}). Put differently, the neutral axis is completely contained in one concrete layer. As a result, each part in tension either contains the neutral axis or does not contribute to the stiffness. This allows for a simple algorithm to decompress a section under the effect of new loads:

1. Apply the load on the section and find the strain and stress distributions. If no cracking has occurred (maximum stress below f_{ct}), these are the final values.

2. Start by assuming the neutral axis is in the bottom layer (or the top layer, if the bending moment is negative).

3. Starting with the uncracked section stiffness, decompress each part below the neutral axis part using (3.17). Record the strain and stress changes that result. The stress in the current layer is now nil. Remove this layer's stiffness from [*d*],

as it will be completely cracked. Finally, decompress the part containing the neutral axis.

4. Partition the load to be applied into $\{F\}_1$ and $\{F\}_2$. Calculate the cracked section properties under the effect of $\{F\}_2$. Check the location of the neutral axis; if the assumption was correct, the analysis is complete. If not, select the part currently containing the neutral axis and return to (3).

To reiterate, this approach is possible because only one part in the section can be partially cracked. A composite section under biaxial bending, however, can easily have a neutral axis that intersects more than one cracked part. Consider a cast-in-place deck sitting on a precast beam, subjected to moments $M_x = M_y$. It is possible that both the deck and the beam will crack (see Figure 3.4).

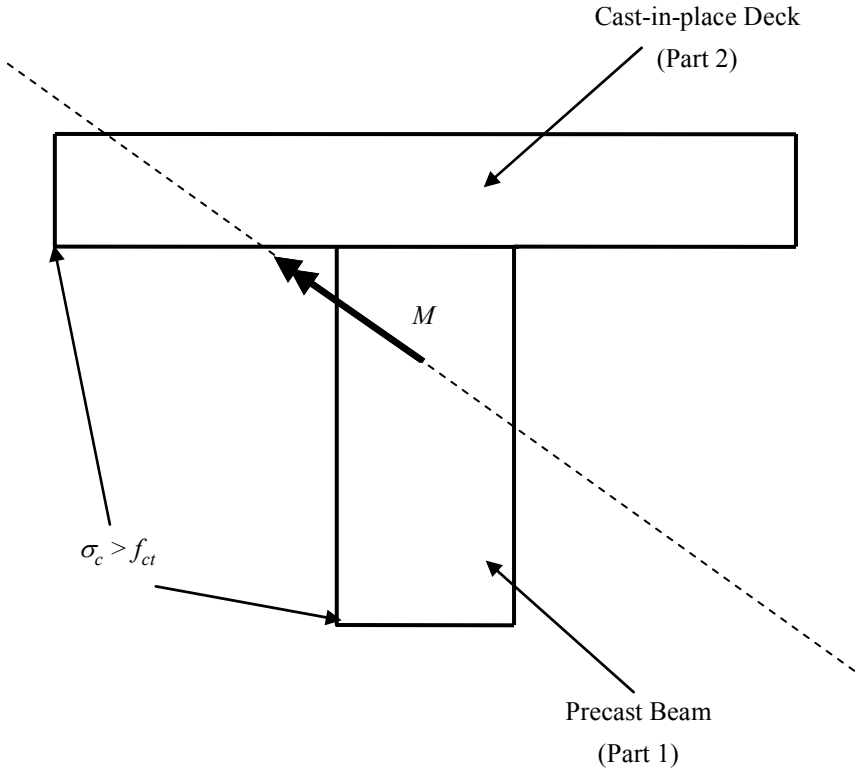

Figure 3.4: Composite Section with Two Cracked Parts

The analysis of cases such as this is not handled in the current model for two reasons: it is beyond the scope of this work to redesign the decompression algorithm, and such cases indicate a poor design. With this in mind, an algorithm can be developed for decompression of sections in the model.

Decompression is required for two separate purposes: the application of load on a section causing new cracking, and the application of load on a precracked section.

The first case can be handled simply enough, since the section does not have any pre-existing cracking. To find the new cracked section properties and the total strain which results from applying load on a section, the following steps are employed:

1. If the section has cracked parts:

    a. Decompress the first part and add the force to the applied force. The decompression strain is $\{\varepsilon\}_1$.

    b. Verify that no part is in tension exceeding f_{ct}. If so, terminate.

    c. Remove the stiffness of the part from the decompression section stiffness matrix.

2. Start with $\{\varepsilon\}_2 = 0$.

3. Using the section stiffness matrix, calculate the resultant forces on the section and the out of balance forces:

$$\{F_r\}_i = \{F\}_0 - [d]_i \{\varepsilon\}_{i-1} \tag{3.18}$$

4. Based on the strain and stress, calculate the geometry and the section properties.

    a. Remove all points where the stress exceeds f_{ct}, and add new ones where required (see below).

    b. Calculate the new properties for the section.

c. Assemble the section's stiffness matrix for this iteration $[d]_i$ by adding the stiffness matrix for each part. Include:

   i. Concrete existing before this interval or precast

   ii. Prestressing steel bonded to the section at the beginning of this interval.

5. Calculate the change in strain from the out of balance forces:

$$\{\Delta\varepsilon\}_i = [d]_i^{-1} \{F_r\}_i \tag{3.19}$$

6. Update the strain and the forces on the section:

$$\{\varepsilon\}_i = \{\varepsilon\}_{i-1} + \{\Delta\varepsilon\}_i \tag{3.20}$$

7. Check for convergence:

$$\{F_{res}\}^T \{F_{res}\} \le \alpha \{F_0\}^T \{F_0\} \tag{3.21}$$

   a. If convergence is not satisfied, go to 2.

8. Verify that no additional parts have cracked. If there are new cracked parts,

   a. Decompress and add the force to $\{F\}_0$.

   b. Verify that the stress in all parts is below f_{ct}. Terminate if not satisfied.

   c. Remove this section from the decompression section stiffness matrix.

Essentially, the initial assumption is that only the first section to crack will remain cracked with the full load applied. If this proves to be false, the next section to crack is used as well, and so forth until equilibrium is satisfied. The check in 8b ensures that if more than one partially cracked part is found, the analysis is halted. This is waived if the decompression of the first part also decompresses the second (consider a double tee section for example). This should not be a significant restriction, and cases where this takes place generally indicate poor design. If new load is applied on a precracked section, it is only necessary to decompress the part which contains the neutral axis (since all other cracked parts are completely cracked and as a result have no stress to decompress).

It should be carefully noted here that the geometry of the cracked section is not determined separately from the strains. Instead, the instantaneous strain is found at the same time as the cracked section properties are determined.

Step 2 in the above procedure considers cracking, and as such, it warrants a detailed explanation here. The method presented by Kawakami and Ghali (1996) for calculation of properties for polygons takes as input a series of (x,y) points. To change the polygon for cracking, the goal is to remove all of the points which are in tension. New points must also be placed wherever one of the boundary lines intersects the neutral axis. The most efficient way to accomplish this is to examine each pair of points in succession. Three cases must be considered:

1. Both points are in tension. Remove them both.

2. Both points are in compression. Leave them both.

3. One point is in tension, the other in compression. Find the zero stress point along the line, remove the point in tension, and add this new point to the new section.

It would also be possible to find the equation for the neutral axis as a line, and test each point to see on which side of the line it lays. However, doing this requires many special case considerations (such as when there is no curvature).

3.8.1 Cracking and Shear Properties

As was explained at the beginning of the chapter, no closed-form solutions are available for determining the shear properties (J, A_{ry}, A_{rz}) of an arbitrary solid section. A method must be found to adjust the initial values to account for a reduction in stiffness from cracking.

The torsional constant, J, can be found using St. Venant's approximation:

$$J \simeq \frac{0.025A^4}{I_x + I_y} \tag{3.12}$$

For the reduced areas, the assumption will be made that the reduction is of the same magnitude as that experienced by the area, ie:

$$\frac{A_r'}{A_r} = \frac{A'}{A} \tag{3.22}$$

where A' and A_r' are the quantities after cracking.

Note that the above assumptions do not account for the difference between closed and open type sections and as a result will give poor results in many cases.

If an initial value for the torsion constant is available, it is also possible to assume that the ratio between the torsion constant and the polar second moment of area remains constant despite the cracking. Mathematically,

$$\frac{J_1}{I_{yy1}+I_{zz1}} = \frac{J_2}{I_{yy2}+I_{zz2}}$$
$$J_2 = J_1 \frac{I_{yy2}+I_{zz2}}{I_{yy1}+I_{zz1}} \tag{3.23}$$

It should be noted, however, that the determination of the cracked torsion and shear properties is the most error-prone part of the model. The largest problem is that cracking can open a closed section, which can cause a sudden decrease of several orders of magnitude in the torsional stiffness. The best way to alleviate this problem is to use FEM or BEM solutions to the internal force-stress distribution relationship. The methods are discussed by Surana (1979). Additionally, Shangchow (1984) showed how the partial boundary element approach could be applied to specific cracked cross sections to determine their torsional resistance. Such implementations are outside of the scope of this analysis.

3.9 Time-Dependent Stress and Strain

Over time, concrete and prestressing steel undergo changes in stress and strain – even under static load. These changes can lead to substantial increases in deflection, and can

radically redistribute the stresses in the cross section. In order to calculate the changes in deflections, member-end forces, and stresses, it is necessary to account for three phenomena: creep and shrinkage of concrete, and relaxation of prestressing steel.

The displacement method is used here. The method requires calculation of the forces required to restrain displacements. The displacements in question are six strains, and the forces are all six stress resultants.

3.9.1 Creep and Shrinkage of Concrete

The calculation of the free strain in concrete which would occur if it were free to do so was presented in Chapter 2. Recall Eq.(2.24):

$$\Delta\varepsilon_f\left(t_{i+1},t_i\right)_{free}=\sum_{j=0}^{i}\left(\varepsilon\left(t_j\right)+\frac{\Delta\sigma\left(t_{j+1},t_j\right)}{E_c\left(t_j\right)}\right)\left(\phi\left(t_{i+1},t_j\right)-\phi\left(t_i,t_j\right)\right)+\Delta\varepsilon_{cs}\left(t_{i+1},t_i\right)$$

The concrete section's stiffness matrix must also be adjusted for time dependent analysis:

$$\left[\overline{d}\left(t_{i+1},t_i\right)\right]_c=\frac{\overline{E_c}\left(t_{i+1},t_i\right)}{E_c\left(t_i\right)}\left[d\left(t_i\right)\right]_c=\frac{1}{\chi\phi\left(t_{i+1},t_i\right)}\left[d\left(t_i\right)\right]_c \tag{3.24}$$

The forces which will restrain creep and shrinkage between t_i and t_{i+1} are:

$$\left\{F\left(t_{i+1},t_i\right)\right\}_r=-\left[\overline{d}\left(t_{i+1},t_i\right)\right]_c\left\{\Delta\varepsilon\left(t_{i+1},t_i\right)\right\}_f \tag{3.25}$$

where $[d]_c$ is the section stiffness matrix for the concrete part in question only. Note that the free shear strains are simply those caused by creep.

3.9.2 Prestress Loss

As discussed in 2.3, the relaxation of prestressed steel can be calculated given some simple parameters and the initial stress.

Calculating the drop in force is a simple matter:

$$\Delta P\left(t_{i+1}, t_i\right) = \Delta \bar{\sigma}_{pr}\left(t_{i+1}, t_i\right) A_{ps} \tag{3.26}$$

Note that the reduced relaxation of the strand, $\Delta\bar{\sigma}_{pr}$, is a negative quantity.

Given the change in the tendon force, the approach shown in section 4.5.2 can be used to find equivalent distributed loads.

3.9.3 Calculation of Stress

To calculate the stresses and strains which occur in the interval, the displacement method is used. Once the restraining forces are known for each section component, they can be reversed and applied on the whole section to find the actual strain that occurs in the interval:

$$\left\{\Delta\varepsilon\left(t_{i+1}, t_i\right)\right\} = -\left[\bar{d}\right]^{-1} \sum \left\{\Delta F\left(t_{i+1}, t_i\right)\right\}_r \tag{3.27}$$

$\left[\overline{\mathrm{d}}\right]$ is the age-adjusted section stiffness matrix, where all properties are transformed relative to $\overline{\mathrm{E_c}}$ as opposed to $\mathrm{E_c}$. The stresses can be calculated, using $A = A_r + A_u D$.

For concrete:

$$\Delta\sigma_c\left(t_{i+1},t_i\right)=\overline{E_c}\left(t_{i+1},t_i\right)\left(\Delta\varepsilon\left(t_{i+1},t_i\right)-\Delta\varepsilon_f\left(t_{i+1},t_i\right)\right) \tag{3.28}$$

For steel:

$$\Delta\sigma_{ps}\left(t_{i+1},t_i\right)=E_{ps}\Delta\varepsilon\left(t_{i+1},t_i\right)+\Delta\overline{\sigma}_{pr} \tag{3.29}$$

Non-prestressed steel is the same as prestressed, but with zero intrinsic loss. Note that for unbonded tendons, the change in stress is simply equal to the loss as no strain in the concrete is transferred to the tendon.

3.9.4 Cracking Due to Time-Dependent Effects

It is entirely possible that the change in stress from creep, shrinkage, and prestress loss could cause or exacerbate cracking. A restrained concrete slab undergoing shrinkage in a dry environment with a high modulus could experience 1MPa of tensile stress.

The problem this presents is that the section geometry and cracked section properties are changing continually as time-dependent stress develops. The forces which determine the geometry, however, result from the geometry. Iteration is required, and two separate cases must be considered: the section initially cracked at the beginning of the interval, and the case where cracking is initiated by the time-dependent effects. El-Badry (1988) suggests the following procedures:

Suppose that the section is initially cracked. To begin, use $[d]_i$ and calculate the strain that develops. Application of the forces on the decompressed section will give new section geometry and hence a new $[d]_{i+1}$. Repeat the calculation, using $[d]_i$ for creep and $[d]_{i+1}$ for everything else.

For sections that are not initially cracked, the proper approach is to find an intermediate time $\bar{t}$ where cracking occurs. By assuming a linear stress-time relationship, this time can be found:

1. Apply the full time-dependent force on the section, assuming cracking does not take place. The stress at the extreme fibre exceeds f_{ct}. Find the stress at this fibre at t_i, $\sigma_c(t_i)$, and the change in stress at that fibre between t_i and t_{i+1}, $\Delta\sigma_c(t_{i+1},t_i)$.

2. Calculate the portion κ of t_{i+1}-t_i for which cracking has not occurred.

$$\kappa = \frac{f_{ct} - \sigma_c(t_i)}{\Delta\sigma_c(t_{i+1}, t_i)} \tag{3.30}$$

3. Reanalyze the uncracked section, using $\kappa\Delta\varepsilon_f(t_{i+1},t_i)$ for the free strain and $\kappa\Delta\bar{\sigma}_{pr}(t_{i+1},t_i)$ for the reduced relaxation. The final stress at the extreme point will be equal to f_{ct} – if not, iteration is required.

4. Calculate the decompression forces for the section, and the changes in stress and strain in the decompression stage.

5. Reverse and apply the decompression forces on a fully cracked section. Find the cracked section geometry and the changes in stress and strain.

6. The total stress and strain that occur up to cracking are the sum of those calculated in 3-5, and are equal to $\Delta\sigma\left(\bar{t},t_i\right)$ and $\Delta\varepsilon\left(\bar{t},t_i\right)$.

7. To simplify the analysis further, assume that this increment of stress $\Delta\sigma\left(\bar{t},t_i\right)$ occurs at t_i. This eliminates the need for additional creep coefficients. The final free strain for the second part of the interval is

$$\Delta\varepsilon_f\left(t_{i+1},\bar{t}\right)=\left(1-\kappa\right)\frac{\Delta\sigma\left(\bar{t},t_i\right)}{E_c\left(t_i\right)}\phi\left(t_{i+1},t_i\right)+\left(1-\kappa\right)\Delta\varepsilon_f\left(t_{i+1},t_i\right) \tag{3.31}$$

The (1-κ) in the first term follows the assumption that $\phi\left(t_{i+1},\bar{t}\right)=\left(1-\kappa\right)\phi\left(t_{i+1},t_i\right)$, which infers that the development of creep is linear between t_i and t_{i+1}. In the second term it accounts for the free strain which was not used in step 3.

This analysis can be greatly simplified if the section properties are assumed to be static between t_i and t_{i+1}. For sections that are already cracked, the error that this introduces is not significant (Ghali, Favre, and El-Badry, 2011). Cracking caused by time-dependent effects is indicative of poor design and should be avoided. For these reasons, the current model neglects the change in section geometry under time-dependent effects. The consequence of this assumption is that nonlinear analysis is not required for time-dependent analysis. Cracking is assumed to happen at t_{i+1}.

3.10 Tension Stiffening and Mean Strain

Suppose that a simply supported reinforced concrete member is subjected to a centre point load which is increased until the extreme fibre stress reaches f_{ct}. Cracking will occur at the centre of the beam. As the load increases to the point just before the second crack occurs, the moment just to the left or right of the first crack exceeds M_{cr} - but no cracks develop. This is because the cracking at the midpoint causes slip of the bond between the bar and the concrete, and the extreme fibre stress just to the left or right of the crack is below f_{ct}. As the distance from the crack increases, the bond slips less, and at some point the strain becomes compatible again. At this distance, however, the stress at the extreme fibre will only reach f_{ct} with an increase in the load. Once it does, the next crack forms, and the process continues. The net result is that the extreme fibre stress is not linear along the beam – even though the bending moment is. Figure 3.5a shows the variation in extreme fibre stress for a cracked member when the first crack forms, and Figure 3.5b shows the distribution when the next cracks develop.

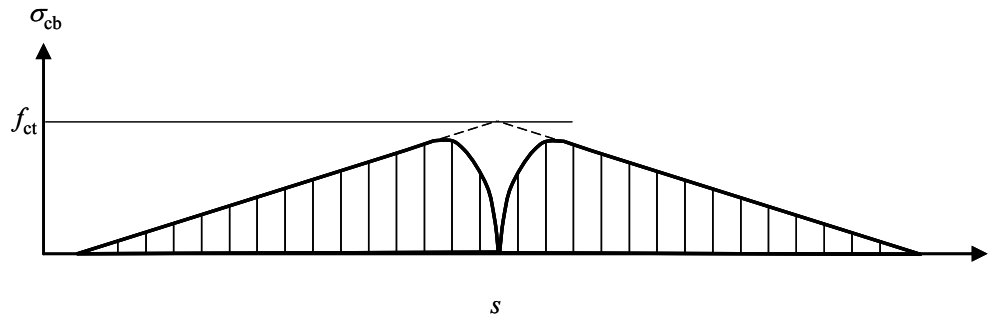

a) immediately after formation of first crack

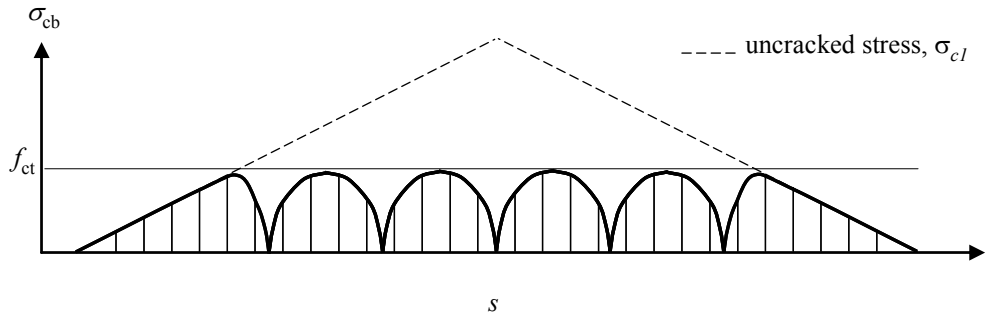

b) cracking becoming extensive

Figure 3.5: Extreme Fibre Stress Variation for a Cracked Member

The ability of sections near cracks to remain uncracked increases the stiffness of the member. This phenomenon is known as "tension stiffening". If the curvature at the cracked section was used to calculate deflections assuming full strain compatibility, they would be overestimated by a large amount because the tension stiffening would be ignored. Tension stiffening also changes the stiffness of a reinforced concrete member. If ignored, it will affect the fixed-end forces as well.

Obviously, the tension stiffening effect is more pronounced when the stress barely exceeds f_{ct}. As the load on the beam mentioned above is increased to a large value, cracking is extensive and the tension stiffening effect becomes small.

Bond quality is also essential to the calculation. A poor bond between the concrete and steel will increase the length over which no strain compatibility exists, and therefore the crack spacing; a better bond will reduce the tension stiffening effect.

Research by several authors, including Favre et al. (1985) was adopted by CEB-FIP in their code and suggests using a coefficient to interpolate between cracked and uncracked states:

$$\zeta = 1 - \beta_1 \beta_2 \left(\frac{\sigma_{sr}}{\sigma_{s2}} \right)^2 \tag{3.32}$$

where σ_{sr} is the steel stress in the cracked section immediately after cracking has occurred and σ_{s2} is the steel stress in the actual cracked section. Ghali, Favre, and El-Badry (2011) modify this to be in terms of concrete stress:

$$\zeta = 1 - \beta_1 \beta_2 \left(\frac{f_{ct}}{\sigma_{\max}} \right)^2 \tag{3.33}$$

where f_{ct} is the rupture stress in the concrete and $\sigma_{\max}$ is the highest stress on an uncracked concrete section. β_1 is a coefficient that takes into account the strength of the bond between the bars and the concrete. For normal bars, $\beta_1 = 0.5$; for high-bond bars,

1.0. β_2 is a coefficient that accounts for the type of loading on the structure. If the load is applied in a sustained fashion or on virgin material, $\beta_2 = 1.0$; for cyclic loads, $\beta_2 = 0.5$. The product $\beta_1\beta_2$ will be referred to below as simply β, and can be taken practically as 0.5.

This approach was analysed by Espion and Halleux (1988) and a slightly more complex approach was taken. They found that while their method more accurately matched observed experimental behaviour, the simplified interpolation approach provided generally acceptable results (within a few percent).

Once the interpolation coefficient is calculated, a "mean strain" can be calculated which accounts for tension stiffening.

$$\varepsilon_m = (1-\zeta)\varepsilon_1 + \zeta\varepsilon_2 \tag{3.34}$$

where ε_1 and ε_2 are the strains in uncracked and cracked states, respectively. Obviously, a larger value for the interpolation coefficient means that tension stiffening has a lesser effect; this will occur when the stress becomes larger, or the bond is better.

Equation (3.34) can also be used for curvatures. Figure 3.6 below shows the resulting moment-curvature relationship (Ghali, Favre, and El-Badry, 2011).

It is important to realize that nonlinear analysis will be required to solve for the displacements in the structure when cracking is involved. While the procedure is

discussed in detail in 5.4, there are some important facets to mean strain calculation that warrant consideration here.

When a member cracks, the stiffness reduces. This can change the fixed-end forces in the member, and will almost certainly change the final member-end forces in statically indeterminate structures. Both of these effects will change the force that acts on any given section (which in turn will change the extent of cracking). There is a small horizontal line BC in Figure 3.6, which indicates that a sudden large jump in strain occurs right at cracking. Even if $\sigma_{\max}$ slightly exceeds f_{ct}, the interpolation coefficient becomes 1-β. Since β is typically taken as 0.5, it is not possible to have a value of ζ below 0.5. This sudden jump can lead to problems where the change in strain is large for small changes in internal force. The strains oscillate heavily and do not converge to an acceptable solution (see 5.4.3 for a discussion about nonlinear convergence).

To avoid this problem, Ghali, Favre, and El-Badry (2011) suggest adopting mean strain calculations when the stress at the extreme fibre exceeds $\sqrt{\beta_1\beta_2}f_{ct}$. This corresponds to following the curve AED in Figure 3.6 instead of ABCD.

One essential note: the mean strain is only used for calculation of displacements. The actual stress and strain at a cracked section are those from state 2.

It will become evident that the analysis will require repeated calculation of strain from stress. As a result, it becomes numerically efficient to calculate a “mean” section stiffness matrix. Recall that

$$
\begin{aligned}
\{\varepsilon\}_m &= (1-\xi)\{\varepsilon\}_1 + \xi\{\varepsilon\}_2 \\
\{\varepsilon\}_1 &= [d]_1^{-1}\{F^*\} \\
\{\varepsilon\}_2 &= [d]_2^{-1}\{F^*\} \\
\{\varepsilon\}_m &= \left((1-\xi)[d]_1^{-1} + \xi[d]_2^{-1}\right)\{F^*\} \\
&= [d]_m^{-1}\{F^*\}
\end{aligned}
\tag{3.35}
$$

where

$$
[d]_m = \left((1-\xi)[d]_1^{-1} + \xi[d]_2^{-1}\right)^{-1} \tag{3.36}
$$

It is more numerically efficient to store the inverse of the mean section stiffness matrix.

The ε_1 term in (3.34) is the strain that develops if the section were to never have cracked. All calculations, including the time dependent forces and strains, must be completed in parallel for a cracked and uncracked section.

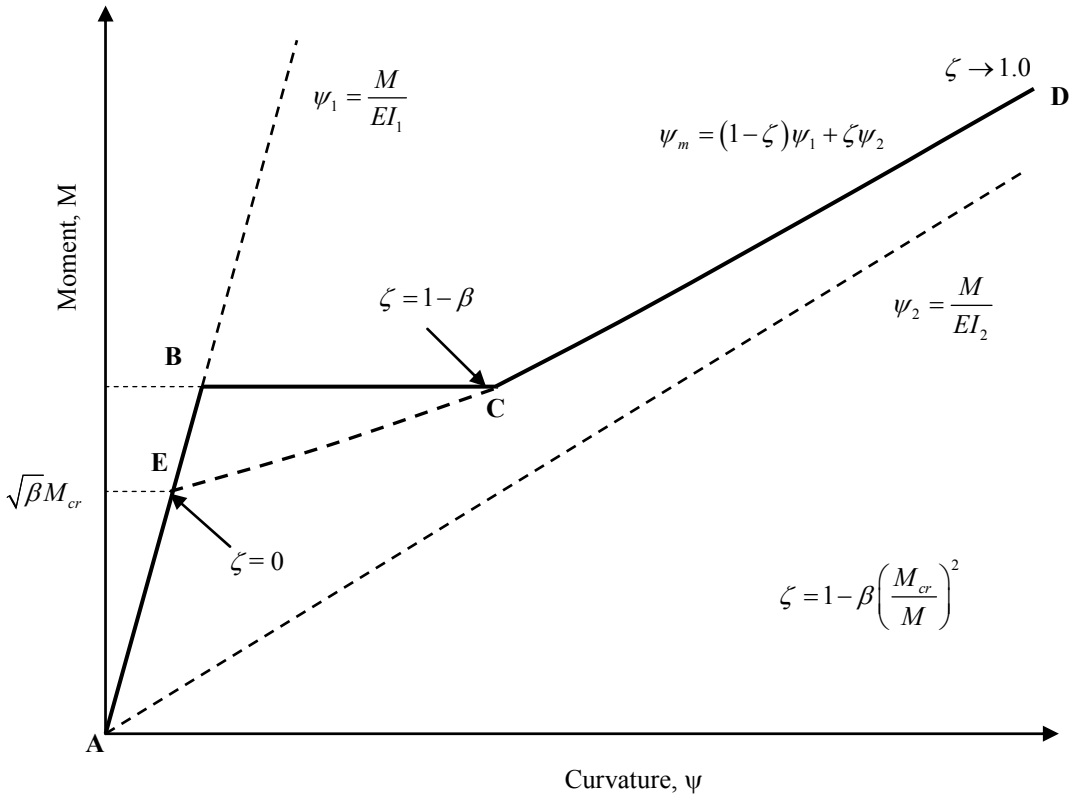

Figure 3.6: Moment-Curvature Relationship Using Interpolation Coefficient

3.11 Summary

This chapter has explored the effects of the resultants of stress and strain on a cross section for the curved beam element in use. Detailed analysis of instantaneous and time dependent phenomena was presented along with matrix formulations for the calculations for arbitrary cross sections constructed in stages.

A detailed look at cracking in cross sections where tensile stress exceeds the capacity of the concrete was undertaken. Simplified equations were presented to account for cracking in the calculation of effective strains.

The next chapter extends this analysis over the element and ties the effects at the nodes into the required calculations at the element level.

Chapter Four: **ANALYSIS OF A MEMBER**

The new formulation's one and only element is a curved beam with an axis defined by an arbitrary curve in 3-dimensional space. At each node or knot, a location and section is given. A sample element is shown in Figure 4.1 below.

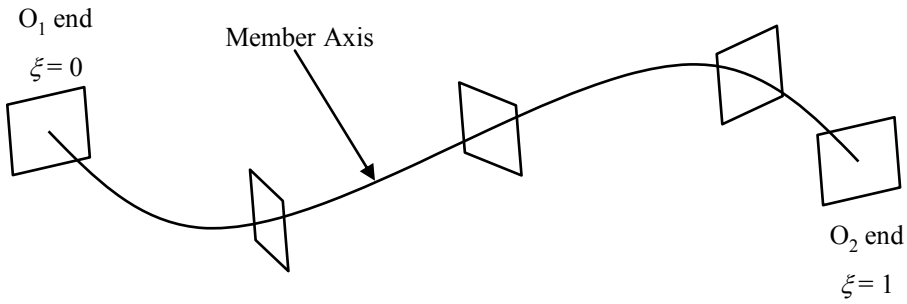

Figure 4.1: Element Layout

4.1 Member Definition

Each beam element axis has two ends: the O_1 end and the O_2 end. The coordinate system for the member is composed entirely of a normal coordinate, ξ, which varies from a value of 0 at the O_1 end to 1 at the O_2 end. The x, y, and z coordinates are modeled as separate functions of the normal coordinate:

$$x = x(\xi) \qquad y = y(\xi) \qquad z = z(\xi) \tag{4.1}$$

Members can be specified by simply providing a series of (ξ, x, y, z) points (sometimes referred to as nodes in the following discussion). The functions listed above are generated using standard Lagrange interpolation. Sections need not have even spacing

along the member, and where abrupt changes in section occur, two sections can be specified at zero distance from each other. Most of the numerical methods presented in section 5.5.1 will simplify greatly if even spacing is used, however.

Note that the formulation used here does not impose any restrictions on the shape of the element. It can model any shape that would be used in practical construction.

4.2 Assumptions

The following assumptions are made for modeling of members in the current model:

1. Plane sections remain plane after deformation. Warping is ignored, and the strain profile is assumed planar. This can be a significant restriction for certain cross-sections if large twisting moments exist. This assumption definitely governs the possible element configurations for the model. While this was also mentioned in the assumptions for section analysis, it warrants reiteration here.

2. The stress profile is also planar. This means that the curvature of the element needs to be small enough that radial stresses do not become significant. The length of the inside of the curve must not be significantly different than the outside; this requires that the dimensions of the cross section be of smaller order than the element's radius of curvature.

3. In order to have the math work out correctly, it is necessary that the normal to the plane of the section through the reference point is collinear with the tangent to the

curve at all points along the element. In other words, the cross sections are not skewed to the element axis.

4. The x, y, and z functions behave appropriately for Lagrange interpolation (see below).

4.3 Parametric Curves

There are many possible ways to define a curve in 3-dimensional space. The y- and z-coordinates can be functions of the x-coordinate, for example. A better system, however, is to have all three coordinates as separate independent functions of a fourth parameter, t.

There are two types of interpolation functions used in this model. They are discussed below.

4.3.1 Lagrange Polynomials

Lagrange polynomials are the simplest to use and are the keystone in isoparametric finite element calculations. Lagrange polynomials use a set of basis functions to interpolate:

$$y(x) = \sum_{i=1}^{n} N_i(x)\, y_i \tag{4.2}$$

where $N_i(x)$ is the Lagrange polynomial and is equal to 1 at x_i and 0 everywhere else. Using this definition, it is relatively simple to derive

$$N_i(x) = \prod_{\substack{j=0 \\ j \neq i}}^{n} \left(\frac{x - x_j}{x_i - x_j} \right) \tag{4.3}$$

For calculation using the computer, it is cleaner to realize that the Lagrange interpolating polynomial for n points is of at most degree n-1. In general,

$$N_i(x) = \sum_{j=1}^{n} a_{ij} x^{j-1} \tag{4.4}$$

In matrix form,

$$\{N\} = [A]\{x\} \tag{4.5}$$

Where [A] is the Vandermonde matrix and is non-singular as long as all x's are distinct. From (4.2),

$$\begin{aligned} y(x) &= \{Y\}^T \{N\} \\ &= \{y\}^T [A]\{x\} \end{aligned} \tag{4.6}$$

[A] will satisfy

$$[A][X] = [I]$$

$$\begin{bmatrix} a_{11} & a_{12} & \cdots & a_{1n} \\ a_{21} & a_{22} & \cdots & a_{2n} \\ \vdots & \vdots & \ddots & \vdots \\ a_{n1} & a_{n2} & \cdots & a_{nn} \end{bmatrix} \begin{bmatrix} x_1^{\,0} & x_2^{\,0} & \cdots & x_n^{\,0} \\ x_1^{\,1} & x_2^{\,1} & \cdots & x_n^{\,1} \\ \vdots & \vdots & \ddots & \vdots \\ x_1^{\,n-1} & x_2^{\,n-1} & \cdots & x_n^{\,n-1} \end{bmatrix} = \begin{bmatrix} 1 & 0 & \cdots & 0 \\ 0 & 1 & \cdots & 0 \\ \vdots & \vdots & \ddots & \vdots \\ 0 & 0 & \cdots & 1 \end{bmatrix} \tag{4.7}$$

$$[A] = [X]^{-1}$$

$$[X]_{ij} = x_j^{\,i-1}$$

Notice that the vector of basis functions $[A]\{x\}$ is independent of the y values. It will frequently be required in the analysis to calculate the derivative of the interpolating function, which can be found by differentiating (4.4):

$$\begin{aligned}\frac{dy}{dx} &= \sum_{i=1}^{n} y_i \frac{dN_i(x)}{dx} \\ \frac{dN_i}{dx} &= \sum_{j=1}^{n} (j-1)\, a_{ij} x^{j-2}\end{aligned} \tag{4.8}$$

In matrix form this becomes

$$\begin{Bmatrix} N_1'(x) \\ N_2'(x) \\ \vdots \\ N_n'(x) \end{Bmatrix} = \begin{bmatrix} a_{12} & 2a_{13} & \cdots & (n-1)a_{1n} & 0 \\ a_{21} & 2a_{22} & \cdots & (n-1)a_{2n} & 0 \\ \vdots & \vdots & \ddots & \vdots & \vdots \\ a_{n1} & 2a_{n2} & \cdots & (n-1)a_{nn} & 0 \end{bmatrix} \begin{Bmatrix} x^0 \\ x^1 \\ \vdots \\ x^{n-1} \end{Bmatrix} \tag{4.9}$$

$$N'(x) = \{y\}^T [A']\{x\}$$

where

$$\begin{aligned} a'_{ij} &= j a_{i,j+1} \quad (j < n) \\ a'_{in} &= 0 \end{aligned} \tag{4.10}$$

Equation (4.10) can be repeated using *a*' in place of *a* to calculate *a*''. Any point in space can be calculated by direct interpolation:

$$\begin{Bmatrix} x(\xi) \\ y(\xi) \\ z(\xi) \end{Bmatrix} = \sum_{i=1}^{n} N_i(\xi) \begin{Bmatrix} x_i \\ y_i \\ z_i \end{Bmatrix} \tag{4.11}$$

Likewise,

$$\begin{Bmatrix} x'(\xi) \\ y'(\xi) \\ z'(\xi) \end{Bmatrix} = \sum_{i=1}^{n} \frac{dN_i(\xi)}{d\xi} \begin{Bmatrix} x_i \\ y_i \\ z_i \end{Bmatrix} \tag{4.12}$$

4.3.2 Spline Functions

While Lagrange polynomials are elegant and simple to use, they can create problems with oscillation depending on the location of selected nodes. Runge's phenomenon demonstrated that the more points that are selected for interpolation, the more significant the oscillation can become. This is because the degree of the interpolating polynomial is one less than the number of selected points. This can cause particular concern in the current study because continuous prestressing tendons can run through several different members. As a result, a prestress tendon may have 15 or more nodes on it.

To illustrate the problem, consider a segmentally constructed bridge with a span illustrated in Figure 4.2. The tendon is composed of parabolic sections in each end with a straight section in the middle. Since each span has 3 section nodes, and there are eight members, there are a total of 17 interpolation points required for the calculation. To simplify matters, the midpoints in the straight pieces are ignored for 11 points.

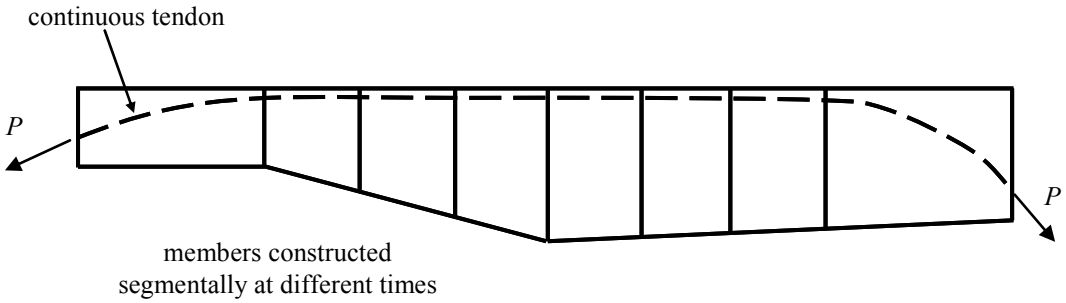

Figure 4.2: Continuity Prestressing Example

The most pronounced effect of this discrepancy is in the calculation of the distributed load produced by the prestressing. The simplified approach to prestressing used by Ghali, Neville, and Brown (2009) shows that the equivalent force is roughly equal to the second derivative of the profile, and that the anchor force is directed along the tangent at the ends. As Figure 4.3 shows below, the second derivative of the continuous polynomial produced by interpolation oscillates heavily through the span and would no doubt produce unacceptable results.

A more suitable approach is to define the function in a piecewise fashion using splines. Spline functions use a lower degree of polynomial to model the tendon's profile, but do so in a segmental fashion. As a result, they do not suffer from the same effects that the interpolating polynomials of high degree do.

The most commonly used spline functions are cubic splines, where each segment of the curve is defined by a different polynomial of order 3. For a function with n segments, this yields 4n unknowns:

$$S_i(x) = a_i x^3 + b_i x^2 + c_i x + d_i \qquad x_{i-1} \le x \le x_i \tag{4.13}$$

However, the values of the function are known at the endpoint of each segment (2n conditions):

$$S_i(x_i) = y_i \qquad S_i(x_{i+1}) = y_{i+1} \tag{4.14}$$

Additionally, the slope and the curvature should be continuous through the central points on the curve:

$$S_i'(x_i) = S'_{i+1}(x_i) \qquad S_i''(x_i) = S_{i+1}''(x_i) \tag{4.15}$$

Since there are only n-1 central points, this only yields 2n-2 conditions. This leaves 2 "free" unknowns, which can be set in any suitable fashion depending on the requirements of the interpolation. The most common condition is zero curvature at the ends, which produces a natural cubic spline:

$$S_1''(x_0) = S_n''(x_n) = 0 \tag{4.16}$$

While NCS are suitable for the majority of analysis, they should not be used to model prestressing tendons with parabolic segments. Parabolic segments have constant curvature, so restricting them to zero values at the ends creates a problem.

A better approach, and the one used in most analysis presented here, is to provide the value of the tangent at each end of the curve:

$$\begin{aligned} S_1'(x_0) &= t_0 \\ S_n'(x_n) &= t_1 \end{aligned} \tag{4.17}$$

Derivation of the coefficients of each of the spline function segments is standard fare in numerical methods texts; one good example is Cheney and Kincaid (1999). The standard method can be easily adjusted for the end tangent.

A comparison of the interpolation for the spline and Lagrange polynomials is shown below:

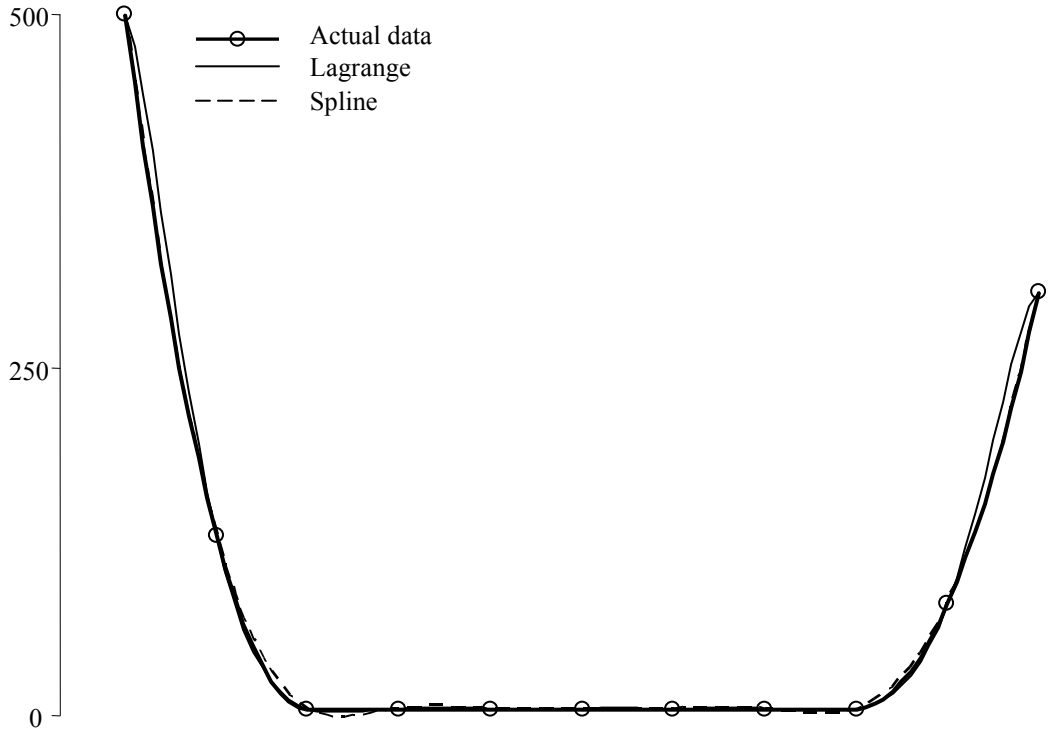

Figure 4.3: Comparison of Spline and Lagrange Functions

To compare the spline modeling to the Lagrange interpolation for the example given above, a simple error function can be used. The results are tabulated below.

$$E = \sqrt{\int_0^1 \left(S(\xi) - y\left(\xi\right)\right)^2} \tag{4.18}$$

Table 4.1: Error for Spline and Lagrange Functions

	Spline	Lagrange
y	2.19	6.94
y''	22500	32100

The other significant advantage with splines is that the error will go down as more points are added – the exact opposite of what happens with polynomial fitting. If, instead of 11 points, the midpoint of each member is considered and 17 points are used, the results become:

Table 4.2: Adjusted Interpolation Error

	Spline	Lagrange
y	0.9	64.1
y''	21600	475000

With the functions to interpolate for each of the x, y, and z coordinates of the beam element's axis defined, the next step is some differential geometry.

4.3.3 Tangent and Principal Normal

It is necessary in the analysis to define a local coordinate system. At any point on the curve, the tangent can be calculated as

$$\mathbf{t} = \mathbf{S}' = \frac{d}{d\xi}\begin{Bmatrix} x(\xi) \\ y(\xi) \\ z(\xi) \end{Bmatrix} \tag{4.19}$$

The plane perpendicular to *t* has infinitely many vectors in it that all satisfy

$$\mathbf{u} \cdot \mathbf{t} = 0 \tag{4.20}$$

The "principal normal" is selected as the vector contained in the plane with the largest positive projection on *S''*. It can be calculated by subtracting the projection of *S''* onto *S'*:

$$\mathbf{n} = \left(\mathbf{S}'' - \frac{\mathbf{t}}{|\mathbf{t}|} \left(\mathbf{S}'' \cdot \frac{\mathbf{t}}{|\mathbf{t}|} \right) \right) \frac{1}{|\mathbf{t}|^2} \tag{4.21}$$

The $1/t^2$ term at the end of the expression corrects the differentiation between dS and $d\xi$.

4.4 Coordinate System/Unit Vectors

In traditional finite-element analysis, there is a difference between the local coordinate system for an element and the global system that the structure exists in. This allows for simple linear transformations to aggregate and combine elements into a structure, which is advantageous because of the amount of repetition typically used in structures. In the current model, however, this is not the case. The stiffness matrix and fixed-end forces for the members are directly calculated in the global coordinate system.

There must be a conversion made, however, between the global coordinate system and the system for a section. Each section along the member may have a completely different coordinate system. The system can be defined by three unit vectors λ_{x^*}, λ_{y^*}, and λ_{z^*}, shown in Figure 3.1. The x* axis lies normal to the section, along the axis of the member, while the y* and z* axes are in the plane of the section. The origin is the reference point of the section. Notice that the section normal is not sufficient to define

the system. The angle φ is introduced as the angle between the local y* axis and the global x-y plane.

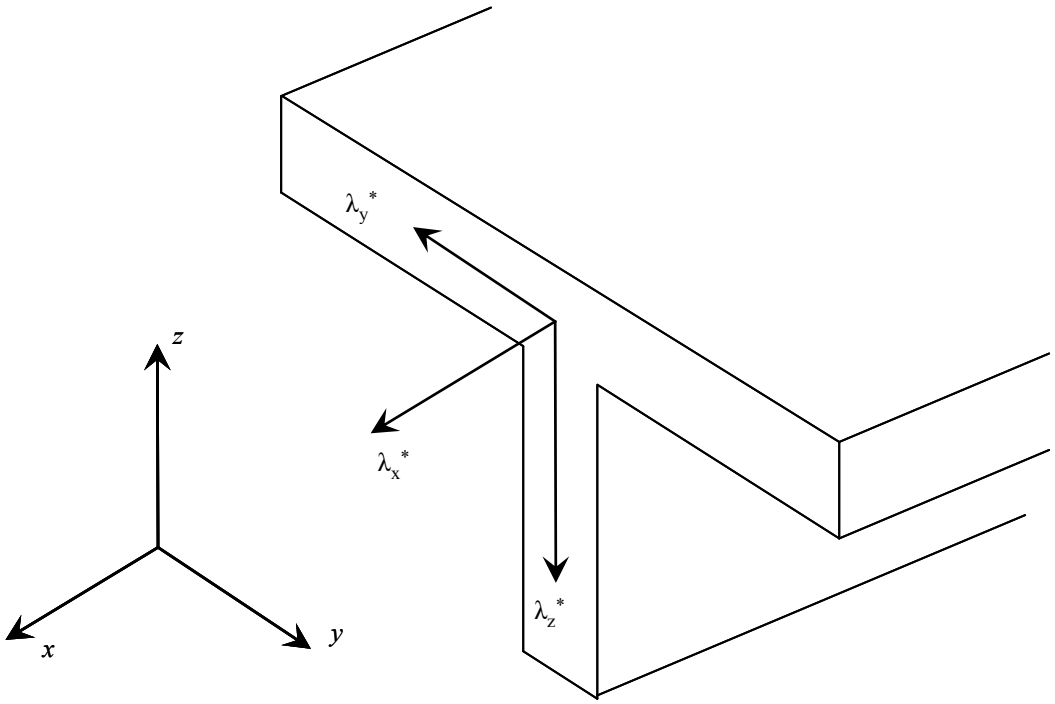

Figure 4.4: Unit Vectors and Direction Cosines

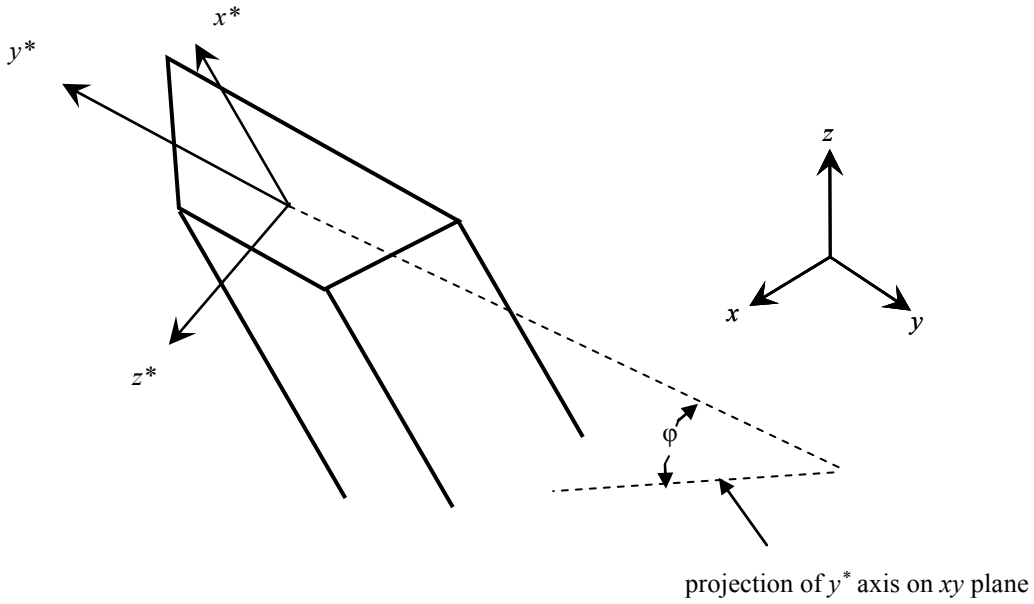

a) Local x*-axis not parallel to global z-axis (Case 1)

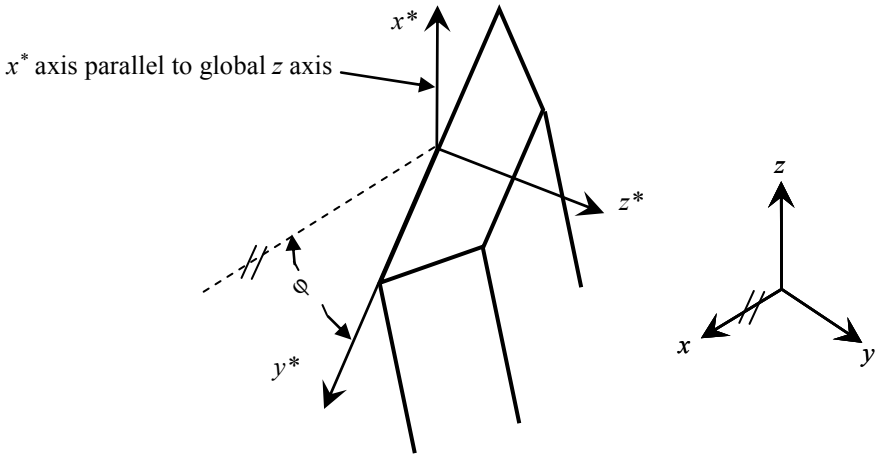

b) Local x*-axis parallel to global z-axis (Case 2)

Figure 4.5: Definition of Angle *φ*

This transformation was presented by Jirousek (1979) and is repeated here for completeness. It begins with calculating λ_{x^*}, which is simply the tangent vector normalized:

$$\boldsymbol{\lambda}_{x^*} = \frac{\mathbf{t}}{|\mathbf{t}|} \tag{4.22}$$

Case 1: t_x and t_y not simultaneously zero :

This case, shown in Figure 4.5a, is applicable whenever the section normal is not parallel to the global z axis.

$$\lambda_{y^*z} = \sin\phi$$
$$\lambda_{y^*y} = \frac{-b - \text{sgn}(t_x)\sqrt{b^2 - 4ac}}{2a}$$

where $a = \left(t_x{}^2 + t_y{}^2\right)$, $b = 2t_y t_z \sin\phi$, and $c = t_z{}^2 \sin^2\phi - t_x{}^2 \cos^2\phi$.

If $t_x \neq 0$, $\lambda_{y^*x} = -\frac{1}{t_x}\left(t_y\lambda_{y^*y} + t_z\lambda_{y^*z}\right)$; if $t_x = 0$, $\lambda_{y^*x} = \text{sgn}(t_y)\sqrt{\cos^2\phi - \lambda_{y^*y}{}^2}$

Case 2: $t_x = t_y = 0$:

In this case, the angle between the local y^* axis and the xy plane cannot uniquely define the orientation because the y^* axis is in the xy plane (see Figure 4.5b). This means that the local x^* axis is parallel to the global z axis and has no projection on the global xy plane. In this case, φ is defined as the angle between the global x axis and the local y axis, measured positive about the global z axis in the right hand sense.

$$\lambda_{y^*x} = \cos\phi$$
$$\lambda_{y^*y} = \sin\phi$$
$$\lambda_{y^*z} = 0$$

4.4.1 Coordinate Transformations

With the unit vectors defined, it is possible to define the transformation between forces or displacements in the global system and the local section system:

$$\begin{aligned} \{D\} &= [t]\{D^*\}` & \{F\} &= [t]\{F^*\}` \\ \{D^*\} &= [t]^T \{D\} & \{F^*\} &= [t]^T \{F\} \end{aligned} \tag{4.23}$$

where the matrix [*t*] is an orthogonal transformation matrix:

$$[t] = \begin{bmatrix} \lambda_{x^*} & \lambda_{y^*} & \lambda_{z^*} \end{bmatrix} = \begin{bmatrix} \lambda_{x^*x} & \lambda_{y^*x} & \lambda_{z^*x} \\ \lambda_{x^*y} & \lambda_{y^*y} & \lambda_{z^*y} \\ \lambda_{x^*z} & \lambda_{y^*z} & \lambda_{z^*z} \end{bmatrix} \tag{4.24}$$

Eqs (4.23) must be applied to both the translational and rotational degrees of freedom, which is done by replacing *t* with *T* where

$$[T] = \begin{bmatrix} [t] & 0 \\ 0 & [t] \end{bmatrix} \tag{4.25}$$

4.4.2 Line Integrals and Length Calculation

Many of the calculations require calculation of the length of a segment or all of a parametric curve. From calculus,

$$L = \oint_C dS = \int_0^1 \frac{dS}{d\xi} d\xi \tag{4.26}$$

where dS is an elemental length along the axis of the member and C is the curve. To carry out the line integral, transform dS into an elemental normal coordinate, dξ.

$$dS = \sqrt{dx^2 + dy^2 + dz^2} = \sqrt{\left(\frac{dx}{d\xi}\right)^2 + \left(\frac{dy}{d\xi}\right)^2 + \left(\frac{dz}{d\xi}\right)^2}\, d\xi = t(\xi)\, d\xi \tag{4.27}$$

$$L = \int_C dS = \int_0^1 \mathbf{t}(\xi)\, d\xi \tag{4.28}$$

where $\{t(\xi)\}$ is again the tangent vector to the curve and $t(\xi)$ is its magnitude. Since all of the integration in the model is done numerically, the values need only be determined at the integration points. Most of the integration required is carried out *dS*, which is directly dependent on the functions $x(\xi)$, $y(\xi)$, and $z(\xi)$.

4.4.3 Internal Forces

Suppose a force is applied at a point on the member, and the internal section force is required. From simple statics,

$$\begin{Bmatrix} F_2 \\ M_2 \end{Bmatrix} = \begin{Bmatrix} F_1 \\ M_1 \end{Bmatrix} + \begin{Bmatrix} 0 \\ \mathbf{r} \times F_1 \end{Bmatrix} \tag{4.29}$$

where **r** is a vector from point 2 to point 1. In matrix form,

$$\begin{Bmatrix} F_{2x} \\ F_{2y} \\ F_{2z} \\ M_{2x} \\ M_{2y} \\ M_{2z} \end{Bmatrix} = \begin{bmatrix} 1 & & & & & \\ & 1 & & & & \\ & & 1 & & & \\ & -\Delta z & \Delta y & 1 & & \\ \Delta z & & -\Delta x & & 1 & \\ -\Delta y & \Delta x & & & & 1 \end{bmatrix} \begin{Bmatrix} F_{1x} \\ F_{1y} \\ F_{1z} \\ M_{1x} \\ M_{1y} \\ M_{1z} \end{Bmatrix} \tag{4.30}$$

Generally, however, the requirement is to calculate the force required at O_2 to maintain equilibrium with an applied force at point 1. This can be expressed as

$$\{F_2\} = [R(\xi_2, \xi_1)]\{F_1\} \tag{4.31}$$

where [*R*] is the negative of the matrix in (4.30).

For these purposes, the internal forces will be considered positive if they align with the local coordinate system on the O_1 side of the section.

4.5 Prestressing Tendons

Prestressing tendons must be modeled in space in the same fashion that the member is. Calculation of losses and forces on sections require information about the angle and length of the tendon, which is not available in any other fashion.

4.5.1 Profile Definition

The definition of the tendon is done at each section where the tendon lies. It is defined by the local *y** and *z** distances from the reference point. By adding these vectors to the

location of the reference point (x_i, y_i, z_i), the point where the tendon intersects the plane of the section can be found.

$$\begin{Bmatrix} x_p \\ y_p \\ z_p \end{Bmatrix} = \begin{Bmatrix} x_o \\ y_o \\ z_o \end{Bmatrix} + [t] \begin{Bmatrix} 0 \\ y_p^* \\ z_p^* \end{Bmatrix} \tag{4.32}$$

This can be done at each node where the tendon exists to define a new set of points. Parametric curves can be used to define the layout of the prestressing tendon; see 4.3.2 for details.

The formulation for prestressing here is similar to that used by Maher (1985) in that only ends of members can be used to anchor tendons. A tendon can go through more than one member.

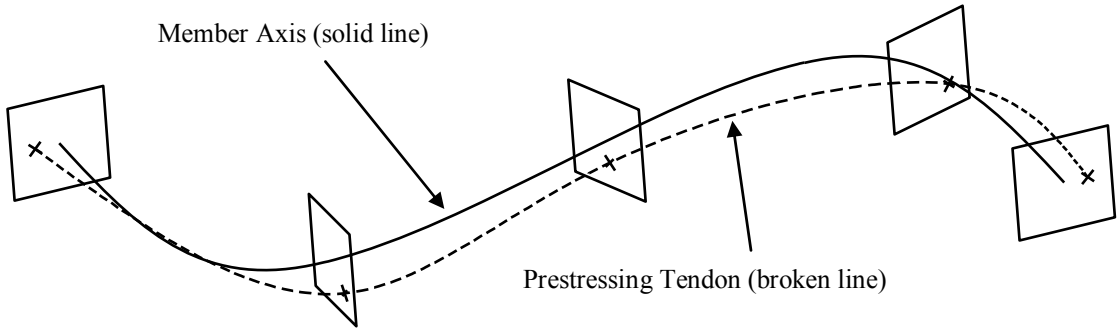

a) Tendon Running Through Member

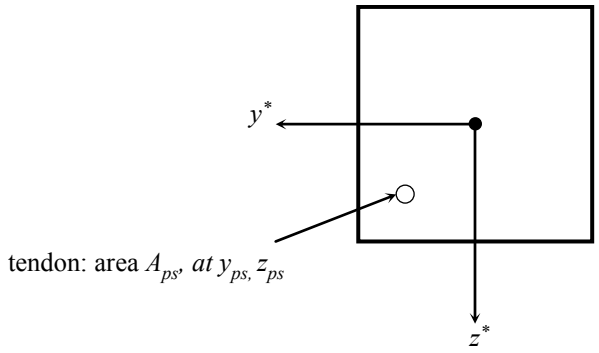

b) Tendon in Typical Cross Section (O_1 Side of Section)

Figure 4.6: Prestressing Tendon Spline Modeling

4.5.2 Prestressing Forces

Prestressing forces are calculated in the same manner as Maher (1985). In summary, both the anchorage forces at the ends as well as the cable forces in the member must be accounted for.

In both cases, it is necessary to calculate the force at the reference point from the tendon force:

$$\{F\}_0 = \left[R_{ps}\right]\{F\}_t \tag{4.33}$$

where $\{F\}_0$ is the force at the reference point (6x1), $\{F\}_t$ is the force at the tendon (3x1), and

$$\left[R_{ps}\right] = \begin{pmatrix} \left[I\right]_3 \\ \left[t\right]\begin{bmatrix} 0 & -z_{ps}^{*} & y_{ps}^{*} \\ z_{ps}^{*} & 0 & 0 \\ -y_{ps}^{*} & 0 & 0 \end{bmatrix}\left[t\right]^T \end{pmatrix} \tag{4.34}$$

The anchorage forces are directed along the tendon at the tendon ends.

$$\{P\} = P\{\lambda_t\} \tag{4.35}$$

The sign above is reversed at the O_2 end.

A cable running through a member produces a distributed load in two directions: one from the change in magnitude of the force, and one from the change in direction of the force. Differentiating (4.35) and applying the product rule,

$$\frac{d\{P\}}{dS} = \frac{dP}{dS}\{\lambda_t\} + P\frac{d\{\lambda_t\}}{dS} = \frac{dP}{d\xi}\frac{1}{|t|^2}t + P\{n\} = q_t + q_n \tag{4.36}$$

where {n} is the principal normal to the tendon. Eq (4.33) is applied afterwards to find the distributed load at the reference point.

Consider a member curved in the x-y plane similar to that in verification example 6.1.1. The tendon's small curvature in the x*-z plane causes a small upward distributed force,

but the tendon's large curvature in the x-y plane causes a larger radial force directed to the centre of the member's curve. Since this force acts well below the shear centre of the beam, it causes torsion on the member.

4.5.3 Instantaneous Losses

There are two types of instantaneous losses that occur from prestressing: friction and anchor set.

Friction losses occur because of resistance at the interface between the tendon and the duct. When the duct is curved, a great deal of the prestressing force pushes against it. This allows friction forces to develop, which gradually reduce the effective prestress through the tendon as the distance from the jacking end grows.

Friction losses can be calculated by

$$P_e = P_i e^{-(\mu\alpha + ks)} \tag{4.37}$$

where s is the distance along the tendon from the jacking end and α is the cumulative change in angle from the jacking end. Mathematically,

$$s = \int_0^{\xi_i} \frac{dS}{d\xi} d\xi = L\xi_i \qquad\qquad \alpha = \int_0^{\xi_i} \left| \frac{d\alpha}{d\xi} \right| d\xi \tag{4.38}$$

The integral for the length is simple and straightforward, but the integration for the change in angle can be difficult. Instead, to calculate the change in angle, sum up all of

the changes in the previous segments. The change in angle between two nodes on the tendon can be found using the dot product of the two tangents:

$$\alpha = \cos^{-1}\left(\lambda_{x^*,i} \cdot \lambda_{x^*,j}\right) \tag{4.39}$$

This assumes that there is no change in curvature of the tendon between the segments. This will never be a problem practically, but if an inflection point exists on a tendon a section node can be added there.

It should be noted that if the jacking end is the right end, the same formulae are used – except the limits of integration will go from ξ_i to 1. If both ends are jacked, the situation is more complicated and is discussed after the single end case.

Anchor set loss takes place due to the small amount of tendon which slips back inside the member at release. It is dependent on the type of anchor, and is characterized by the length of slip, δ. Anchor set analysis is complicated, however, because the same friction losses that affect the jacking also affect the slip. The anchor slip loss is highest at the anchor, and decreases along the tendon at the same rate that the friction losses take place. It is possible that at some distance L_s along the tendon, the anchor set loss has no more effect as the friction loss has completely isolated it. If friction loss is low, however, the anchor set can affect the entire tendon. This distance along the tendon where anchor set has influence is denoted L_s, and its value is the cornerstone of the analysis. Anchor set loss in a prestressing tendon is shown in Figure 4.7.

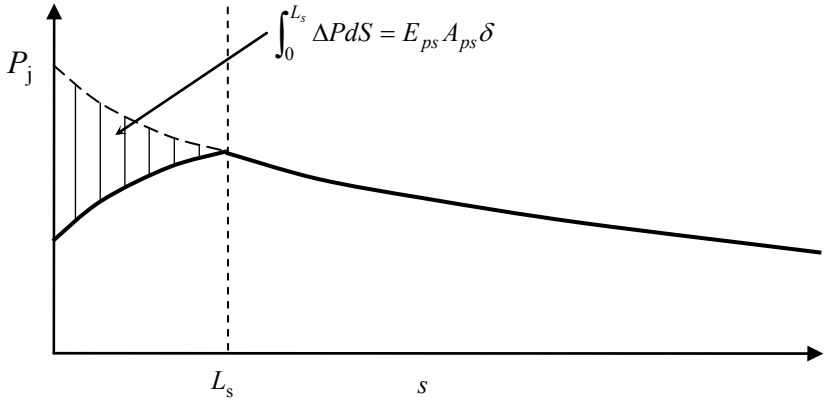

Figure 4.7: Anchor Set Loss in Prestressing Tendon

The total slip in the tendon will be equal to the integral of the change in strain over L_s:

$$\delta = \int_0^{L_s} \Delta\varepsilon \, dS = \int_0^{L_s} \frac{\Delta P}{E_{ps} A_{ps}} dS \tag{4.40}$$

E_{ps} and A_{ps} are constant over the tendon, therefore

$$E_{ps} A_{ps} \delta = \int_0^{L_s} \Delta P dS \tag{4.41}$$

Since the slope of the P-s curve is the same as for friction loss, but inverted, it is a simple matter to calculate the change in prestressing force due to anchor set loss:

$$\Delta P = 2\left(P_i - P_{L_s}\right) \tag{4.42}$$

where P_{Ls} is the value of the prestressing force at L_s. The only unknown in the expression is the value L_s. Rather than deriving a closed form expression for it, an

iterative procedure is presented which follows El-Badry (1988). The goal is to find the two section nodes which bracket L_s.

1. Start by choosing the section next to the jacking end.

2. For the chosen section, calculate the integral $\int_0^{L_i} \Delta P dS$. Gaussian quadrature is the most suitable method for this purpose.

3. If the integral is larger than $\delta A_{ps} E_{ps}$, then the true value for L_s lies somewhere between the last section and the current one. Bisection can be used to determine the value of L_s.

4. If the drop over the entire tendon is still insufficient, the anchor set loss affects the entire member. A certain drop in prestress, ΔP_0, will affect the entire member including the opposite anchor. This drop in force can be calculated by removing the amount of shortening that would occur if $L_s = L_{tendon}$:

$$\begin{aligned} \delta E_{ps} A_{ps} &= 2\int_0^{L_{tendon}} P_i - P_{end}\, dS + \Delta P_0 \cdot L_{tendon} \\ \Delta P_0 &= \frac{\delta E_{ps} A_{ps} - 2\int_0^{L_{tendon}} P_i - P_{end}\, dS}{L_{tendon}} \end{aligned} \tag{4.43}$$

The final prestressing force at any section can be calculated:

$$P_e = P_i - 2\left(P_i - P_{end}\right) - \Delta P_0 = 2P_{end} - P_i - \Delta P_0 \tag{4.44}$$

The case when $L_s > L$ is illustrated in Figure 4.8.

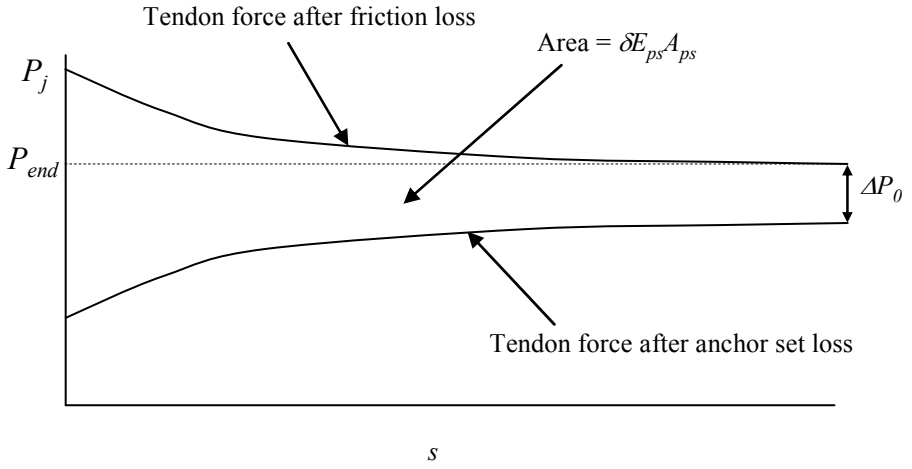

Figure 4.8: Anchor Set Loss Affecting Entire Tendon

What if both ends are jacked? Consider no anchor set losses first. Since jacking from the second end overcomes the friction losses from the first end, the larger of the two prestressing forces at any section is taken as shown in Figure 4.9.

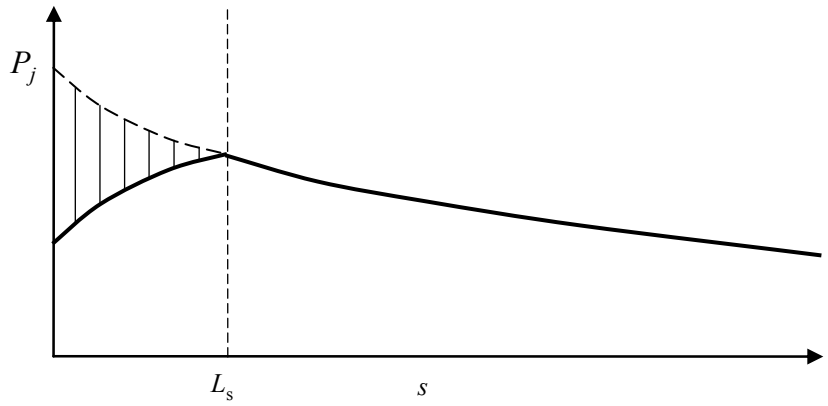

a) Anchor Set Losses with One End Jacked

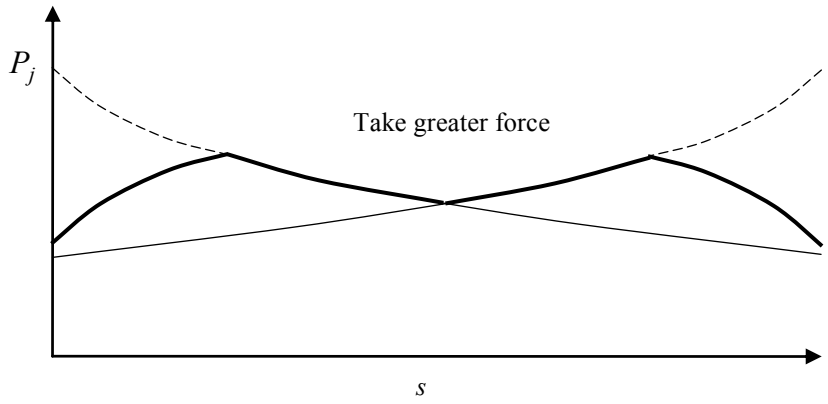

b) Net Prestress Force with Both Ends Jacked

Figure 4.9: Anchor Set Loss From Each End Independent

However, if L_s is large, the anchor set losses from the first end will overcome the jacking force from the second end as shown in Figure 4.10b. In this case, the smaller of the two forces should be taken. The decision can be made based on L_s. First, calculate the final prestressing force at every section for each jacking end separately. This will result in two values for L_s: L_{s1}, for when the tendon is jacked from the O_1 end, and L_{s2}, for jacking from the O_2 end. If the location indicated by L_{s2} on the tendon is closer to the O_1 end than L_{s1}, the minimum of the two forces should be taken (since the losses are the greater

of the two cases). In this case, $L_{s1} > L_{tendon} - L_{s2}$. Otherwise, the larger of the two forces is taken (smaller losses). Note that while the figures shown here indicate symmetric tendons, this may not be the case in practice.

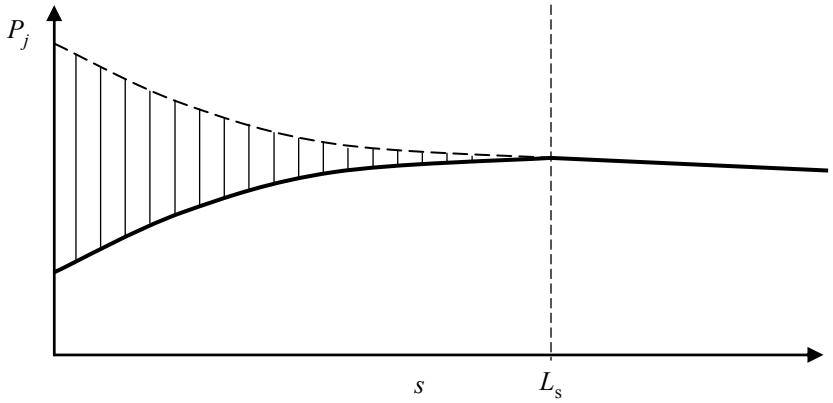

a) Anchor Set Losses with One End Jacked

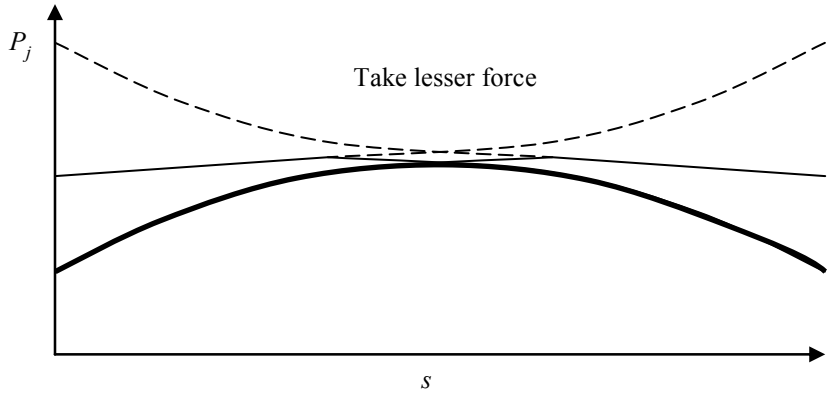

b) Net Prestress Force with Both Ends Jacked

Figure 4.10: Anchor Set Loss From Each End Overlapping

It is this final force, after all instantaneous losses, which should be used for calculating the fixed-end forces for the member (see 4.8).

4.6 Force Method and Deflection Calculation

As will be shown below, all of the computations involving members centre around the calculation of deflections for given loads on a member. For any node in 3-dimensions, there are 6 deflections that can take place: 3 translations (w_x, w_y, and w_z) and 3 rotations (θ_x, θ_y, and θ_z). The calculations at the basic level for members in the model involve extensive use of the force method. It is worthwhile at this point to review the force method as used by Ghali, Neville, and Brown (2009). It has five steps, which are explained below with reference to the current model.

1. Introduce releases to render the system statically determinate, and define the actions which are the unknowns to be found. In the current model, this means completely freeing the O_1 end while the O_2 end remains fixed. The actions are the internal forces $\{F^*\}$ at every section in the section coordinate system, which are required for calculations of stress and strain. The actions should also include the O_2 forces (the O_1 forces will be solved in step 4).

2. Due to the loadings on the released structure, calculate the displacements $\{D\}$ that would be caused by the loading if they were free to occur.

$$\{D\} = \{w_x \quad w_y \quad w_z \quad \theta_x \quad \theta_y \quad \theta_z\}^T \tag{4.45}$$

   The displacements are calculated using virtual work, which is explained in detail below.

3. Apply unit values of the redundants on the structure one by one and calculate the flexibility matrix [*f*] and the unit values of the actions. Each column of the flexibility matrix is equal to the deflections at the released end due to a unit redundant. The A_u matrix will give the O_1 reactions and internal forces at each section for each unit redundant.

4. Solve the geometry equation $[f]\{F\}+\{D\}=\{0\}$ for the redundant forces $\{F\}$.

5. Calculate the values of the actions by superposition: $\{A\}=\{A_s\}+[A_u]\{F\}$. These actions are the restrained actions for the overall displacement method, since step 4 enforces zero displacement at the nodes.

The bulk of the computations in the force method come from steps 2 and 3. Since flexibility is a matrix of displacements for unit loadings, the problem boils down to a simple one: given internal forces at every section in the member, calculate the free displacement of the O_1 end assuming that the O_2 end is fixed. Note that the calculation of the internal forces for external loading is not handled here, but is discussed in 4.8.1.

Virtual work is the most suitable method for this undertaking. The principle is fairly straightforward. In a structure with internal strain $\{\varepsilon\}$, a system of displacements $\{D\}$ is desired. If virtual forces $\{F\}$ are applied to the system causing stress $\{\sigma\}$, the work done by the virtual forces $\{F\}$ moving through the displacements $\{D\}$ is equivalent to the strain energy stored by the virtual stress $\{\sigma\}$ moving through the strains $\{\varepsilon\}$. Mathematically (Ghali, Neville, and Brown, 2009),

$$\sum_{i=1}^{n} F_i D_i = \int_v \{\sigma\}^T \{\varepsilon\}\, dv$$

or (4.46)

Virtual work = Virtual strain energy

The strain energy in the beam element is the sum of contributions from six sources: axial strain, two bending strains, two shear strains, and a twisting strain. By making the virtual forces unit values, equation (4.46) becomes

$$D = \int N_u \varepsilon\, dS + \int M_{xu} \psi_x\, dS + \int M_{yu} \psi_y\, dS + \int V_{xu} \gamma_x\, dS + \int V_{yu} \gamma_y\, dS + \int T_u \theta\, dS \quad (4.47)$$

where N_u, etc. are the internal forces due to the virtual load, and ε, ψ, etc. are the strains due to the real loads. The i,jth element of the flexibility matrix, by definition, is equal to the displacement at the ith coordinate due to a unit load acting at the jth coordinate. In this case, the "real" load is the one acting at the jth coordinate, while the "virtual" load is the one placed at the ith coordinate to calculate the displacement there.

The line integrations are carried out over the whole curve. Recall from section 4.4.2 that the differential dS can be transformed into a normal coordinate $d\xi$ to simplify the integration.

Note, however, that information about internal forces and strains is only available at the section nodes. El-Badry (1988) and Ghali, Favre, and El-Badry (2011) both use elastic weights for calculating deflections. This method works well because the shape of both the internal force and strain diagram is often linear or parabolic (though cracking and use of mean strain obviously alters the shape substantially). Furthermore, the differential dS

is simply equal to dx for a straight plane frame element. In the current model, however, the curvature of the beam element distorts the common parabolic shape of the bending moment diagram. Numerical methods can be used to calculate the integrals.

4.6.1 Numerical Integration Schemes

The most efficient form of numerical integration is quadrature. In general,

$$\int_a^b f(x)\,dx = \sum_{i=1}^{n} w_i f(x_i) \tag{4.48}$$

where w_i are the quadrature weights and x_i are the integration points or knots.

Maher (1985) and Debaiky (1997) both employ Gaussian quadrature extensively in their analysis. Gaussian quadrature selects the knots and weights so as to minimize the error in the integration. In general, Gaussian quadrature with n points is exact for polynomials of order 2n-1. This assumes a smooth curve that behaves in a polynomial-like fashion. Additionally, to employ Gaussian quadrature, the integrand must be computable at many different arbitrary points.

By introducing cracking into the equation, this no longer applies. The model gives the strains and stresses at the knots only, and as such, it is advantageous to use these values in computing the integral. A more suitable integration scheme for this is Simpson's rule, which can be adapted from its usual textbook form into one that allows uneven spacing of the knots. Simpson's rule can be expressed in quadrature form as

$$
\begin{aligned}
w_i &= a\left(h_{i+1}\left(2h_i - h_{i+1}\right)\right) \\
w_{i+1} &= a\left(h_i + h_{i+1}\right)^2 \\
w_{i+2} &= a\left(h_i\left(2h_{i+1} - h_i\right)\right)
\end{aligned} \tag{4.49}
$$

where

$$
\begin{aligned}
h_i &= x_{i+1} - x_i \\
h_{i+1} &= x_{i+2} - x_{i+1} \\
a &= \frac{\left(h_i + h_{i+1}\right)}{6h_i h_{i+1}}
\end{aligned} \tag{4.50}
$$

Equations (4.49) and (4.50) need to be repeated and summed for i=0 to n-2. Note that the number of sections must be odd to use Simpson's rule.

In general, the integrals in (4.47) can be calculated as

$$
\int_0^L M_u \psi \, dS = \int_0^1 M_u \psi \frac{dS}{d\xi} d\xi = \int_0^1 M_u \psi \left|t\right| d\xi = \sum_{i=1}^{n} w_i M_u\left(\xi_i\right)\psi\left(\xi_i\right)\left|t\left(\xi_i\right)\right| \tag{4.51}
$$

It is worth noting here that in practice, many members will not have smooth continuous internal force and strain diagrams. A good illustration is a member where bars are suddenly cut off. Whenever there is an abrupt change in section properties, two sections should be added with zero distance between them. The integrations above can be split and carried out on both sides.

4.7 Stiffness Matrix

At the core of structural and finite-element analysis is the stiffness matrix. It represents the effect of deflections on member end forces. Simply put, the $(i,j)^{th}$ element of the stiffness matrix represents the force required at the i^{th} coordinate when the displacement is unity at the j^{th} coordinate and all other displacements are nil.

It is essential to note that calculations for element stiffness are usually done in the element's local coordinate system. As discussed in 4.3.2, however, there is no difference between the element and the structure coordinate systems. The numerical nature of the model allows all of the calculations that follow to be done in a fashion that requires no transformation at the end.

Each row or column of the 12x12 stiffness matrix for the element represents a system of forces in equilibrium. Partition the matrix:

$$[S] = \begin{bmatrix} S_{11} & S_{12} \\ S_{21} & S_{22} \end{bmatrix} \tag{4.52}$$

where S is the 12x12 element stiffness matrix, and each submatrix is 6x6. Ghali, Favre, and El-Badry (2011) show the stiffness matrix as

$$[S] = \begin{bmatrix} [S_{11}] & [S_{11}][R]^T \\ [R][S_{11}] & [R][S_{11}][R]^T \end{bmatrix} \tag{4.53}$$

where $[R] = [R(1,0)]$ from equation (4.31). El-Badry (1988) completed the stiffness matrix using a single matrix transformation:

$$\begin{aligned} \left[S^*\right] &= \left[H\right]^T \left[S_{11}\right]\left[H\right] \\ \left[H\right] &= \begin{bmatrix} 1 & & -1 & & \\ & 1 & & -1 & L \\ & & 1 & & -1 \end{bmatrix} \end{aligned} \tag{4.54}$$

By examining (4.53) and (4.54), it becomes clear that

$$\left[H\right] = \left[\left[I\right] \quad \left[R(1,0)\right]^T\right] \tag{4.55}$$

S_{11} is calculated by inversion of the flexibility matrix. Once the problem is isolated at O_1, the beam becomes a simple cantilever, fixed at O_2 and free at O_1. The flexibility is the inverse of stiffness; the i,j^{th} element is equal to the displacement that occurs at the i^{th} coordinate when a force of unity acts at the j^{th} coordinate. To generate each column of the flexibility matrix for the member, unit loads are applied at each coordinate in turn and the deflection at all others is measured.

The deflection can be calculated using equation (4.47), modified slightly:

$$f_{ij} = \int N_{u_i}\varepsilon_{u_j}\,dS + \int M_{xu_i}\psi_{xu_j}\,dS + \int M_{yu_i}\psi_{yu_j}\,dS + \int V_{xu_i}\gamma_{xu_j}\,dS + \int V_{yu_i}\gamma_{yu_j}\,dS + \int T_{u_i}\theta_{uj}\,dS \tag{4.56}$$

where the unit strains are those resulting from the application of the unit load at j, and the unit internal forces are from the unit load at i.

Calculating the internal force on each section is a simple matter of combining equations (4.31) and (4.23):

$$\left\{F^*\right\}_i = \left[T\right]_i^T \left[R\right]_i \left\{F_u\right\}_i \tag{4.57}$$

Since the vector $\{F_u\}_i$ is simply the i^{th} column of I_6, it is more efficient to use

$$\left[F^*\right] = \left[T\right]_i^T \left[R\right]_i \tag{4.58}$$

where each column of $[F^*]$ represents the internal forces at the section due to the corresponding unit force. Recalling eq. (3.36), the strains can be calculated easily:

$$\left[\varepsilon\right]_m = \left[d\right]_m^{-1} \left[F^*\right] \tag{4.59}$$

Again, $[\varepsilon]_m$ is a 6x6 matrix whose i,j^{th} element is the i^{th} component of strain caused by a unit load applied at the j^{th} coordinate. Combining eqs. (4.56) through (4.59) yields a convenient equation for the flexibility:

$$\begin{aligned}\left[f_{11}\right] &= \int_0^1 \left[R(\xi,0)\right]^T \left[T(\xi)\right] \left[d_m\right]^{-1} \left[T(\xi)\right]^T \left[R(\xi,0)\right] \left|t(\xi)\right| d\xi \\ &= \sum_{i=0}^{n} w_i \left[R(\xi_i,0)\right]^T \left[T(\xi_i)\right] \left[d_m\right]^{-1} \left[T(\xi_i)\right]^T \left[R(\xi_i,0)\right] \left|t(\xi_i)\right|\end{aligned} \tag{4.60}$$

Note that the first two matrices in the integrand are simply the transpose of the product of the transformation matrix and the equilibrating matrix. This works because it will multiply each element in the column of the "virtual" force matrix with each element in

the "real" strain matrix. The mean section stiffness matrix can be replaced with the age-adjusted matrix for time-dependent analysis.

At this stage, the A_u matrix must also be calculated. It can be expressed as

$$\left[A_u\right]=\begin{bmatrix}\left[A_u\right]_1\\ \left[A_u\right]_2\\ \vdots\\ \left[A_u\right]_n\end{bmatrix} \qquad \left[A_u\right]_i=\left[T\left(\xi_i\right)\right]_i^T\left[R\left(\xi_i,0\right)\right]_i\left[f_{11}\right]^{-1} \tag{4.61}$$

In summary, once the flexibility matrix is generated,

$$\left[S\right]=\left[H\right]^T\left[f_{11}\right]^{-1}\left[H\right] \tag{4.62}$$

4.8 Instantaneous Analysis

4.8.1 Instantaneous Fixed-End Forces

The other information necessary in the analysis is the coordinate forces that are equivalent to or restrain the applied loads on the structure. Using the methods outlined in 4.6, it is only necessary to calculate the internal forces at every section due to the applied load with the O_1 end free.

For a point load P applied at ξ_L, there is no internal force at a section if it lies on the O_1 side.

$$\begin{aligned}\left\{F^*\right\}_i &= 0 \text{ if } \xi_i < \xi_L\\ \left\{F^*\right\}_i &= \left[T\left(\xi_i\right)\right]^T\left[R\left(\xi_i,\xi_L\right)\right]\left\{P\right\} \text{ if } \xi_i \geq \xi_L\end{aligned} \tag{4.63}$$

The effects of a distributed load q can be calculated using Gaussian quadrature. In general,

$$\left\{F^*(\xi_0)\right\} = \left[T(\xi_0)\right]^T \int_0^{\xi_0} \left[R(\xi_0,\xi)\right]\left\{q(\xi)\right\}\left|t(\xi)\right| d\xi \tag{4.64}$$

Note that equation (4.64) allows the load q to vary as a function of position along the beam. This is required for non-uniform beams under self-weight, for example.

Once the forces are known in the global coordinate system, it is a simple matter of applying eq. (4.23) to find them locally. If the loads are projected on one of the axes (eg: wind load), the integrations should be done using dx, dy, or dz instead of dS as required. The $t\,d\xi$ in the above equations would be replaced with $x'\,d\xi$, $y'\,d\xi$, or $z'\,d\xi$.

Self-weight is handled tidily with the equations above. The load is a negative z-direction force with intensity at each section equal to $\Sigma\gamma A$, where γ is the unit weight of the part and A is the cross-sectional area (uncracked area for concrete parts).

Equation (4.64) applies for a distributed load applied over the full length of the member. It is a simple matter of changing the integration limits if only a portion of the member is loaded.

Once all of the section forces are known, the deflections can be calculated using the methods outlined in 4.6. More directly,

$$\begin{aligned}\{D_1\} &= \int_0^1 \left[R(\xi,0)\right]^T \left[T(\xi)\right]\left[d_m(\xi)\right]^{-1}\left\{F^*(\xi_i)\right\}\left|t(\xi)\right|d\xi \\ &= \sum_{i=0}^{n} w_i \left[R(\xi_i,0)\right]^T \left[T(\xi_i)\right]\left[d_m(\xi_i)\right]^{-1}\left\{F^*(\xi_i)\right\}\left|t(\xi)\right|\end{aligned} \tag{4.65}$$

The $\{A_s\}$ vector is simply the static values of $\{F^*\}_i$ from (4.65). The $[A_u]$ matrix can be expressed as

$$\left[A_u\right] = \begin{bmatrix} \left[A_u\right]_1 \\ \left[A_u\right]_2 \\ \vdots \\ \left[A_u\right]_n \end{bmatrix} \qquad \left[A_u\right]_i = \left[T(\xi_i)\right]_i^T \left[R(\xi_i,0)\right] \tag{4.66}$$

The final values of the actions represent the internal force in every section in the restrained condition.

4.8.2 Effect of Displacements

Once the fixed-end forces for all of the members are calculated, they are amalgamated at the structure level and the equilibrium equation is solved to yield displacements at each node. It is now necessary to calculate the member-end forces that result, along with the internal forces at the sections (so that the stresses and strains may be calculated).

The member-end forces can be calculated easily (Ghali, Neville, and Brown, 2009):

$$\{A\} = \{A_r\} + [S]\{D\} \tag{4.67}$$

where $[S]$ is the element's stiffness matrix. Again, there is no difference between the local and global stiffness. The restrained member-end forces are equal to the restraining

forces calculated in 4.8.1. Since non-linear analysis is often required to calculate the final effects, it is beneficial to calculate the changes in the member-end and section forces instead. Start with the actions in the restrained state and adjust them as the displacements change. The increment in member-end forces from the first iteration is equal to $[S]\{D\}$; the effect at each section is simply the statical equivalent of the O_1 partition of the force at the section node.

For time-dependent analysis, the procedure is exactly same except that $\left[\overline{S}\right]$ is used instead of $[S]$. In both cases, the final values obtained in the analysis are the change in member-end and section internal forces for the current timestep.

4.8.3 Nonlinearity Caused by Cracking

Once the displacements are calculated and the internal forces determined, it is possible that the stress in the concrete will exceed f_{ct}. The cracking of the section does not just change the stress - it also changes the stiffness. As a result, there may be a redistribution of the internal forces as the structure cracks.

A detailed discussion of nonlinear analysis and the techniques applicable to the model is left to 5.4.

4.9 Time-Dependent Fixed-End Forces

Section 4.8 deals with the calculation of restraining forces resulting from applied external loads on an element. It is also necessary to calculate the forces which are required at the

ends of the element to prevent the displacements that would occur because of creep and shrinkage of concrete and relaxation of prestressing steel.

After the first part of the analysis, the instantaneous strain at each section is calculated. Following the steps of the force method, it is necessary to calculate the O_1 displacements that would occur if free to do so. The "free strains" mentioned here should not be confused with the free strain of concrete; they are the final strains that result from the application of the restraining forces on each section (see 3.9 for details). Once the free strains are known, the corresponding O_1 displacements are

$$\begin{aligned}\left\{\Delta D_f\left(t_{i+1},t_i\right)\right\} &= \int_0^1 \left[R\left(\xi,0\right)\right]^T \left[T\left(\xi\right)\right]\left\{\Delta\varepsilon_f\left(t_{i+1},t_i\right)\right\}\left|t\left(\xi\right)\right| d\xi \\ &= \sum_{j=0}^{n} w_j \left[R\left(\xi_j,0\right)\right]^T \left[T\left(\xi_j\right)\right]\left\{\Delta\varepsilon_f\left(t_{i+1},t_i\right)\right\}\left|t\left(\xi_j\right)\right|\end{aligned} \tag{4.68}$$

Once the O_1 displacements are calculated, the fixed-end forces that develop between t_i and t_{i+1} can be calculated using the force method:

$$\left[\overline{f_{11}}\left(t_{i+1},t_i\right)\right]\left\{\Delta F\left(t_{i+1},t_i\right)\right\} = -\left\{\Delta D_f\left(t_{i+1},t_i\right)\right\} \tag{4.69}$$

where $\left[\overline{f_{11}}\left(t_{i+1},t_i\right)\right]$ is the age-adjusted flexibility matrix, calculated using the method outlined in 4.7. To reiterate,

$$\begin{aligned}\left[\overline{f_{11}}\right] &= \int_0^1 \left[R\left(\xi,0\right)\right]^T \left[T\left(\xi\right)\right]\left[\overline{d}\left(\xi\right)\right]^{-1}\left[T\left(\xi\right)\right]^T \left[R\left(\xi,0\right)\right]\left|t\left(\xi\right)\right| d\xi \\ &= \sum_{j=0}^{n} w_j \left[R\left(\xi,0\right)\right]^T \left[T\left(\xi\right)\right]\left[\overline{d}\left(\xi\right)\right]^{-1}\left[T\left(\xi\right)\right]^T \left[R\left(\xi,0\right)\right]\left|t\left(\xi\right)\right|\end{aligned} \tag{4.70}$$

where $\left[\overline{d}\right]$ is the age-adjusted mean section stiffness matrix for the specified interval.

Prestress relaxation is represented by distributed loads (see 4.5.2). Since the loss is assumed to be uniform along the tendon, $dP/dS = 0$, and only q_n is required in (4.36).

$$\Delta q_{ps} = q_n = \left[R_{ps}\right]\Delta P\{n\} \tag{4.71}$$

For the force method stage of the analysis,

$$\{\Delta A_r\} = \{\Delta A_s\} + \left[A_u\right]\{\Delta F\} \tag{4.72}$$

where $\{\Delta A_s\}$ is zero and $[A_u]$ is defined in (4.66).

Once the nodal displacements are calculated, the change in member end and internal forces can be calculated following the method of 4.8.2, but using $\overline{S}$ instead of S.

4.10 Intermediate Displacements

The method outlined above provides the stress and strain throughout the member given the displacements at the nodes. While the calculation of nodal displacements is discussed in Chapter 5, an important requirement of the calculation is to determine the intermediate displacements in the member.

Ghali, Neville, and Brown (2009) show that when using virtual work to calculate the displacements in a structure, the unit load can be applied on any statically determinate structure and the forces calculated. El-Badry (1988) releases the moments at the ends

and considers the element as a simple beam, then uses the method of elastic weights to calculate intermediate displacements. A similar approach is adopted here. To keep the math consistent with the force vector and stiffness matrix calculations, the released structure will consider the O_1 end free. The member becomes a cantilever, and the goal is to calculate the displacement of and section of the member. Unit loads are applied at the section in question and the familiar integration is carried out. The formulation is very similar to (4.68), except instead of the displacement at $\xi = 0$, intermediate section values are used, and instead of the free strain, the final cumulative mean strain is used.

The matrix of internal forces at any section j from a unit load applied at i is

$$\left[F^*\left(\xi_j\right)\right]_u = \left[T\left(\xi_j\right)\right]^T \left[R\left(\xi_j,\xi_i\right)\right] \tag{4.73}$$

The displacement equation becomes

$$\begin{aligned}\left\{D\left(\xi_i\right)\right\} &= \int_{\xi_i}^{1} \left[R\left(\xi,\xi_i\right)\right]^T \left[T\left(\xi\right)\right]\left\{\varepsilon_m\left(\xi\right)\right\}\left|t\left(\xi\right)\right| d\xi \\ &= \sum_{j=i}^{n} w_j \left[R\left(\xi_j,\xi_i\right)\right]^T \left[T\left(\xi_j\right)\right]\left\{\varepsilon_m\left(\xi_j\right)\right\}\left|t\left(\xi_j\right)\right|\end{aligned} \tag{4.74}$$

Note the integration limits – only the part of the element between and including the section in question and the support need to be included.

What exactly are the displacements that have been calculated above? Obviously, if the O_2 end ($\xi = 1$) is evaluated, the result is zero. These displacements are relative to the displacements of the O_2 end, assuming no rotation at the end. More directly, eq (4.74)

provides the displacements tangent to the member O_2 end. To calculate the total displacements in the global coordinate system, these displacements need to be added to the position the section would be in if there were no strain in the member. This can be calculated using eq (4.23). The final equation for the displacement of any section in the member in the global coordinate system is

$$\{D(\xi_i)\} = -\left[R(1,\xi_i)\right]^T \{D(O_2)\} + \sum_{j=i}^{n} w_j \left[R(\xi_j,\xi_i)\right]^T \left[T(\xi_j)\right] \{\varepsilon_m(\xi_j)\} \left|t(\xi_j)\right| \quad (4.75)$$

4.11 Summary

A contrast was presented between the conventional method of parametric curve representation using Lagrange polynomials and a better approach for certain functions using splines. Spline functions become particularly useful when the number of interpolation points becomes large, such as in continuity prestressing.

A robust formulation for curved members was developed, based on points in space and the orientation of each section's local axes. Simple matrix equations can be used along with numerical integration techniques to determine stiffness and forces throughout the element based on displacements at its ends, external loads, prestressing, and time dependent effects. These equations support the commonly used displacement method of analysis.

With the methods presented in Chapter 3, the element's framework is now complete. The next chapter investigates some nuances of the basic analysis that need to be considered in the modeling of real world structures.

Chapter Five: **ANALYSIS OF A STRUCTURE**

The preceding chapters have all dealt with the analysis of different components of the model. The highest level of analysis is that of the structure, where all of the elements are connected and their interactions are calculated.

The structure is essentially a group of elements. It is also necessary to consider the boundary conditions which govern the structure's response, and the external nodal forces which are applied on it. The first step is to assemble the stiffness matrix for the entire structure. These equations are modified to account for the boundary conditions, and then they are solved for displacements and the reaction components which maintain equilibrium.

Many structural boundary conditions are not simple supports; sometimes a support can be restrained to move along a line or even a plane. If the line or plane is inclined, it is called a skew support. Skew supports require manipulation of the stiffness matrix which is covered in 5.2.1.

While the essence of the displacement method is simple, there are a few aspects of segmental construction which impact the analysis. A section of this chapter is devoted to the consideration of the sequence of construction.

The last part of this chapter presents the model as a numerical procedure and discusses its implementation in a computer program.

5.1 Stiffness Matrix Assembly

The first step in the analysis is to generate the stiffness matrix for each of the structure's elements. This was covered in 4.7. Once all of the matrices have been generated, they must be aggregated to form the structure's stiffness.

The stiffness matrix can be partitioned into submatrices as follows:

$$S = \left[\begin{array}{c|c|c|c} S_{11} & S_{12} & \cdots & S_{1n} \\ \hline S_{21} & S_{22} & \cdots & S_{2n} \\ \hline \vdots & \vdots & \ddots & \vdots \\ \hline S_{n1} & S_{n2} & \cdots & S_{nn} \end{array}\right] \tag{5.1}$$

where n is the number of nodes, and the i,jth partition is a 6x6 submatrix which represents the forces that develop at the ith node as a result of displacements at the jth node.

Recall that the element stiffness matrix is partitioned as well:

$$S_e = \left[\begin{array}{c|c} S_{e_{11}} & S_{e_{12}} \\ \hline S_{e_{21}} & S_{e_{22}} \end{array}\right] \tag{5.2}$$

The structure's i,jth partition can be calculated as

$$S_{ij} = \sum \begin{cases} S_{e_{11}} & n_1 = i = j \\ S_{e_{22}} & n_2 = i = j \\ S_{e_{12}} & n_1 = i, n_2 = j \\ S_{e_{21}} & n_1 = j, n_2 = i \end{cases} \tag{5.3}$$

where n_1 and n_2 are the node numbers of the element in question and the summation is carried out over all elements in the structure. The force vector can be assembled in a similar manner.

The effects of construction schedule on the stiffness are important. It is possible to have large portions of the structure which do not exist at a timestep, and as such, they will have zero stiffness. A row or column of zeros in the stiffness matrix will make it singular and will not allow solution of the system. For this reason, the matrix should be scanned for such problems. If the force vector is also zero, it is acceptable to replace the i^{th} equation with $D_i = 0$; this involves simply replacing the zeroed diagonal in the stiffness matrix with a 1. If, however, the i^{th} element in the force vector is non-zero, there is no solution to the system. This would indicate that force is being applied on part of the structure with no capacity to resist it.

5.2 Boundary Conditions and Reaction Components

The stiffness matrix generated by equation (5.3) is not quite sufficient to analyse the structure as a whole. The elemental stiffness matrix for any valid element is singular; that is, it has a determinant of zero. The assemblage of the elemental matrices is no different; these indicate that the fundamental force-displacement relation, SD=-F, has no solution other than the trivial one. In the real-world sense, there are no actions to resist the applied loads on the structure. The boundary or support conditions for the structure must be accounted for in the equations to complete the analysis.

The unadjusted stiffness matrix and force vector represent a system with n known forces and n unknown displacements. The boundary conditions change the situation at the i^{th} coordinate into a known displacement (c_i) but unknown force (reaction) problem. Ghali, Neville, and Brown (2009) show that the simplest way to change this is to directly change the equations so that the i^{th} equation becomes

$$D_i = c_i \tag{5.4}$$

If this approach is taken, the force vector must be modified as well to reflect the effect of this displacement. The forcing of the displacement to c at coordinate i will apply a force at every other coordinate j equal to $S_{ji}c_i$ (by definition). The restraint of this force will be equal to $-S_{ji}c_i$. The system of equations becomes

$$\begin{array}{c} \\ 1 \\ \\ i \\ \\ n \end{array} \begin{array}{c} \begin{array}{ccccc} 1 & & i & & n \end{array} \\ \begin{bmatrix} & & 0 & & \\ & & \vdots & & \\ 0 & \cdots & 1 & \cdots & 0 \\ & & \vdots & & \\ & & 0 & & \end{bmatrix} \end{array} \begin{Bmatrix} D_1 \\ \vdots \\ D_i \\ \\ D_n \end{Bmatrix} = \begin{Bmatrix} -F_1 - S_{1i}c_i \\ \vdots \\ c_i \\ \vdots \\ -F_n - S_{ni}c_i \end{Bmatrix} \tag{5.5}$$

This method is especially effective because it preserves the banded nature of the equations. It is problematic, however, because it requires manipulation of the stiffness matrix and force vector, and the original values are lost. The matrices must be reconstructed to find the reactions (but this can be accomplished instead by assembling the fixed end forces and subtracting the force vector; see equation (5.8)).

Another very effective method for boundary conditions is to add equations to the system. Bathe (2003) details this approach, which can be used to add any arbitrary restraint condition (not just setting a certain displacement to a prescribed value). In this approach, the system becomes

$$\begin{bmatrix} [S] & [S']^T \\ [S']^T & [0] \end{bmatrix} \begin{Bmatrix} \{D\} \\ \{R\} \end{Bmatrix} = \begin{Bmatrix} -\{F\} \\ \{D\}_0 \end{Bmatrix} \tag{5.6}$$

where $\{D\}_0$ is a mx1 vector of the m prescribed displacements, and $[S']$ is an mxn matrix with all elements zero except for $S_{ij}'=1$ where i is the i^{th} prescribed displacement at the j^{th} node. For example, if a 9 degree-of-freedom problem requires prescribed displacements at the 2^{nd}, 5^{th}, and 6^{th} coordinates, the matrix would be

$$[S'] = \begin{bmatrix} 0 & 1 & 0 & 0 & 0 & 0 & 0 & 0 & 0 \\ 0 & 0 & 0 & 0 & 1 & 0 & 0 & 0 & 0 \\ 0 & 0 & 0 & 0 & 0 & 1 & 0 & 0 & 0 \end{bmatrix} \tag{5.7}$$

The vector $\{R\}$ will contain the forces which are required to maintain equilibrium at the displaced nodes.

This second method is desirable because it preserves the original stiffness matrix, and it directly calculates the reaction forces. It can also be used to add equations that relate displacements at more than one coordinate (eg: $D_2+D_5=1$). It has a very significant drawback, however, in that the banded nature of the system is lost. For smaller systems where banded storage is not a necessity, it is not a significant penalty and is superior.

However, if space is limited or the problem is large, the inefficient storage can make it impractical.

Once the nodal displacements are calculated, the member end forces can be computed using the procedures outlined in 4.8.2. To calculate the reaction components, the basic displacement method relationship is used:

$$\{F\} = \{F_r\} + [S]\{D\} \tag{5.8}$$

$\{F_r\}$ is the force vector from the analysis, and [S] is the stiffness matrix for the structure *before* the boundary conditions are taken into account. The $[S]\{D\}$ term can also be found by assembling the member-end forces for all of the elements in the structure. The final $\{F\}$ vector will be zero everywhere except at the nodes where displacements have been prescribed.

It is important to note that when multiple stages are considered, the prescribed displacements must be set to zero for every stage after the initial displacement. This ensures that the cumulative displacement for all stages is equal to the imposed value. If the condition is removed at some later time, the cumulative reaction must be applied in the reverse direction on the structure (see 5.3.3).

5.2.1 Skew Supports

Many structures have boundary conditions that are not expressed in the nodal coordinate directions. A roller on a bridge support may allow motion at some angle θ to the

coordinate axes. It is essential that modeling of skew supports be included in bridge analysis software. Figure 5.1 shows an example of a skew support.

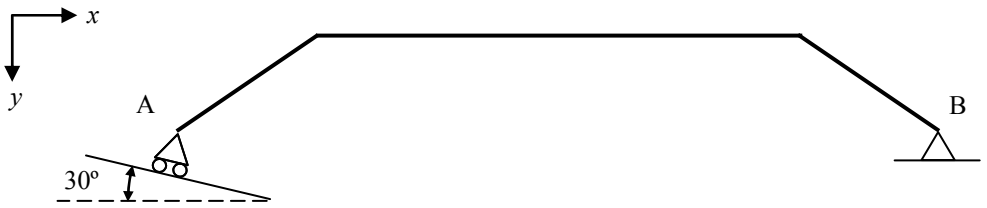

Figure 5.1: Skew Support Example

Support A is confined to move along a 30º angle – or, put differently,

$$D_1 = D_2 \tan 30° \tag{5.9}$$

While this does not prescribe a displacement per se, it adds a single piece of information to the system of equations, which increases the determinacy by one if the system is already determinate (and will increase the rank of stiffness matrix by 1 if it is not). Ghali, Neville, and Brown (2009), present a procedure to relate the displacements at coordinate i and coordinate j by some constant β:

$$D_j = \beta D_i \tag{5.10}$$

The new system of equations becomes

$$\begin{array}{c} \\ 1 \\ i \\ j \\ n \end{array}\begin{array}{c} \begin{array}{cccccc} 1 & & i & & j & n \end{array} \\ \begin{bmatrix} S_{11} & \cdots & S_{1i}+\beta S_{1j} & \cdots 0 & \cdots S_{1n} \\ \vdots & & \vdots & \vdots & \vdots \\ S_{i1}+\beta S_{j1} & \cdots S_{ii}+2\beta S_{ij}+\beta^2 S_{jj} & \cdots 0 & \cdots S_{in} \\ \vdots & & \vdots & \vdots & \vdots \\ 0 & \cdots & 0 & \cdots 1 & \cdots 0 \\ \vdots & & \vdots & \vdots & \vdots \\ S_{n1} & \cdots & S_{ni} & \cdots 0 & \cdots S_{nn} \end{bmatrix} \end{array} \begin{Bmatrix} D_1 \\ \vdots \\ D_i \\ \vdots \\ D_j \\ \vdots \\ D_n \end{Bmatrix} = -\begin{Bmatrix} F_1 \\ \vdots \\ F_i+\beta F_j \\ \vdots \\ 0 \\ \vdots \\ F_n \end{Bmatrix} \quad (5.11)$$

Note that the j[th] equation has been replaced with a dummy equation: $D_j = 0$, which will obviously yield the same in the final displacements. The actual value for D_j can be calculated from (5.10). The skewed boundary condition does not have any effect on the calculation of internal or member-end forces.

To handle supports constrained to a plane instead of a line, the model must handle constraints of the form

$$D_j = \beta_i D_i + \beta_k D_k \quad (5.12)$$

If the support's plane contains one of the principal axes, then one of the β's is zero. If it is orthogonal to one of them, they are both zero, and the constraint takes the familiar form $D_j = 0$.

To handle constraints like (5.12), the equations above are repeated with β_k for the k[th] row and column before the j[th] equation is replaced with the dummy one.

5.3 Segmental Construction

The sequence of construction for complex structures can have a substantial impact on the intermediate and final stresses in a structure. Furthermore, because concrete develops strength with time, it is probable that the stress at some point during construction will exceed that which the structure experiences once it is complete. Most complex structures experience their highest utilization factor during construction.

This section will consider how the analysis must handle the addition of future members, the use of temporary supports or shoring, and how continuity prestressing can be handled.

5.3.1 Incremental Analysis

It is worthwhile to briefly recap the displacement method of analysis. The restraining forces at the coordinates are calculated, the stiffness matrix is composed, and the displacements are calculated by solving the resulting system. The restrained actions are added to those caused by the displacements to find the final effects. These equations are shown below:

$$\begin{aligned} [S]\{D\} &= -\{F\} \\ \{A\} &= \{A_r\} + [A_u]\{D\} \end{aligned} \tag{5.13}$$

This needs to be adjusted slightly for a structure built in stages. Instead, the forces and restrained actions are assembled for each timestep due only to the loading introduced at the stage in question. Next, the stiffness matrix is assembled for parts existing at the

current time. The solution of the system results in the increment of displacement at the current timestep. The modified equations become

$$\begin{aligned} \left[S\right]_i \left\{\Delta D\right\}_i &= -\left\{\Delta F\right\}_i \\ \left\{\Delta A\right\}_i &= \left\{A_r\right\}_i + \left[A_u\right]_i \left\{\Delta D\right\}_i \end{aligned} \tag{5.14}$$

The final values of the displacements and the actions can be obtained by summation.

5.3.2 Member Sequencing

Consider the simple two span bridge shown in Figure 5.2.

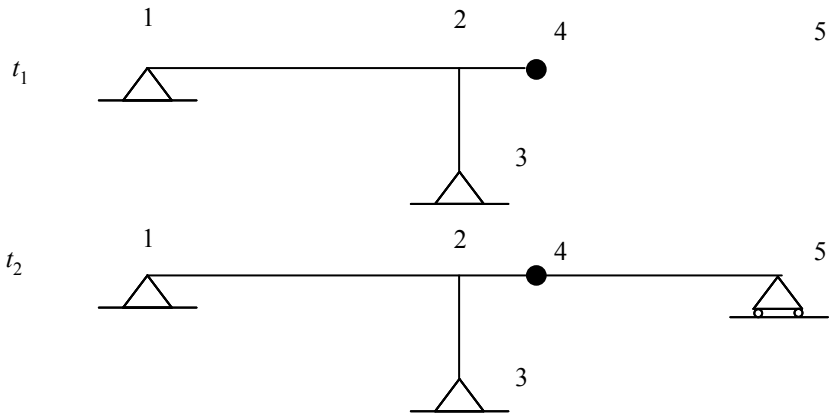

Figure 5.2: Segmentally Constructed Two-span Bridge

This simple structure contains four nodes. The stiffness matrix of the structure at time t_1 is

$$\begin{bmatrix} S_{11} & S_{12} & 0 & 0 & 0 \\ S_{21} & S_{22} & S_{23} & S_{24} & 0 \\ 0 & S_{32} & S_{33} & 0 & 0 \\ 0 & S_{42} & 0 & S_{44} & 0 \\ 0 & 0 & 0 & 0 & 0 \end{bmatrix} \tag{5.15}$$

where S_{ij} represents a 3x3 submatrix.

This presents a problem. Node 5 does not have a member attached to it, and as such is unstable. Two of its three degrees of freedom (horizontal translation and rotation) have no restraint. The final assembled stiffness matrix in this case will be singular; it cannot be inverted.

The most obvious answer to alleviate this problem is to introduce an imaginary restraint at the coordinate in question. In this case, it would be analogous to replacing the roller at coordinate 5 with a fixed support. While this seems like an easy solution, it creates a problem: what if a user has accidentally applied a force at this coordinate? Such an error would normally be detected because the matrix is singular, but the imaginary restraint imposed above would prevent this from occurring.

The answer becomes evident when one examines the system of equations corresponding to the system instead of just the stiffness matrix:

$$\begin{bmatrix} S_{11} & S_{12} & 0 & 0 & 0 \\ S_{21} & S_{22} & S_{23} & S_{24} & 0 \\ 0 & S_{32} & S_{33} & 0 & 0 \\ 0 & S_{42} & 0 & S_{44} & 0 \\ 0 & 0 & 0 & 0 & 0 \end{bmatrix} \begin{Bmatrix} D_1 \\ D_2 \\ D_3 \\ D_4 \\ D_5 \end{Bmatrix} = \begin{Bmatrix} F_1 \\ F_2 \\ F_3 \\ F_4 \\ F_5 \end{Bmatrix} \tag{5.16}$$

The fifth system will be 0 * $D_5 = F_5$. The only way for this to be enforceable is if $F_5 = 0$. Clearly, there must be no force applied in the DOFs that are unsupported for the process to work. An imaginary constraint of $D_5 = 0$ can be applied, but no reaction components should develop. If they do, the analysis should be halted.

5.3.3 Removal of Supports

In many construction sequences, it is possible to have an intermediate system that may be unstable. There may also be cases where temporary support may be necessary to reduce the span in order to protect young concrete. Consider the segmentally built structure shown in Figure 5.3.

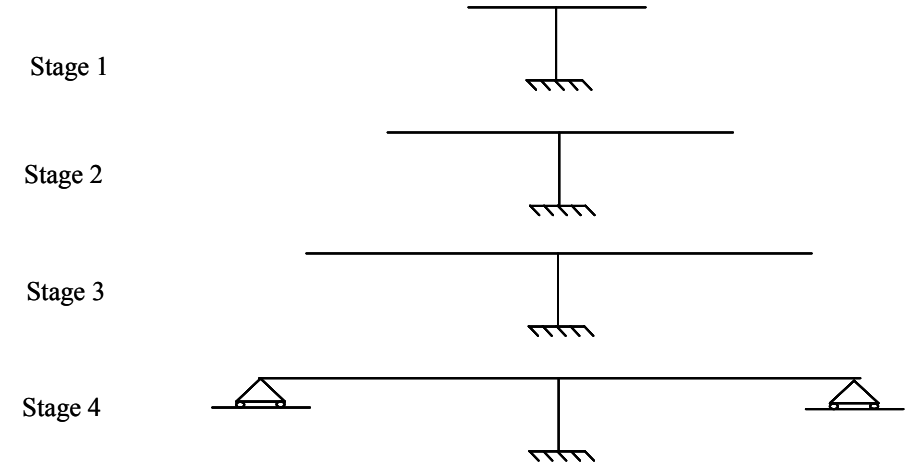

a) balanced launching

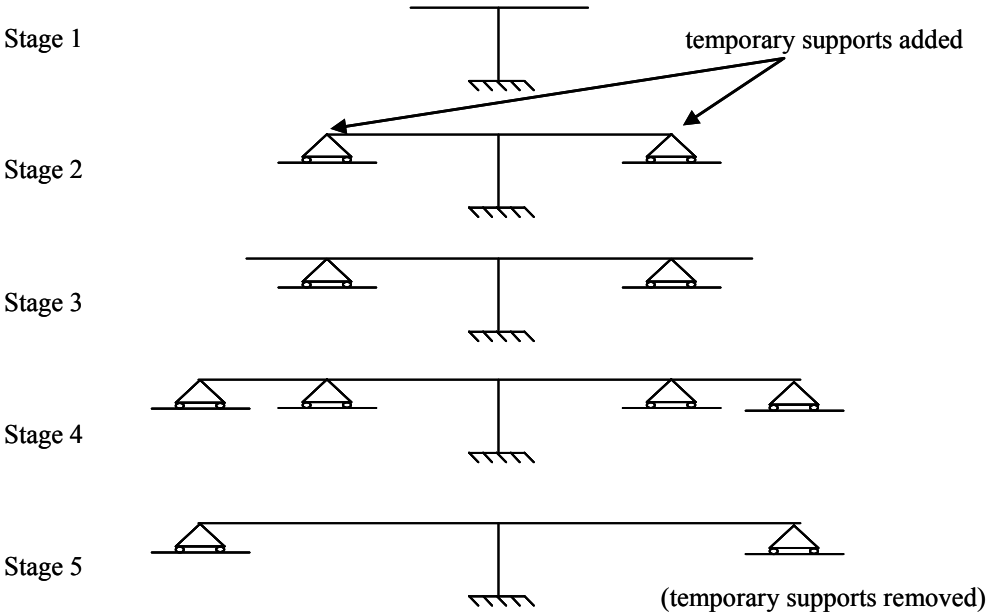

b) using temporary supports

Figure 5.3: Segmentally Constructed Bridge

The bridge in Figure 5.3a is built in four stages and is launched outward from the centre support. The problem with this method is that the negative bending moment over the support becomes very large in the third stage and may in fact cause cracking over the

support. It would be difficult (though not impossible) to apply prestressing in the top of the section to counteract this, but a better solution to the problem is presented in b). By introducing temporary supports, the negative moment over the support decreases. Furthermore, the structure is more efficient as there is less difference between the maximum moment in the span and the negative moment at the support. Once the final supports at the ends of the span are in place, the temporary supports can be removed.

How does the addition and removal of temporary supports affect the analysis? The addition of the supports simply implies boundary conditions (covered in 5.2). The removal of supports is slightly more complicated. Consider stage 4 in Figure 5.3b. The reactions from the temporary supports are exerting a vertical upward force on the bridge. The removal of these supports is equivalent to first removing the boundary conditions from the system, then applying a force equal but opposite to the reaction components exerted by the supports. The new structural system is used for the analysis from this time point on, and the support removal does not affect the displacements or actions from the previous timesteps.

5.3.4 Prestressing Considerations

Perhaps the largest growth in the concrete industry in the past few years has been in the precast section. Many bridge girders are now precast offsite, shipped to the field, and installed in place. This requires much less formwork in place and allows tighter quality control for the concrete.

It is often desirable, however, to set a series of precast girders and then use prestressing cables to make them behave in a continuous manner. This creates a problem because a member can no longer contain a tendon uniquely. To enable continuity prestressing, a tendon must be able to pass through members. This can be accomplished by defining a tendon externally to the member, then indicating where the tendon intersects each section. The profile can then be constructed and the losses calculated. Once the internal force exerted by the cable at each section is known, the actual profile of the cable is no longer relevant to the analysis.

Debaiky (1997) used prestressing tendons as independent members linked at the nodes. This works well because the Jirousek element analysis yields displacements at every node. The method presented here only yields the member end displacements, so the techniques in section 4.5 are used instead.

5.4 Nonlinear Analysis

The basic assumption that underlies the use of displacement or force method is that the displacements that occur at the coordinates are directly proportional to the forces that develop as a result. This applies both at the section and member level. This is obviously not the case; the moment-curvature diagram is not linear but instead follows the mean strain relationship described in section 3.10.

Nonlinearity also develops geometrically; the equilibrium condition may be satisfied in the pre-displacement condition, but in many cases (such as cable-stayed bridges) it is

necessary to consider equilibrium after the nodes have displaced. Geometric nonlinearity is not considered in the current model.

5.4.1 General Solution Techniques

There are several well-documented methods available for solving nonlinear equations. The goal is simple: given a function f(x), find the value x_0 such that $f(x_0) = y_0$ for a given value y_0.

As explained by El-Badry (1988), the solution techniques can be divided into two categories: incremental and direct iterative. Incremental techniques involve splitting the desired value y_0 into slices and solving for each one, then adding up all incremental solutions.

Direct iterative techniques operate with a current approximation for the solution, and recursive formulae are applied to close in on the solution. More iterations generally give more accurate results, though this is not always the case (see section 5.4.3 on convergence).

In the case of structural analysis, the equations relate displacements (the x_i's) and forces (the y_i's). By definition,

$$S_{ij} = \frac{\partial F_i}{\partial D_j} \tag{5.17}$$

The Jacobian for the system is simply the stiffness matrix.

The actual approach used in the model to solve nonlinear problems is a straight-up Newton-Rapshon technique. See the procedures in section 5.6 for how this is implemented. A modified NR approach is often not effective because of the large changes in the stiffness that result from cracking. Incremental techniques are not suitable because of their propensity to accumulate error.

5.4.2 Residual Forces

At the end of each iteration, there is a difference between the force at the current displacement and the desired full force level. This difference represents a force which is out of balance and should be applied on the structure in the next iteration.

This "residual" force results because the displacements at the ends of the member are not compatible with the strains at all of the sections. This will occur if cracking takes place. The goal, then, is to calculate the displacement which would occur at the end of the member if the O_1 end were free, and compare it to the actual displacement that occurred in the real structure. The stiffness matrix can be used to convert these out of balance displacements into residual forces. It is at this juncture that the stiffness matrix is (optionally) recalculated, taking into account the change in section stiffness due to cracking. The procedure for calculating the residual forces for a member is as follows (Ghali, Favre, and El-Badry, 2011):

1. Calculate the total mean strain at each section from the stresses. Take cracking into account. Apply equation (3.34), where ε_1 and ε_2 are the total cumulative strain ignoring and considering cracking, respectively.

2. Integrate the strains to find the corresponding O_1 displacement $\{D\}_s$. This is a 6x1 vector:

$$\begin{aligned}\{D\}_s &= \int_0^1 \left[R(\xi,0)\right]^T \left[T(\xi)\right]\{\varepsilon_m(\xi)\}\left|t(\xi)\right| d\xi \\ &= \sum_{i=0}^{n} w_i \left[R(\xi_i,0)\right]^T \left[T(\xi_i)\right]\{\varepsilon_m(\xi_i)\}\left|t(\xi_i)\right|\end{aligned} \tag{5.18}$$

3. The residual displacement can be found using the following equation:

$$\{D\}_{error} = [H]\{D\} - \{D\}_s \tag{5.19}$$

$\{D\}_{\text{error}}$ is a 6x1 vector representing the out-of-balance displacement at O_1, and $\{D\}$ is a 12x1 vector representing the displacements at the O_1 and O_2 ends in the real structure.

4. Regenerate the stiffness matrix, using the new section properties calculated in step 1. Note that this is an optional step; it is possible, if using the modified Newton-Raphson method, to use the same stiffness throughout the calculations.

5. The residual forces can be calculated using

$$\{F\}_r = [H]^T [S_{11}]\{D\}_{error} \tag{5.20}$$

Since the change in cross-section geometry due to time-dependent effects is neglected in the analysis, no iteration is necessary in that section of the analysis.

5.4.3 Convergence

The conditions at which the analysis is deemed complete for the current timestep are essential to the model. It is sufficient to stop iteration when the magnitude of the residual force drops below some fraction of the originally applied force vector:

$$\left(\{\Delta F\}_i^T \{\Delta F\}_i\right)^{1/2} \leq \alpha \left(\{F\}_0^T \{F\}_0\right)^{1/2} \tag{5.21}$$

Some analysis will have zero applied force but nonzero reactions (prescribed displacements, for example). In these cases, the reactions can be used as a convergence benchmark:

$$\left(\{\Delta F\}_i^T \{\Delta F\}_i\right)^{1/2} \leq \alpha \left(\{R\}^T \{R\}\right)^{1/2} \tag{5.22}$$

Notice that the units of $\{F\}$ are not consistent through the vector. The first through the third have units of force, while the fourth through sixth have units of force-length. This leads to distortion of the convergence calculation. To avoid this problem, the fourth through sixth elements of the force vector should be divided by some arbitrary length. Ghali, Favre, and El-Badry (2011) suggest the longest dimension of the frame. This approach is adopted here.

As discussed in section 3.10, adopting the "smooth cracking" approach greatly improves the convergence of the model. However, there are still problems where the resdistribution of forces from the change in stiffness causes sections to crack. When the stiffness is calculated again using the new properties and the residual forces are applied,

the force on these sections decreases and cracking no longer occurs. It is possible to reach a lockstep where the iterations continue and convergence is not achieved. A numerical example of this is investigated in section 6.1.3.

In these cases, a simple approach to break the lock is to only apply a portion of the residual force for one iteration:

$$\{F\}_r = \theta\left[H\right]^T \left[S_{11}\right]\{D\}_{error} \tag{5.23}$$

If the problem is oscillating symmetrically about the solution, using θ= 0.5 is an acceptable strategy that typically results in convergence. Generally speaking however, using the smooth line on Figure 3.6 provides better results.

It should be carefully noted that in large structures convergence may be reached for the structure though an individual element may still have considerable residual force. For this reason it is prudent to carry forward any remaining residual force to the next iteration. This approach allows for slightly higher error tolerance. It also picks up any difference in cracking caused by time dependent effects.

5.5 Algorithm

The algorithm for analysis is summarized below:

5.5.1 Instantaneous Effects

1. Generate member stiffnesses
    a. Generate [f_{11}] with O_1 end free and invert to get [S_{11}]

b. $[S^*] = [H]^T[S_{11}][H]$

2. Generate loads from prestressing added at this time
3. Generate fixed end forces
    a. Apply loads on member with O_1 end free
        i. Calculate force at each section
        ii. Calculate strain at each section
        iii. Integrate strains to get displacement $\{D^*_s\}$ at O_1
    b. $\{A_r\}_{O1} = -[S_{11}]\{D^*_s\}$
    c. $\{F_s\}$ = static effect of load at O_2
    d. $\{A_r\}_{O2} = [R]\{A_r\}_{O1} - \{F_s\}$
4. Assemble stiffness matrix
5. Account for boundary conditions
6. Assemble fixed end forces
7. Solve system $[S]\{D\}=-\{F\}$
8. Solve actions in each member $\{A\}=\{A_r\}+[S^*]\{D^*\}$
9. Update $\{D\}$ and $\{A\}$
10. Find internal forces at each section from $\{A\}$
    a. Calculate stresses
11. Calculate strain at each section
    a. Check for cracking and update properties accordingly
12. Integrate strains to get free end displacement $\{D^*_s\}$
13. Calculate displacement error $\{D^*\}_{err} = [H]\{D^*\}-\{D^*_s\}$
14. Recalculate stiffness based on new strains
15. Calculate residual force $\{A\}_{res} = [H]^T[S_{11}]\{D^*\}_{err}$

16. Assemble $\{A\}_{res}$ to get $\{F\}_{res}$
17. Check for convergence $(\{F\}^T\{F\})^{1/2} < \alpha(\{F_0\}^T\{F_0\})$, stop or goto 4

5.5.2 Time-Dependent Analysis

1. Generate member stiffnesses
2. Generate distributed loads from prestress loss
3. Generate fixed-end forces
    a. Calculate internal force at every section with O_1 end free
    b. Calculate free strain at each section and integrate to get $\{D^*_s\}$ at O_1
    a. $\{A_r\}_{O1} = -[\bar{S}_{11}]\{D^*_s\}$
    b. $\{F_s\}$ = static effect of load at O_2
    c. $\{A_r\}_{O2} = [R]\{A_r\}_{O1} - \{F_s\}$
4. Assemble stiffness matrix
5. Account for boundary conditions
6. Assemble fixed end forces
7. Solve system $[S]\{D\}=-\{F\}$
8. Solve actions in each member $\{A\}=\{A_r\}+[S^*]\{D^*\}$
9. Update $\{D\}$ and $\{A\}$
10. Find internal forces at each section from $\{A\}$
    d. Calculate stresses
11. Calculate strain at each section, and subtract free strain
    c. Calculate stresses

5.6 Numerical Procedure and Computer Program

With all of the pieces in place, the framework for a computer program can be presented. The flowchart for the developed model is shown in Figure 5.4. The member loops for stiffness and fixed end force generation are Loop A and C. The member loop for the calculation of stress and strain at each section are Loop B. Flowcharts for each loop are shown in Figure 5.5.

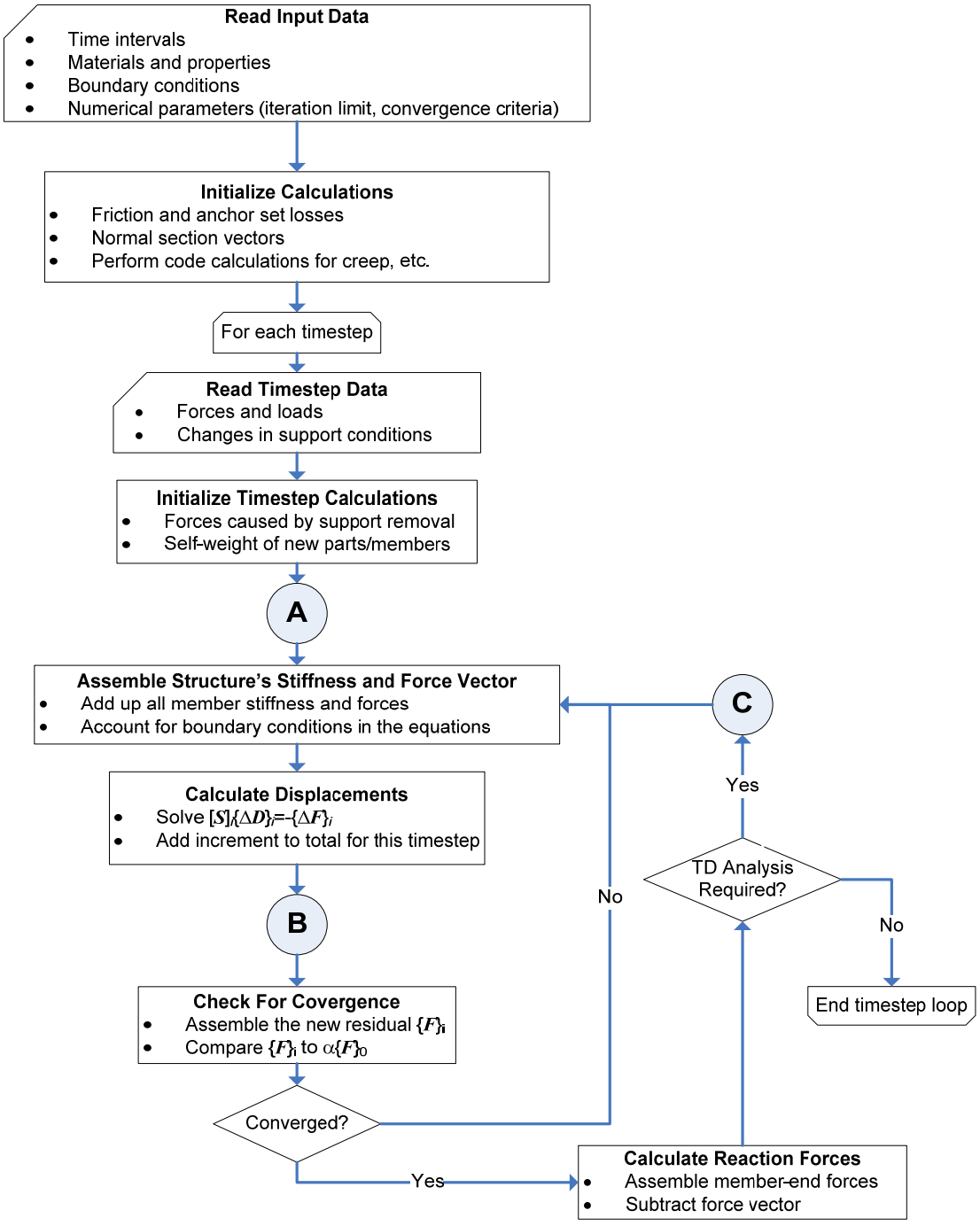

Figure 5.4: Program Flowchart

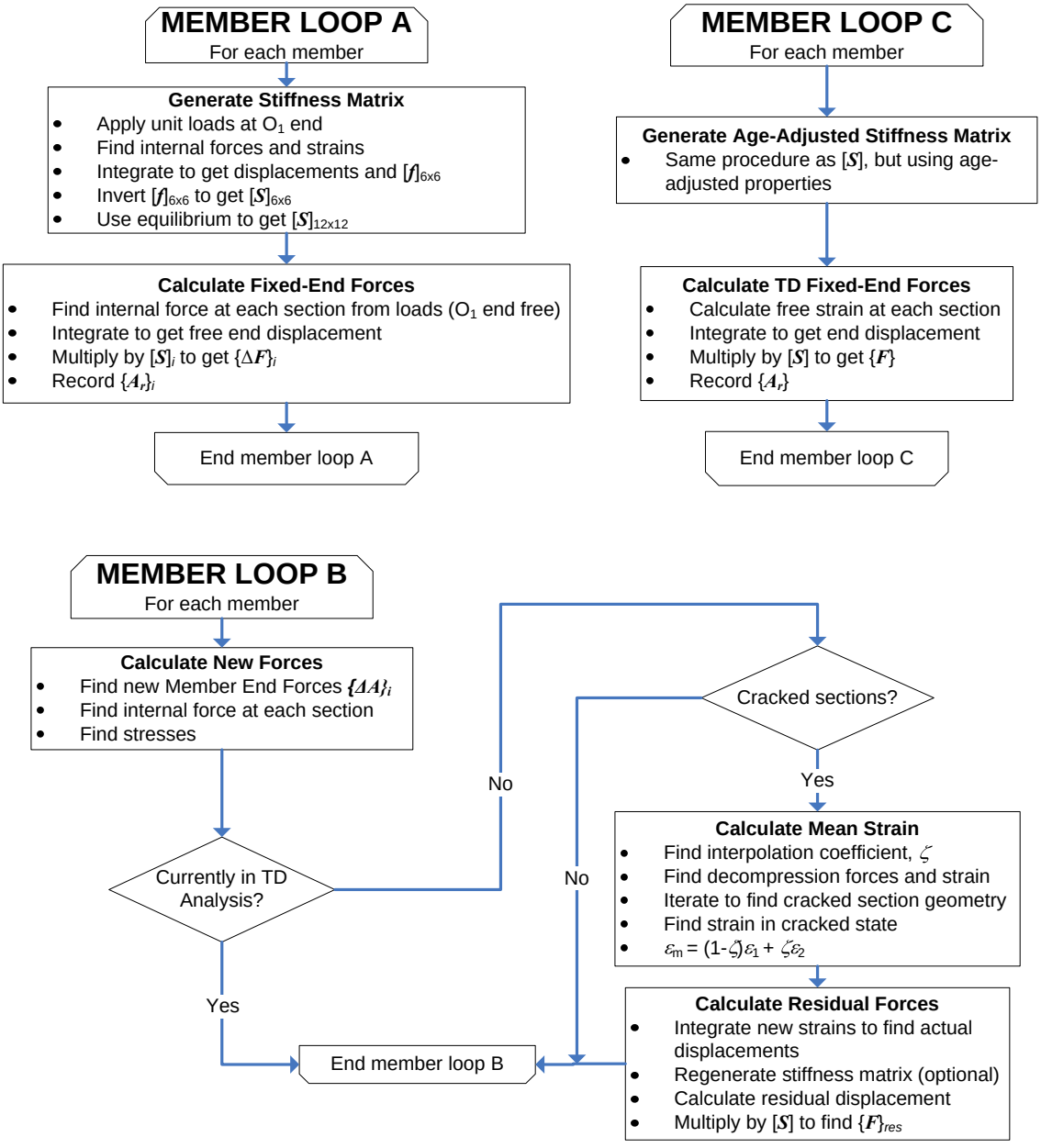

Figure 5.5: Program Flowchart for Loops

5.7 Program Input and Output

To demonstrate the simplicity of the model, a summary of the required inputs is included below. Additionally, a summary of the output is provided.

5.7.1 Input Data Requirements

The required input data for the program is summarized below.

1. PROGRAM DEFINITIONS

- Number of intervals for analysis
- Tolerance for convergence during non-linear analysis
- Maximum number of iterations during non-linear analysis
- Interpolation coefficient β
- Flag to use "smooth" cracking ($\beta^{0.5} f_{ct}$)
- Flag to print the stress at every point in the cross section or only min/max
- Direction vector for self weight calculations
- Flag to calculate properties using code equations or to use provided values
- If code equations are used:
    - Time in days of each timestep
    - Relative humidity

2. MATERIAL PROPERTIES

- Concrete properties, one set for each type being used
    - Timestep of introduction
    - Poisson's ratio, ν
    - Unit density for self-weight calculations
    - For code calculation:
        - Age at first loading (in days)
        - Characteristic strength (in MPa)
        - Notional thickness (in mm)
    - For user-defined values:
        - E, f_{ct}, xi, ε_{cs}, and ϕ for each timestep or interval
- Non-prestressed steel properties

    - E_{ns}
- Prestressed steel properties
    - Time of introduction
    - E_{ps}
    - μ, k, d
    - For code calculation:
        - Total intrinsic loss
    - For user-defined values:
        - Reduced relaxation in each interval

3. SECTION DATA

- For each section, number of concrete parts, and for each concrete part:
    - Material type from material data
    - List of points (y,z) defining cross section geometry
    - α_y, α_z, reduction factors for shear area
    - (y_s, z_s), location of shear center
    - J, torsion constant
- For each section, number of steel parts, and for each steel part:
    - Material type from material data
    - Flag for whether bar or not
    - For bars:
        - (y_{ns}, z_{ns}), specific location
        - A_{ns}, area of steel
    - For "smeared" or ratio reinforcement:
        - Concrete part for reference
        - ρ_{ns}, reinforcing ratio (A_{ns}/A_c)

4. STRUCTURAL GEOMETRY

- Number of nodes, and for each node:
    - Number for reference
    - (x, y, z), location in space of the node

5. MEMBER DATA

- Number of members, and for each member:
    - Member number for reference
    - Number of sections
    - For each section:

        - ξ, parameter value at section
        - Node number for section from structural geometry
        - Value of phi angle for section orientation
        - Section number from section data

6. TENDON DATA

- Number of tendons, and for each tendon:
    - Number for reference
    - Material from material data
    - A_{ps}, A_{duct}
    - Timestep of bonding
    - Number of members tendon passes through
    - List of members tendon passes through
    - Type of parametric curve to use (spline or Lagrange)
    - Number of control points on tendon, and for each point:
        - ξ, parametric variable
        - (y_{ps}, z_{ps}) location of tendon at that point
    - Number of jacking timesteps, and for each timestep:
        - Time of jacking
        - Jacking force
        - Whether jacked from O_1, O_2, or both ends

7. LOADING DATA

- For each timestep, number of loads, and for each load:
    - Type, whether nodal, point load, or varying distributed load
    - For nodal loads:
        - Node number
        - 6 element vector for load
    - For member point loads:
        - Member number
        - ξ, parametric variable where load acts
        - 6 element vector for load
    - For distributed loads:
        - Member number
        - Direction of applied load
        - Constant value, or list of ξ points with value at each

8. BOUNDARY CONDITIONS

- Number of fixed supports, and for each support:
  - Starting timestep
  - Ending timestep, or -1 for permanent support
  - Node number
  - 6 sets of values, either 1 for free, or 0 and another number for prescribed displacement
- Number of skewed supports, and for each skew:
  - Starting timestep
  - Ending timestep, or -1 for permanent support
  - Node number
  - Slave degree of freedom (1-6)
  - β_1, ratio of slave to master displacement, and master degree of freedom
  - β_2, ratio of slave to master displacement, and master degree of freedom

5.7.2 Summary of Program Output

The following information is produced in two formats: first, a narrative showing salient values for each timestep, and second, a tabular format with the changes in and cumulative values at the end of each timestep.

1. **Nodal displacements for each connected node**
2. **Reaction forces at each supported node**
3. **Member end forces for each member**
4. **Internal forces at each section in each member**
5. **Strains at each section in each member, for cracked, uncracked, and mean state**
6. **Displacements at each section in each member**
7. **Stress at each point in each concrete section part**

8. **Stress in each bar of non-prestressed steel, or stress vector for smeared reinforcing**
9. **Stress in each prestressing tendon**

5.8 Summary

This chapter has summarized the analysis required at the aggregated structure level. It includes considerations for segmental construction and non-linear analysis techniques. Together with the material in the previous chapters, it completes the formulation for a method for serviceability analysis of instantaneous and time dependent effects in concrete structures. The next chapter includes a comparison to problems solved with other techniques, and some demonstration of the model's capability.

Chapter Six: **VERIFICATION AND DEMONSTRATION EXAMPLES**

This chapter contains several numerical problems. The first section is concerned with the verification of element behaviour, and there is quantified discussion about the quality of the modeling. The latter half of the chapter contains a demonstration of the capabilities of the model.

Any new model must be verified before it can be used on full-scale problems. This chapter contains examples for which either simple closed-form solutions or computer analysis is available to verify that the model works as it should. It is also important to test problems which the model is known to solve to ensure that the computer programming is sound.

Once the verification is complete, the program is used to demonstrate capabilities on a complex multi-stage real world structure under real design code requirements.

6.1 Verification Examples

6.1.1 Curved Cantilever

Maher (1985) developed a method to minimize the internal forces in a structure by optimizing the prestressing. To demonstrate the method, he presented the following bridge:

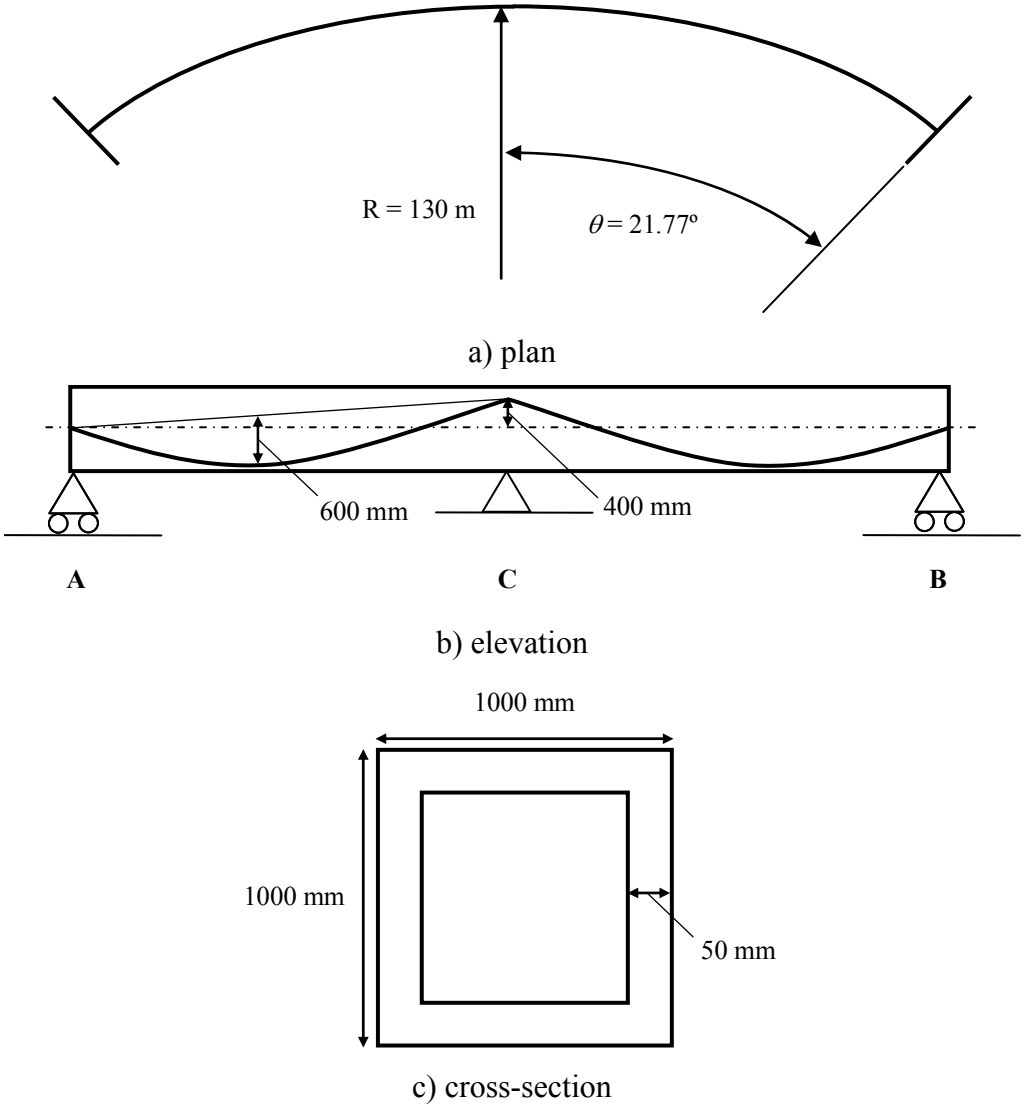

Figure 6.1: Maher's Curved Cantilever

Due to symmetry, only one span requires analysis.

The bridge is subjected to its self weight (1.967 kN/m) and prestressing (P = 1.0 MN). The torsional stiffness ratio, EI/GJ = 1.595. Anchor set and friction losses are neglected.

Maher used two elements each with 6 nodes. For verification, a single 11 node element is used here.

Maher analysed the prestressing and dead load cases separately and compared the results to commercially available software. The same presentation is used here. The bending and twisting moment diagrams are shown in Figure 6.2. Numeric results are presented for the midspan and support locations in Table 6.1.

Table 6.1: Internal Forces for Verification Example 1

	Dead Load Only			
	Bending (M_y*, kNm)		Torsion (M_x*, kNm)	
	Ford	Maher	Ford	Maher
Support A (ξ=0)	-608.1	-610.4	0.94	1.00
Midspan (ξ=0.5)	297.3	298.4	-9.67	-9.73
Support B (ξ=1.0)	0.0	0.0	37.66	37.80

	Prestressing Only			
	Bending (M_y*, kNm)		Torsion (M_x*, kNm)	
	Ford	Maher	Ford	Maher
Support A (ξ=0)	597.1	597.2	-25.32	-25.36
Midspan (ξ=0.5)	-299.2	-299.2	3.14	3.14
Support B (ξ=1.0)	0.0	0.0	12.75	12.74

	Combined (DL+PS)			
	Bending (M_y*, kNm)		Torsion (M_x*, kNm)	
	Ford	Maher	Ford	Maher
Support A (ξ=0)	-10.95	-13.25	-24.38	-24.36
Midspan (ξ=0.5)	-1.88	-0.81	-6.52	-6.59
Support B (ξ=1.0)	0.0	0.0	50.40	50.54

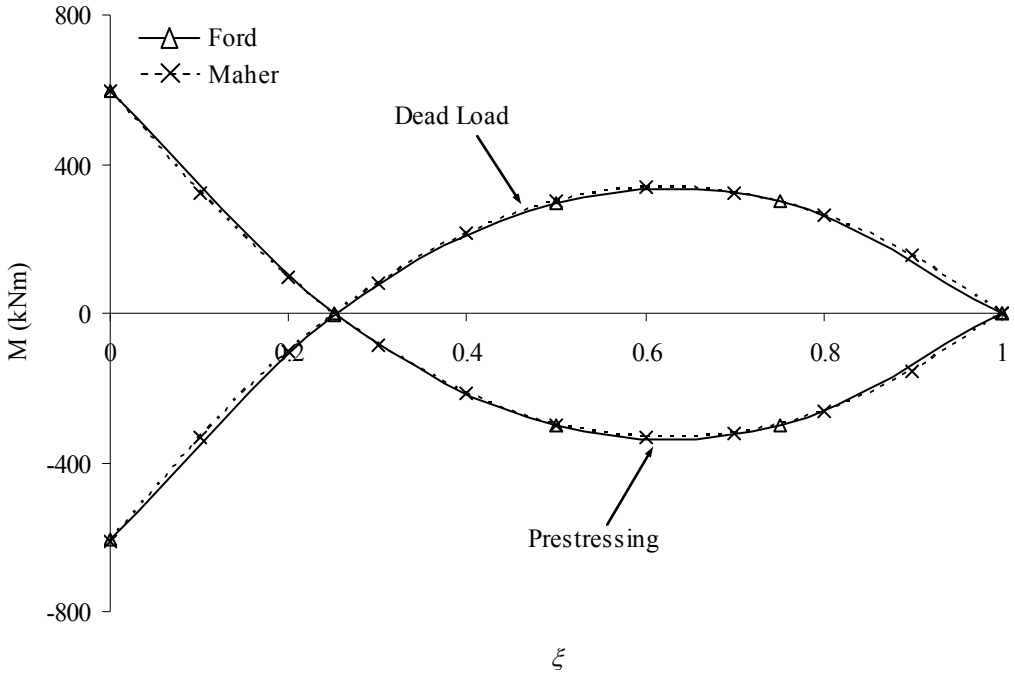

a) Bending (M_y*)

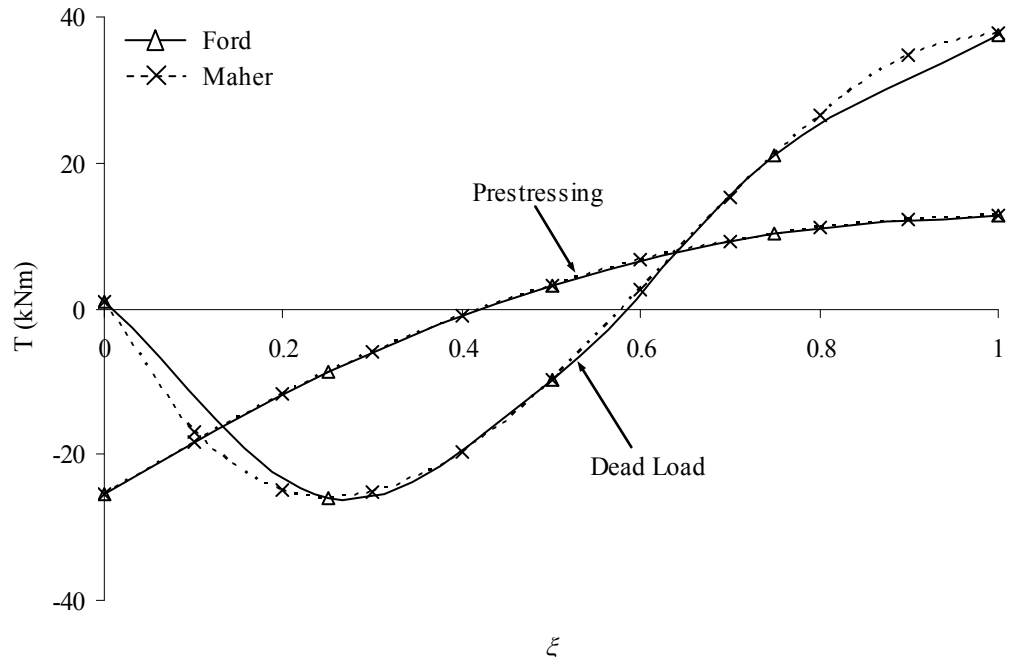

b) Torsion (M_x*)

Figure 6.2: Internal Force Diagrams for Verification Example 1

The combined results are also presented to demonstrate a fundamental catch-22 in curved prestress design: while the bending moments from prestressing counteract the dead load moments, the torsion is magnified in some parts of the beam. The combined internal force diagrams are shown in Figure 6.3.

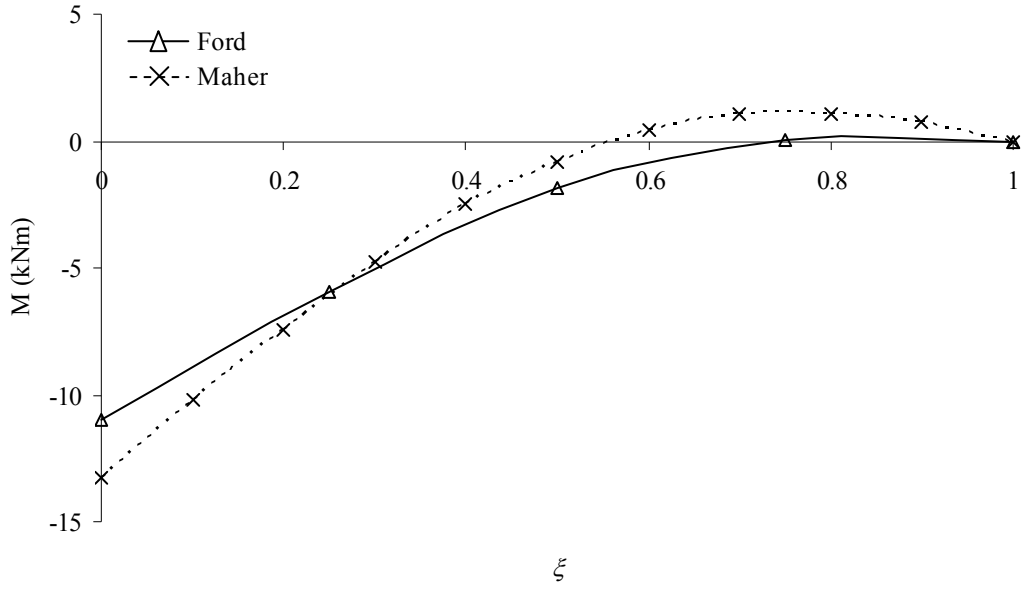

a) Bending (M_y*) – all moments in kNm

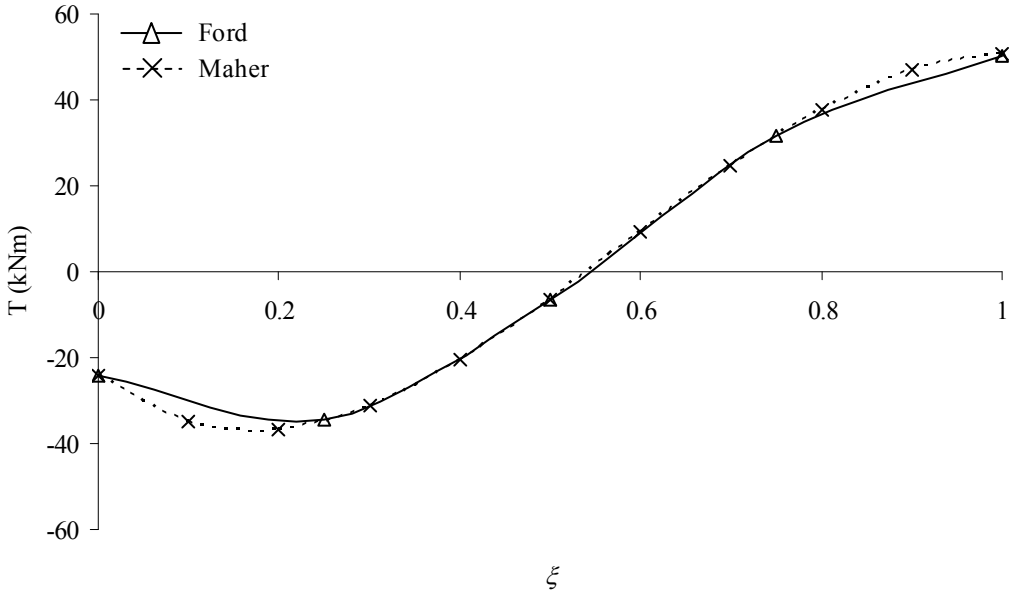

b) Torsion (M_x*) – all moments in kNm

Figure 6.3: Combined Moment Diagrams for Verification Example 1

The above example shows that despite excellent correlation for the individual load cases (well under 1% difference), the superposition of the forces results in a nearly 20% difference in the bending moment at the support. While this may initially seem like a large difference, the normal force on the section will reduce the difference in axial stresses. In fact, Maher's larger bending moment gives 5.49MPa, while the result from this formulation is 5.45MPa (a difference of less than 1%).

El-Badry (2008) presented closed form solutions for curved structures, beginning with the Maher bridge as a cantilever fixed at end B and free at end C. Closed form equations for the displacements at C under the effect of dead load only are presented. They are tabulated in Table 6.2 against the results from the model analysis.

Table 6.2: Displacements for Verification Example 1

	Closed Form	Closed Form	Ford	Error
D_z (mm)	$-0.00274\frac{qr^4}{EI}$	-293	-291	0.7%
$\theta_{x*}(10^3$ rad)	$-0.00129\frac{qr^3}{EI}$	-1.06	-1.05	0.8%
$\theta_{y*}(10^3$ rad)	$-0.00944\frac{qr^3}{EI}$	-7.78	-7.74	0.5%

The analysis is extended to consider the effect of fixing support C at some later time t_1 and calculating the effects between t_1 and some later time t_2.

El-Badry (2005) shows that for a curved cantilever of with radius r and included angle α with both ends fixed and loaded with a uniform load q, the internal forces at any angle β

$$\begin{aligned} M_0 &= -qr^2\left(1-\gamma\cos\left(\beta-\frac{\alpha}{2}\right)\right) \\ T_0 &= -qr^2\left(\beta-\frac{\alpha}{2}-\gamma\sin\left(\beta-\frac{\alpha}{2}\right)\right) \end{aligned} \tag{6.1}$$

where

$$\gamma = \frac{4(1+k)\sin\frac{\alpha}{2}-2k\alpha\cos\frac{\alpha}{2}}{a(1+k)+(1-k)\sin\alpha} \tag{6.2}$$

and

$$k = \frac{EI}{GJ} \tag{6.3}$$

Furthermore,

$$\{\Delta F(t_2,t_1)\} = \frac{\phi(t_2,t_0)-\phi(t_1,t_0)}{1+\chi\phi(t_2,t_1)}\{F\} \tag{6.4}$$

where {F} is the force that would have developed if end C were totally fixed when the load was applied. A comparison between the forces at C between t_1 and t_2 is presented in below.

Table 6.3: Time Dependent Effects for Verification Example 1

	Closed Form	Ford	Error
Q_z (kN)	143	143	0.0%
M_{x*} (MNm)	-1.20	-1.20	0.0%
M_{x*} (kNm)	-1.44	-1.45	0.6%

The results are excellent and demonstrate that for typical elements, the model behaves exactly as it should (even with a limited number of nodes).

6.1.2 Semicircular Beam

Hassoun and Al-Manaseer (2008) included a section on the design of beams curved in plan. The formulation begins with a semicircular beam fixed at each end under the effect of self weight, and includes an additional analysis where a one-way slab spans between the beam and another support connecting the fixed ends. Figure 6.4 shows the configuration.

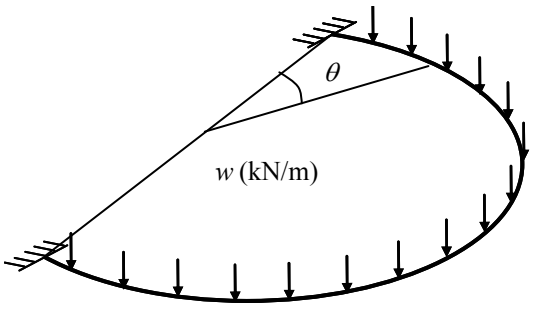

a) Case 1: self weight only

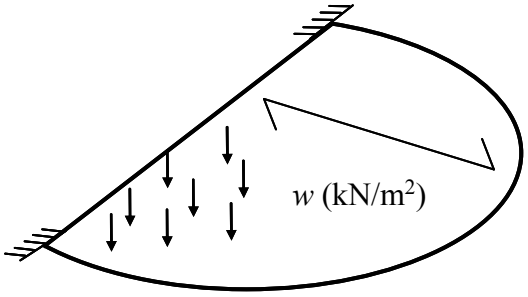

b) Case 2: slab weight only (one-way action)

Figure 6.4: Semicircular Beam Fixed at Both Ends

For this comparison, a single member was used with 9 nodes. The authors presented closed form equations for the bending moment and torsion at any section.

Under self weight:

$$M_N = wr^2\left(\frac{4}{\pi}\sin\theta - 1\right)$$
$$T_N = wr^2\left(\theta - \frac{\pi}{2} + \frac{4}{\pi}\cos\theta\right) \quad (6.5)$$

Under a distributed area load:

$$M_N = wr^3\left(\frac{\pi}{8}\sin\theta - \frac{1}{6}\left(1+\cos^2\theta\right) + \frac{4}{\pi}\left(\frac{2}{9}-\frac{\pi^2}{32}\right)\sin\theta\right)$$
$$T_N = wr^3\left(\frac{\pi}{8}\left(\cos\theta - 1\right) + \frac{\theta}{4} + \frac{1}{24}\sin 2\theta + \frac{4}{\pi}\left(\frac{2}{9}-\frac{\pi^2}{32}\right)\cos\theta\right) \quad (6.6)$$

A dimensionless comparison between these closed form equations and the numerical results from the model run are indicated below:

Table 6.4: Comparison to Closed Form Equations

	Case 1 Self-weight (w kN/m)				Case 2 Slab load (w kN/m^2)			
	Bending (M/wr^2 x1000)		Torsion (T/wr^2 x1000)		Bending (M/wr^3 x1000)		Torsion (T/wr^3 x1000)	
s/L	CF	Ford	CF	Ford	CF	Ford	CF	Ford
0	-1000	-1000	298	299	-333	-333	110	110
0.25	-100	-100	-115	-115	-50	-50	-45	-45
0.5	273	273	0	0	116	116	0	0
0.75	-100	-100	115	115	-50	-50	45	45
1	-1000	-1000	-298	-299	-333	-333	-110	-110

The correlation between the results is exceptional for both cases. Bending and torsion moment diagrams for both cases are shown below.

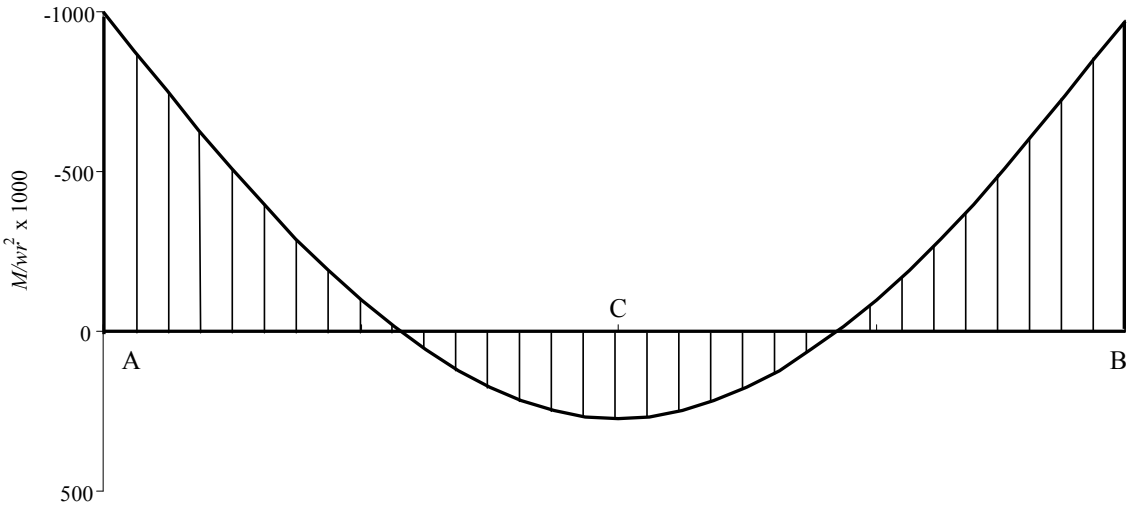

a) Bending Moment Diagram

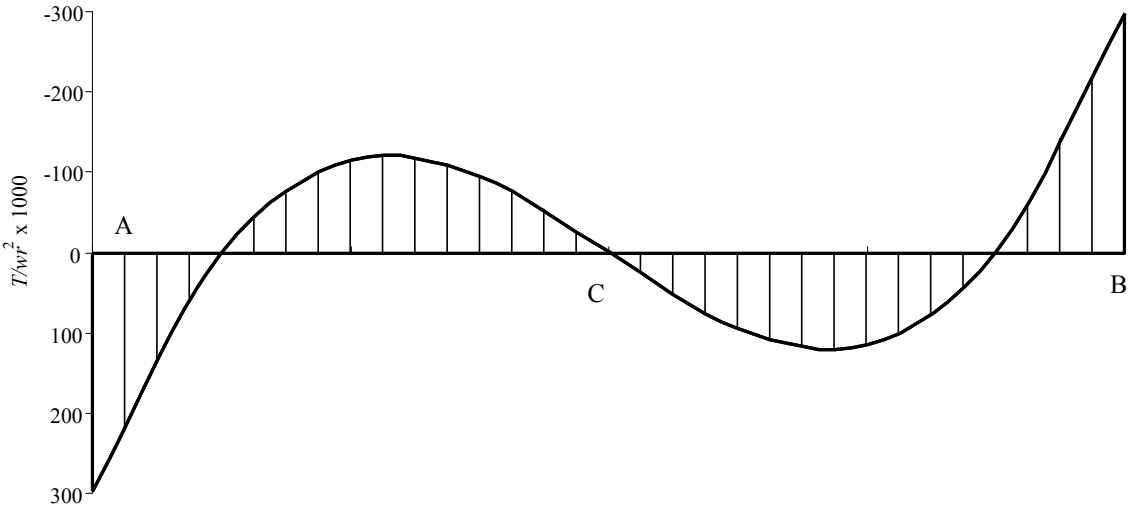

b) Torsion Moment Diagram

Figure 6.5: Internal Forces for Semicircular Beam Under Self Weight

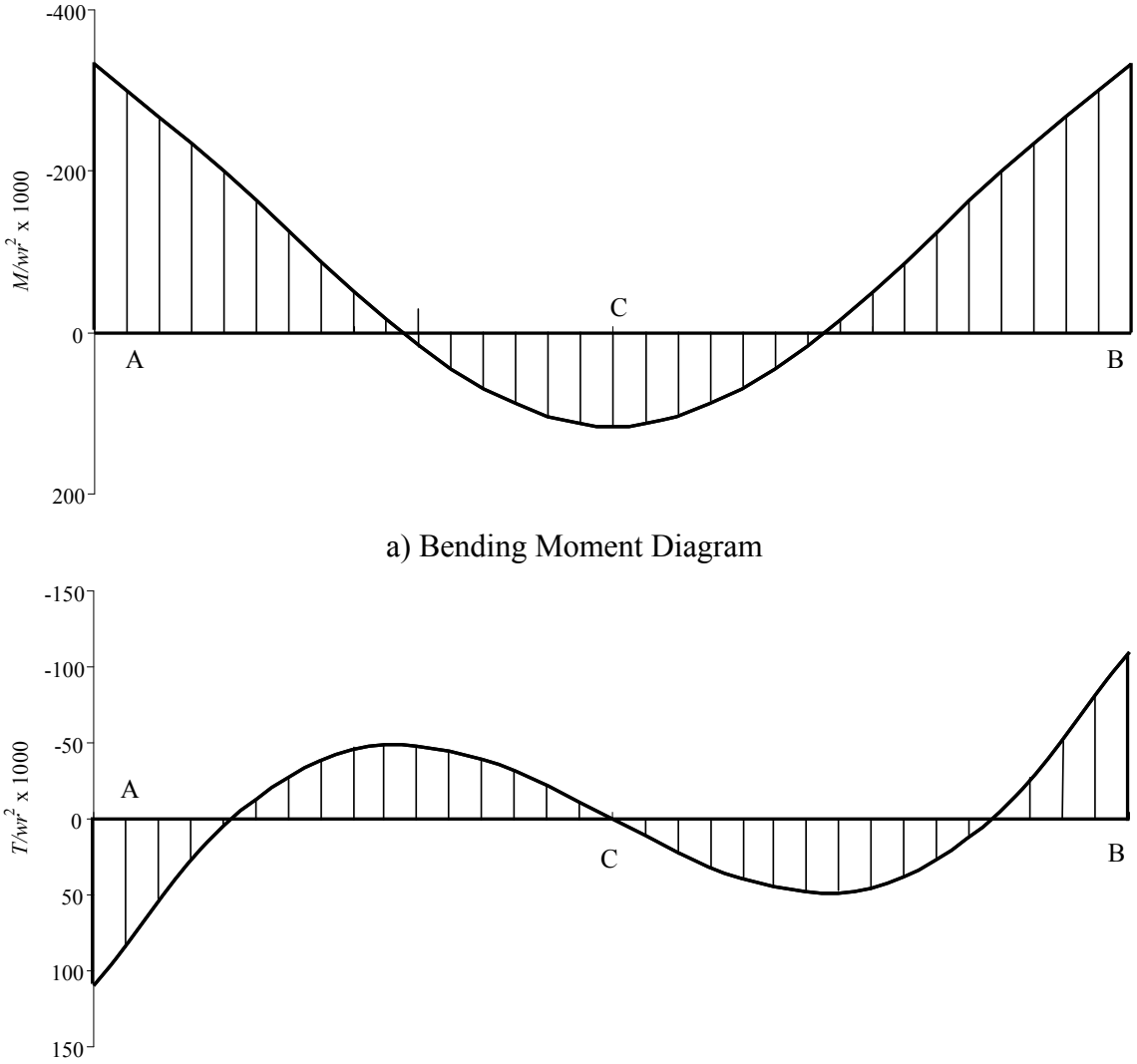

a) Bending Moment Diagram

b) Torsion Moment Diagram

Figure 6.6: Internal Forces for Semicircular Beam Under Slab Weight

6.1.3 Propped Cantilever

Ghali, Favre, and El-Badry (2011) analysed a simple cantilever propped at the end with a point load applied at midspan. Using iterative analysis, a solution is found to converge. The problem is illustrated below.

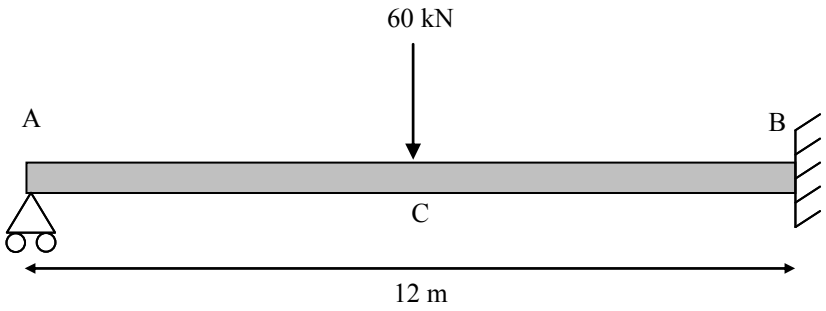

a) profile

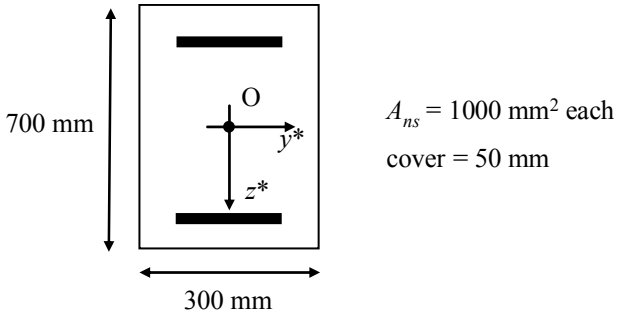

b) section

Figure 6.7: Ghali's Propped Cantilever

To ensure adequate coverage during cracking, 2 members with 6 points each are used. The results of an elastic analysis of the beam are shown in Figure 6.8. The elastic rotation at end A is 0.938 x 10^{-3} rad and the midspan displacement is 3.28 mm.

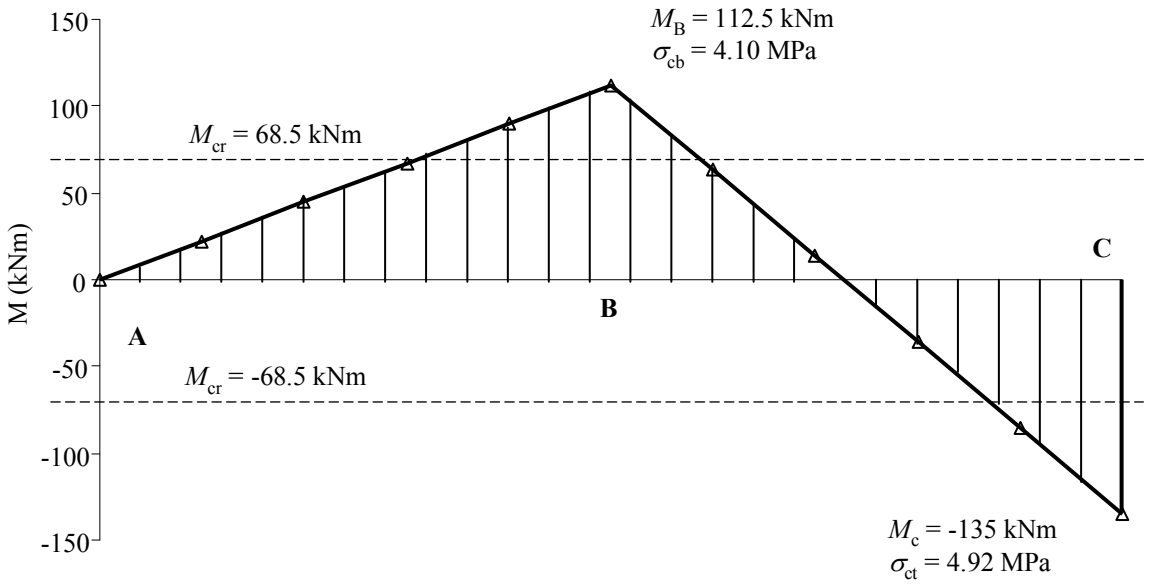

Figure 6.8: Elastic Analysis of Propped Cantilever

As indicated in the figure, the load causes cracking at both the midspan of the beam and at the support B. For the given cross section and properties, $I_t = 9.595 \times 10^9$ mm^4 and M_{cr} = 68.5 kNm. The table below shows the moment distribution in the beam and the relationship to M_{cr}.

Table 6.5: Results from 1st Iteration

Section	**1**	**2**	**3**	**4**	**5**	**6**	**7**	**8**	**9**	**10**	**11**
$\xi = x/L$	**0**	**0.1**	**0.2**	**0.3**	**0.4**	**0.5**	**0.6**	**0.7**	**0.8**	**0.9**	**1.0**
M (kNm)	0	22.5	45	67.5	90	112.5	63	13.5	-36	-85.5	-135
σ_{cb} (MPa)	0	0.82	1.64	2.46	3.28	4.10	2.30	0.49	-1.31	-3.12	-4.92
ζ	0.000	0.000	0.000	0.485	0.710	0.814	0.408	0.000	0.000	0.679	0.871
y_t (mm)	-350.0	-350.0	-350.0	-350.0	-350.0	-350.0	-350.0	-350.0	-350.0	196.4	196.4
y_b (mm)	350.0	350.0	350.0	-196.4	-196.4	-196.4	-196.4	350.0	350.0	350.0	350.0
ε_{01} ($\mu\varepsilon$)	0.0	0.0	0.0	0.0	0.0	0.0	0.0	0.0	0.0	0.0	0.0
ψ_1 ($\mu\varepsilon$/mm)	0.00	0.08	0.16	0.23	0.31	0.39	0.22	0.05	-0.13	-0.30	-0.47
ε_{02} ($\mu\varepsilon$)	0.0	0.0	0.0	230.4	307.2	384.0	215.0	0.0	0.0	291.8	460.8
ψ_2 ($\mu\varepsilon$/mm)	0.00	0.08	0.16	1.10	1.46	1.83	1.02	0.05	-0.13	-1.39	-2.19
ε_{0m} ($\mu\varepsilon$)	0.0	0.0	0.0	111.6	218.1	312.7	87.8	0.0	0.0	198.1	401.4
ψ_m ($\mu\varepsilon$/mm)	0.00	0.08	0.16	0.65	1.13	1.56	0.55	0.05	-0.13	-1.04	-1.97

Note that cracking has occurred in sections 4 through 7 and 10 and 11 as shaded above. Notice that the interpolation coefficient, ζ, is being carried for sections 4 and 7 even though it is less than 0.5. This ensures smooth convergence. However, for the purposes of comparison, the integrations below are carried out ignoring cracking at sections 4 and 7. The mean strains are integrated and the residual displacement is calculated:

Ford	Ghali et al. (2011)
$\{D^*_s\} = \int_0^1 [TR]^T \{\varepsilon\}_m \lvert t \rvert d\xi = \begin{Bmatrix} -1.161 \\ 6.410 \\ 1.603 \end{Bmatrix}$	$\{D^*_s\} = \begin{Bmatrix} -1.119 \\ 6.922 \\ 1.530 \end{Bmatrix}$
$\{D\}_{err} = [H]^T \{D^*\} - \{D^*_s\} = \begin{Bmatrix} 1.161 \\ -6.410 \\ -0.652 \end{Bmatrix}$	$\{D\}_{err} = \begin{Bmatrix} 1.119 \\ -6.922 \\ -0.592 \end{Bmatrix}$

where the displacements are in mm and the rotation is in 10^{-3} rad. The stiffness is recalculated and the residual forces to be applied in the next iteration are

Ford	Ghali et al. (2011)
$\{F\}_{res} = \begin{Bmatrix} 166.6 \\ 6.764 \\ -52.48 \end{Bmatrix}$	$\{F\}_{res} = \begin{Bmatrix} 163.1 \\ 7.165 \\ -53.57 \end{Bmatrix}$

where forces are in kN and moments are in kNm. This process is repeated until the final result is achieved and (5.21) is satisfied, which requires roughly 20 iterations. The final value of the moment at B is 131.4 kNm, which is within 3% of the 126.3 kNm that Ghali et al. (2011) provide. The final rotation at A is 2.686 x 10^{-3} rad, and the final displacement at midspan is 11.0 mm. Slight differences in the results can be attributed to a slightly different numeric integration algorithm (Simpson's rule vs. a "trapezoid product" rule).

As discussed in section 3.10, this problem demonstrates convergence problems unless the cracking limit is taken as $\sqrt{\beta} f_{ct}$. Figure 6.9 shows a comparison of the two methods.

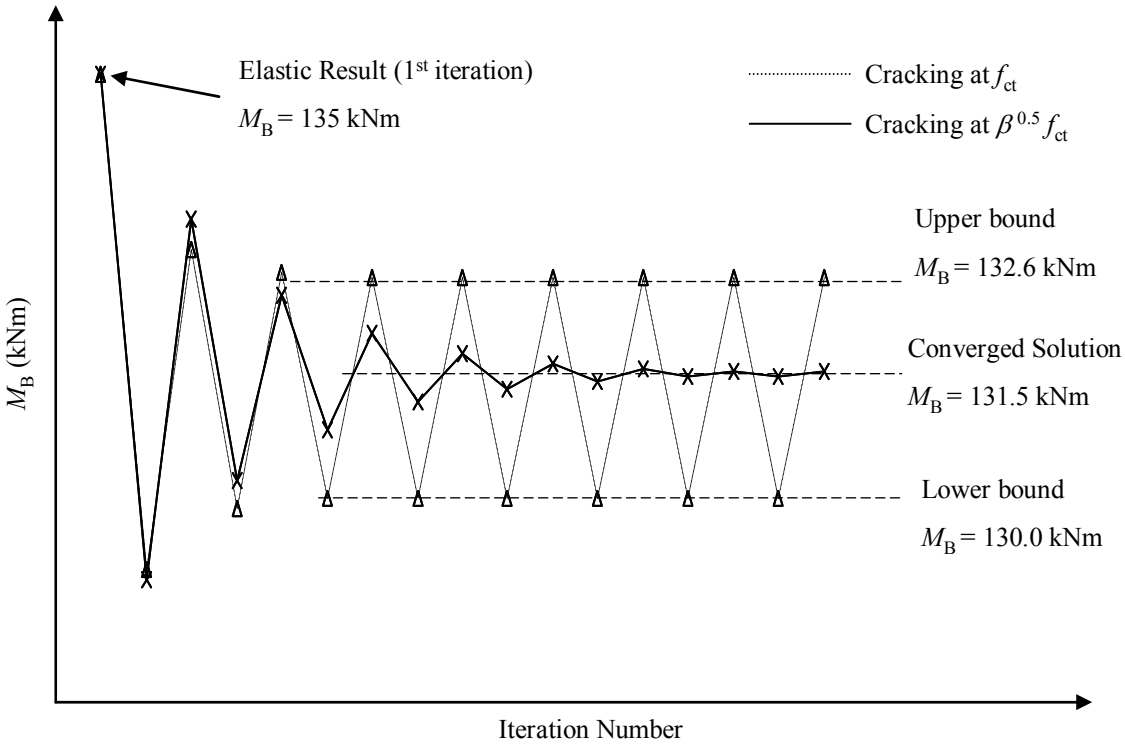

Figure 6.9: Convergence Comparison

The normal method of considering cracking results in oscillation from 132.6 kNm and 130.0 kNm, while the smooth method closes in on the solution of 131.5 kNm. The average of the oscillations is 131.3 kNm, which is close to the solution. Ghali et al. (2011) provide 126.3 kNm.

6.1.4 Prestressed Continuous Beam

Ghali, Favre, and El-Badry (2011) also presented a continuous beam with prestressing and plotted the deflection curve from an increasing uniformly distributed load. The beam has equal layers of reinforcing steel, except for the quarter of the length closest to the

support where additional steel is added at the top. The problem is illustrated in Figure 6.10.

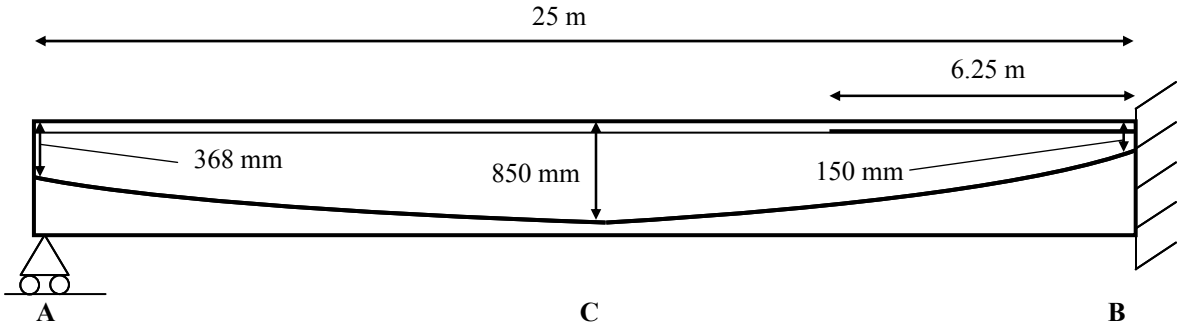

a) profile

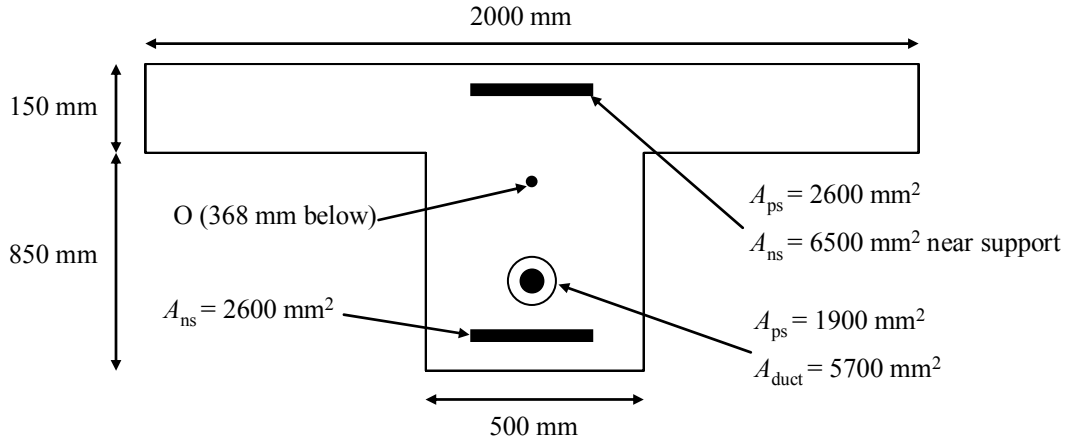

b) section

Figure 6.10: Prestressed Continuous Beam

The following properties are used in the analysis:

$$E_c = 30 \text{ MPa}$$

$$f_{ct} = 2.5 \text{ MPa}$$

$$E_{ns}, E_{ps} = 200 \text{ GPa}$$

$$q_{DL} = 18 \text{ kN/m}$$

$$P_i = 2.2 \text{ MN}$$

The given prestress value includes the effect of time-dependent losses. The given dead load includes the self-weight of the beam.

For this analysis, Ghali used 22 sections, with the section at 0.75L duplicated because of the reinforcing change. For this model, two members with 9 and 10 sections respectively were used (again, with an extra section in the second member because of the step change in the reinforcing). To keep the results comparable, cracking was ignored until f_{ct} rather than using the smooth cracking limit. In this case, convergence was achieved without this modification, but at a few values of q/q_{cr} convergence issues manifested.

Table 6.6 shows a comparison of the results of analysis of Ghali et al. (2011) with those from the developed model.

Table 6.6: Results for Prestressed Beam of Ghali et al. (2011)

	Ghali	Ford
D_{zC}, DL+PS (mm)	1.10	1.35
q_{cr} (kN/m)	13.4	13.3
$D_{zC,cr}$ (mm)	12.80	12.83
$D_{zC}/D_{zC,cr}$ at $1.5q_{cr}$	2.02	2.10
$D_{zC}/D_{zC,cr}$ at $2.0q_{cr}$	3.52	3.53

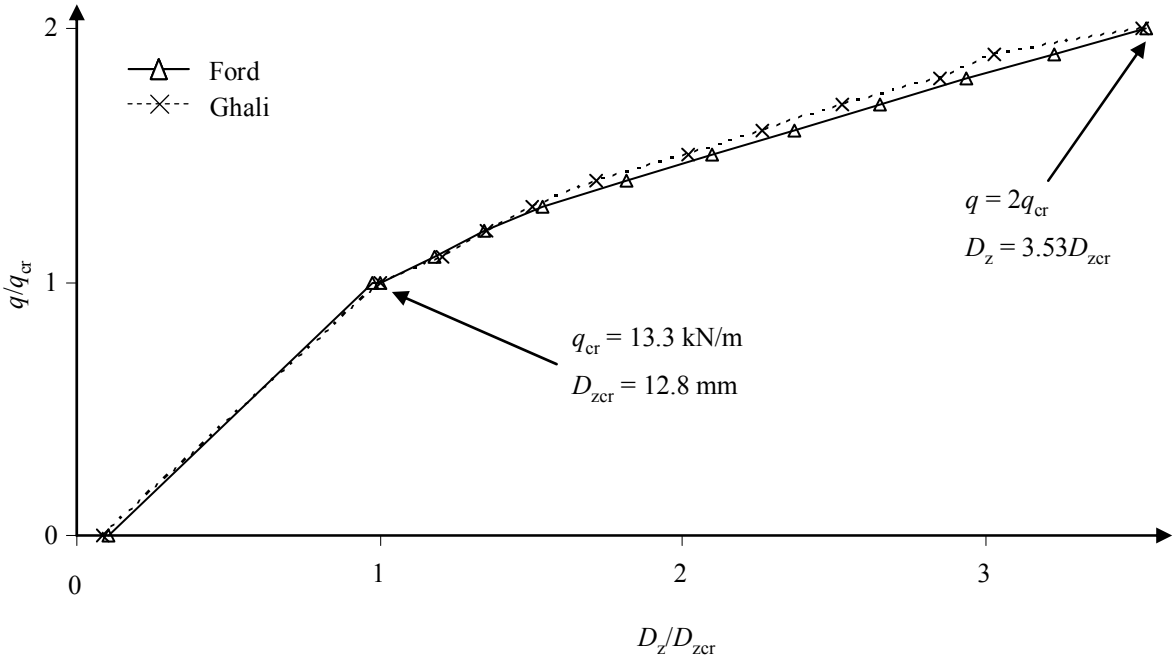

Figure 6.11: Comparison of Deflections

The results correlate extremely well, as shown in the figure. It is evident that as the load increases, so does the extent of cracking, which leads to a reduction in stiffness. To illustrate this effect, Table 6.7 below shows the value of the interpolation coefficient at

each section for increasing values of load. For this purpose, the cracking was assumed to start as soon as $\beta^{0.5} f_{ct}$ was exceeded. The load at which this stress is exceeded is reached at q = 11.2 kN/m, or 84.2% of the load that causes f_{ct}.

Table 6.7: Interpolation Coefficient vs. Live Load

	ξ = x / L								
q/q_r	**0**	**0.125**	**0.25**	**0.375**	**0.5**	**0.625**	**0.75**	**0.875**	**1**
0	0	0	0	0	0	0	0	0	0
0.842	0	0	0	0	0	0	0	0	0
1	0	0	0	0.305	0.278	0	0	0	0.498
1.2	0	0	0	0.642	0.623	0	0	0	0.757
1.4	0	0	0.460	0.787	0.777	0	0	0	0.852
1.6	0	0	0.672	0.858	0.851	0	0	0	0.902
1.8	0	0	0.779	0.898	0.893	0	0	0	0.930
2	0	0	0.841	0.924	0.919	0.273	0	0.285	0.948

Note that cracking starts at the support and proceeds into the midspan of the beam. The stiffness reduces further as more sections start to crack.

6.1.5 Prestressed Continuous Beam- Time Dependent Effects

El-Badry and Ghali (1990) analysed a similar beam in the demonstration section of the manual for Cracked Plane Frames in Concrete (CPF), a program developed to implement the formulation shown in El-Badry (1988). The example included time dependent effects and live load causing cracking.

The reference point is 400 mm from the top fibre, and the prestressing tendon is on the reference point at A again (32 mm lower than in the previous example). The deck is only 100 mm thick as opposed to 150 mm. The additional nonprestressed steel only extends 5.0 m into the beam instead of 6.25 m.

The properties follow:

At t_0	From t_0 to t	At t
E_c = 25 MPa	ϕ = 3.0	E_c = 30 MPa
f_{ct} = 2.5 MPa	χ = 0.8	f_{ct} = 2.5 MPa
E_{ns}, E_{ps} = 200 GPa	ε_{cs} = -300 με	q_{LL} = 16 kN/m
q_{DL} = 14 kN/m	$\Delta\sigma_{pr}$ = -90 MPa	
P_i = 2.9 MN		

An elastic analysis is completed for all three stages; the cumulative results are shown in Figure 6.12. The cumulative displacement at the centre of the beam in mm is 5.95 upwards, 4.35 upwards, and 8.97 downwards for after t_0, just before t, and after t respectively. Time dependent effects cause a downward displacement of 1.6 mm, and live load would cause 13.3 mm displacement if cracking did not occur.

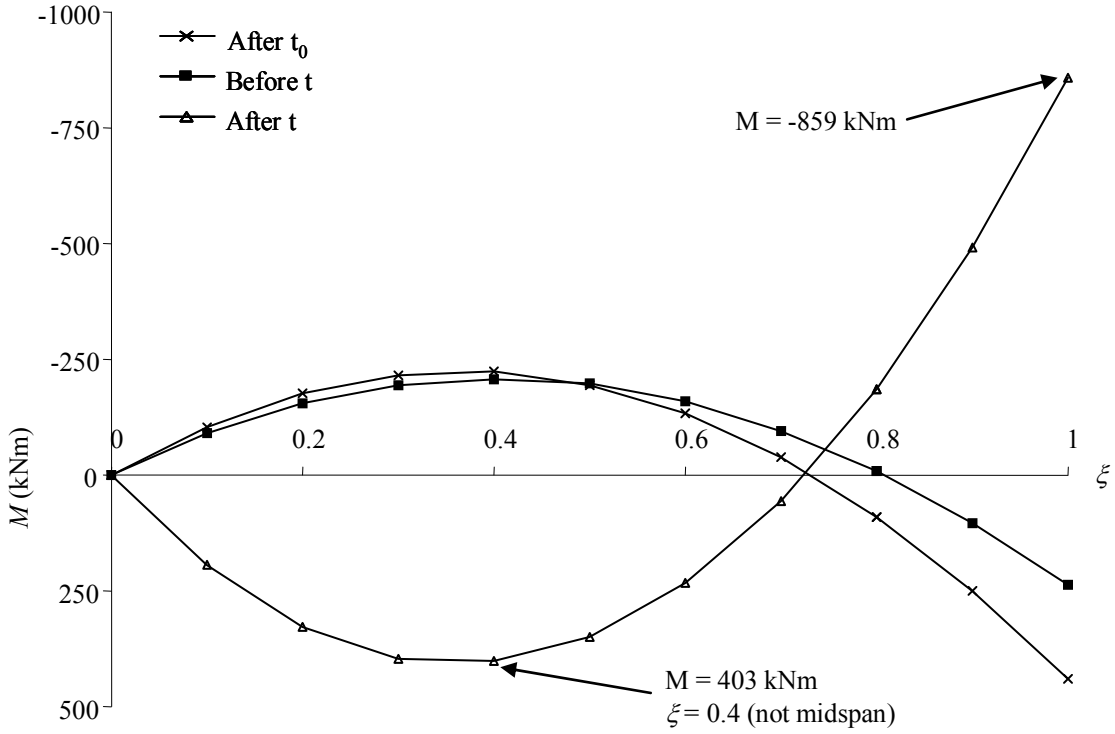

a) Bending Moment Diagram

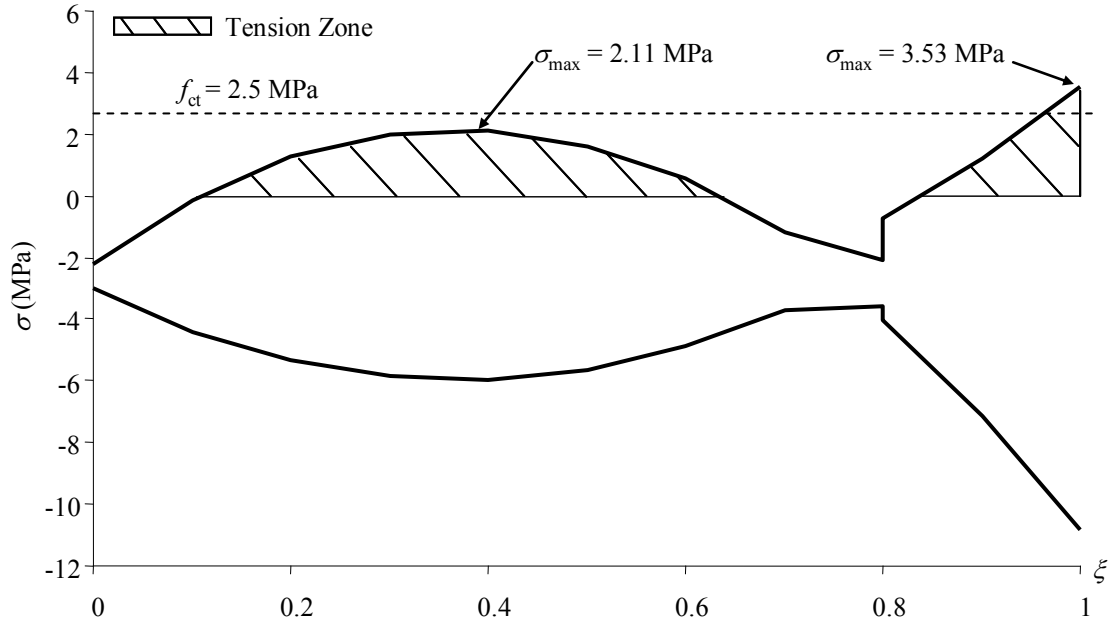

b) Stress Envelope

Figure 6.12: Bending Moment and Stresses for Elastic Uncracked Analysis

As the figure shows, the tensile stress limit is exceeded at the support and at midspan. Cracking occurs. Convergence is reached in 3 additional iterations.

Comparisons of results from cracked and uncracked analysis are shown below.

Table 6.8: Effect of Cracking

	Uncracked	Cracked
D_{zB} (mm)	8.97	9.97
At B (Support)		
M (kNm)	-859.0	-804.2
σ_{ct} (MPa)	3.54	0.0
σ_{cb} (MPa)	-10.8	-13.1
At C (Midspan)		
M (kNm)	348.0	375.4
σ_{ct} (MPa)	-5.63	-5.78
σ_{cb} (MPa)	1.63	1.85

As the results in the table indicate, cracking at B forces redistribution of a 27.4 kNm bending moment. The deflection at B increases by 11%. This effect would be even more pronounced if the middle sections of the beam started to crack. As shown in Figure 6.12b, the maximum tensile stress near (but not at) midspan is 2.10 MPa before cracking occurs. This increases to 2.29 MPa with the additional redistributed moment, which is still not enough to cause cracking there. Cracking is limited to the support, where $\zeta = 0.705$.

Table 6.9 shows a comparison to the results of CPF.

Table 6.9: Comparison to CPF Results

	Ford	El-Badry	%
$D_C(t_0)$ (mm)	5.95	5.86	1.5
$\Delta D_C(t,t_0)$ (mm)	-1.60	-1.54	3.9
$\Delta D_C(t)$ (mm)	-14.3	-13.7	4.3
Final values at B (Support)			
M (kNm)	-804.2	-776.6	3.6
σ_{ct} (MPa)	0.0	0.0	-
σ_{cb} (MPa)	-13.1	-13.4	2.3
ζ	0.705	0.719	2.0
Final values at C (Midspan)			
M (kNm)	375.4	288.0	30.3
σ_{ct} (MPa)	-5.78	-5.72	1.0
σ_{cb} (MPa)	1.85	1.78	3.9

The correlation is fairly good – except for the final value of the moment at the midspan, where CPF's result is 30% less despite good correlation in stress result. Furthermore, the moments at the support should be larger in CPF as the stress shows.

A simple way to check the moments is to consider the net distributed load that should be satisfied. Recall that the equivalent uniformly distributed load that results from the application of prestressing is

$$q_{eff} = \frac{8Pc}{L^2} \tag{6.7}$$

The 90 MPa prestress loss over the 1900 mm^2 tendon results in a 171 kN drop in force, for a net prestressing force of 2729 kN. The equivalent load for the net prestressing, using c = 0.575 m, is 20.1 kN/m applied in an upward direction. Balancing against the total 30 kN/m load applied on the beam yields a net distributed load of 9.91 kN/m.

Since the beam must satisfy equilibrium, the difference between the midspan moment and half of the support moment should be equal to $qL^2/8$, or 774.6 kNm. For the developed model's result, (-804.2)/2 – (375.4) = 777.5 kNm, which is very close. Some difference is expected here because the developed model takes into account the angle the prestress acts at. For the CPF reported result, (-776.6)/2 – (288.0) = 676.3 kNm. This moment difference represents an effective load of 8.66 kN/m, or exactly the value that would occur if the 90 MPa tendon loss was not included.

If the moments reported by CPF are adjusted for prestress loss by adding ΔP times e, the following results are obtained.

Table 6.10: Results Corrected for Prestress Loss

	Ford	El-Badry	%
Moment at Support	-804.2	-819.4	1.9
Moment at Midspan	375.4	365.0	2.8

Not only do these values make more sense, but the fact that the error difference is very close to that reported for the stress difference shows that this is simply a reporting issue.

6.2 Demonstration Examples

The following examples are shown to demonstrate the capabilities of the model. First, a fictitious bridge is presented and compared with similar analysis; second, a real bridge in Calgary, Alberta is examined.

6.2.1 Complex Curved Bridge

Van Zyl (1979) developed software to analyse prestressed curved concrete bridges built in stages. He presented a fictitious bridge which was later analysed by Debaiky (1997) using Jirousek elements. The bridge is shown below.

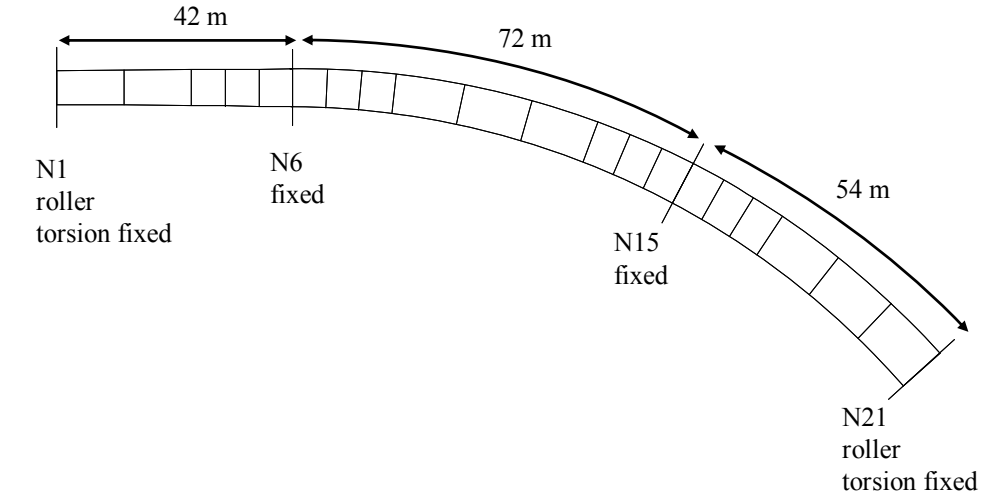

a) Plan

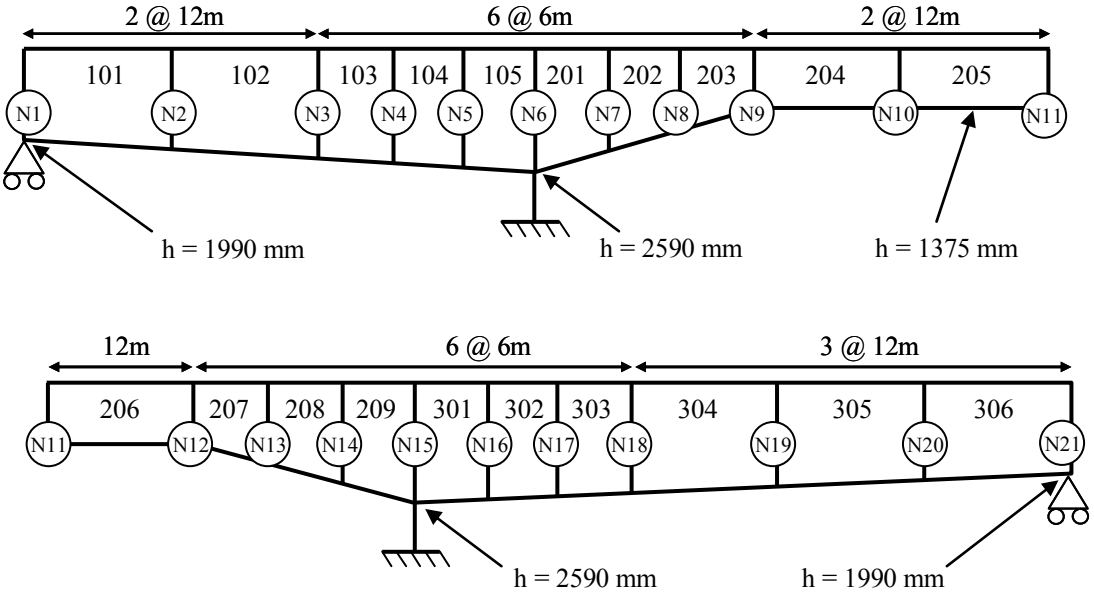

b) Profile w/ Member and Node Numbers

Figure 6.13: Van Zyl's Bridge

The bridge is made of three spans and 17 segments (not to be confused with members). The first span is 140' (42 m) long and straight, while the second and third spans are 240' (72 m) and 180' (54 m) on a 500' (150 m) radius. The width of the bridge varies linearly

over its entire length, while the depth varies throughout. The cross section information and variation across the bridge is shown in the figure below. The horizontal dimensions vary linearly along the bridge while the vertical ones vary to make up the total height shown in Figure 6.13.

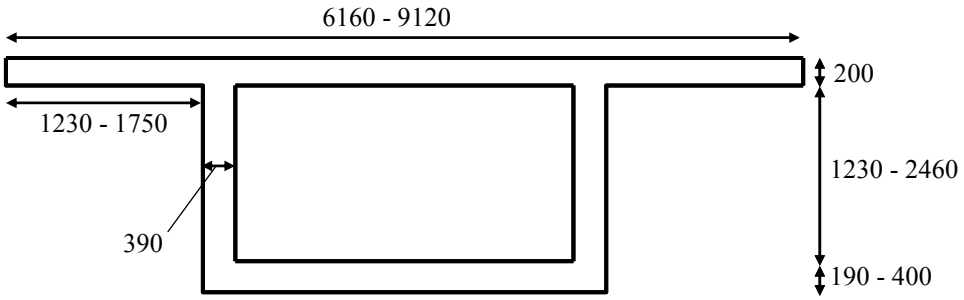

Figure 6.14: Cross Sectional Geometry

Van Zyl's bridge includes temporary supports and removal of prestressing tendons. While Debaiky (1997) used concrete piers at nodes 6 and 15, Van Zyl's actual analysis included totally fixed supports at these locations. The input data for the analysis are shown in the table below.

Table 6.11: Input Data for Van Zyl Analysis

# of members	20
Nodes per member	3
Self weight of concrete, γ	25.1 kN/m^3
Code for calculation	CEB-FIP (MC90)
Relative humidity, RH	40%
Characteristic strength, f_{ck}	27.6 MPa
Poisson's ratio, ν	0.18
Prestressing modulus, E_{ps}	190 MPa
Wobble coefficient, k	.000656/m
Friction coefficient, μ	0.2/rad

Note that both Van Zyl (1979) and Debaiky (1997) ignored the effect of prestress relaxation, while friction loss is included in the analysis. Van Zyl (1979) included the effect of variable relative humidity and temperature; the relative humidity was increased to 60% at day 100 in the analysis. He also included the effect of seasons in the construction, varying the temperature between 20°C and 40°C. To simplify the analysis, this variance was ignored by Debaiky (1997). As neither model incorporates the effect of cracking, it is ignored in all three analysis models.

The erection sequence and loading are shown in the figure below.

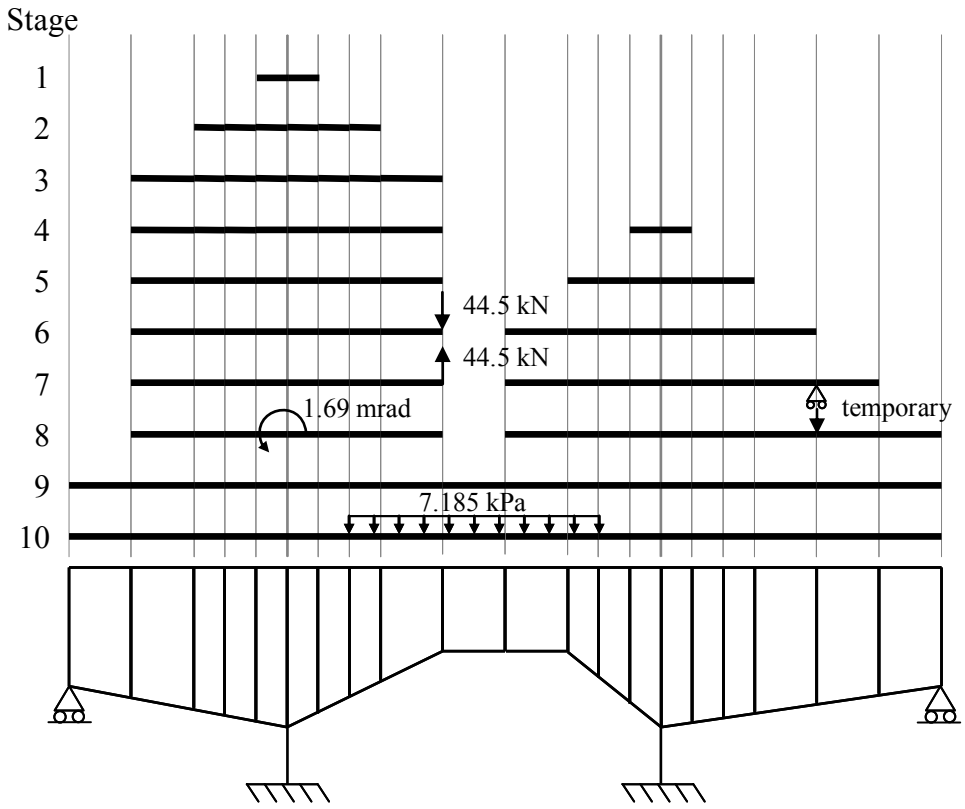

Figure 6.15: Erection Sequence and Loading

The bridge is erected using the balanced cantilever technique. In practice, segments would be shorter than used here; this is done to simplify the analysis. The left hand side of the bridge (segments 2 through 7) are erected in stages 1-3 first; the right hand side (segments 9 through 16) are erected next in stages 4-7. The bridge is finally completed by connecting the right side to the support at node 21 in stage 8 with segment 1, then connecting the left side to node 2 in stage 9 with segment 17. Segment 8 is cast in stage 9, which makes the bridge continuous. The left side of the bridge is rotated to match the vertical displacements of nodes 10 and 11 before the closure span is cast. The required rotation is calculated by separate analysis.

A construction load of 10 kip (44.5 kN) is added to the left end of the right side (node 11) in stage 6; it is removed in stage 7. A temporary support is added at node 19 in stage 7 and removed in stage 8. A superimposed dead load of 7.2 kN/m^2 (0.15 psf) is added to the five centre segments (6 though 10) in stage 10.

The properties of the concrete members are shown in Table 6.12.

Table 6.12: Segment Casting History

Segment	Members	Cast in Stage	Age at Introduction (d)	Self Weight (kN/m)	
				Start	End
1	101	9	91	81.0	86.0
2	102	3	35	90.3	95.4
3	103, 104	2	25	99.9	108.2
4	105, 201	1	15	117.5	116.8
5	202	2	15	107.2	103.6
6	203	2	15	100.3	96.6
7	204	3	15	91.7	84.1
8	205	9	61	84.1	85.8
9	206	6	25	85.8	87.6
10	207	5	15	93.0	101.7
11	208	5	15	105.3	114.1
12	209, 301	4	5	125.2	134.0
13	302	5	5	122.6	122.3
14	303	5	5	118.5	118.1
15	304	6	5	114.3	113.5
16	305	7	10	109.5	108.6
17	306	8	10	104.5	103.6

The bridge contains 16 prestressing tendons. Their geometry and construction sequence are shown in Figure 6.16 and Table 6.13.

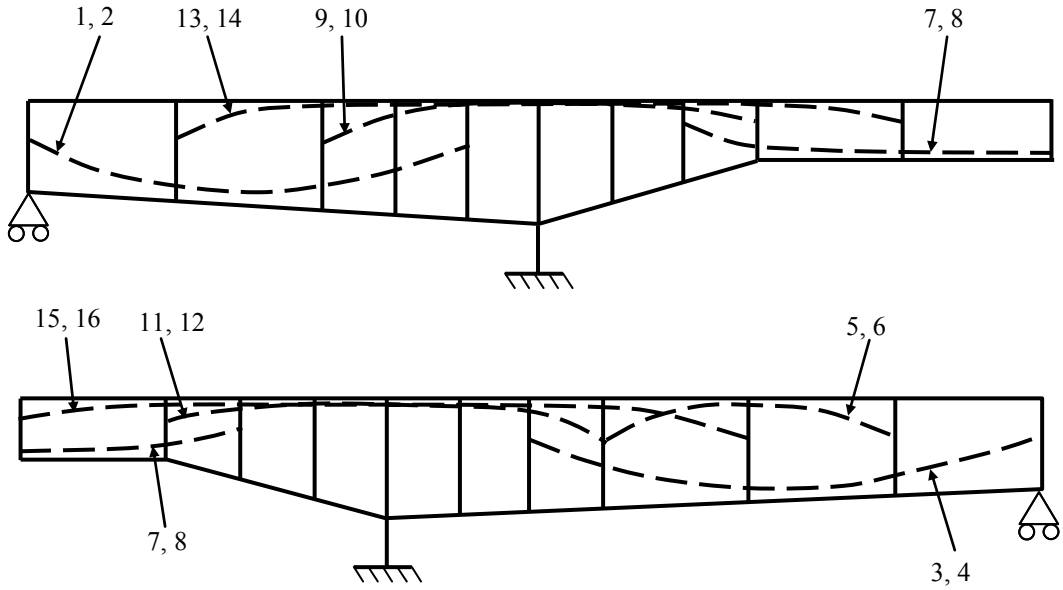

Figure 6.16: Prestressing Tendon Geometry

Table 6.13: Prestressing Geometry Data

Tendon	Stage Added	A_{ps} (mm^2)	P_i (MN)	z_{ps}^* (mm)		c_1 (mm)	c_2 (mm)	Inflection nodes
				Start	End			
1, 2	9	1395	1.34	1076	1119	-698	-	-
3, 4	8	2787	3.11	1076	1119	-960	-	-
5, 6	7*	2787	3.11	1192	1094	768	-	-
7, 8	9	2787	2.67	1192	1094	-314	-	-
9, 10	2	9290	11.1	1158	1094	216	91	5, 7
11, 12	5	11148	13.4	1158	1094	104	223	14, 16
13, 14	3	3716	4.45	872	875	183	91	3, 9
15,16	6	4645	5.56	872	875	91	198	12, 18

*Tendons 5 and 6 are removed at stage 8.

Tendons 9 through 16 are located 150 mm below the deck between their inflection points.

A summary of the construction sequence is shown in Table 6.14.

Table 6.14: Construction Sequence Summary

Stage	Time (d)	Segments Added	Tendons Stressed	Loads	Boundary Conditions
1	30	4			N6 fixed
2	35	3,5,6	9,10		
3	40	2,7	13,14		
4	50	12			N15 fixed
5	55	10,11,13,14	11,12		
6	60	9,15	15,16	44.5 kN at N11	
7	70	16	5,6	-44.5 kN at N11	Vert at N19
8	75	17	3,4		N21 skew .0017 rad at N6 Remove N19
9	91	1,8	1,2,7,8		N1 skew
10	150			7.2 kPa on [6,10]	

The results from the analysis are compared with both the work of Debaiky (1997) and Van Zyl (1979) below. It is important to note, however, that Debaiky (1997) was not able to obtain good correlation with the results of Van Zyl (1979). Van Zyl (1979) also analysed the structure using commercial software (SAP) and did not obtain a good match. Still, given the curved nature of the problem, the staged construction, the variety of prestressing and the varying cross sectional properties, the analysis is worthwhile.

The displacements of the bridge are shown below just before closure and after t = 1000 days.

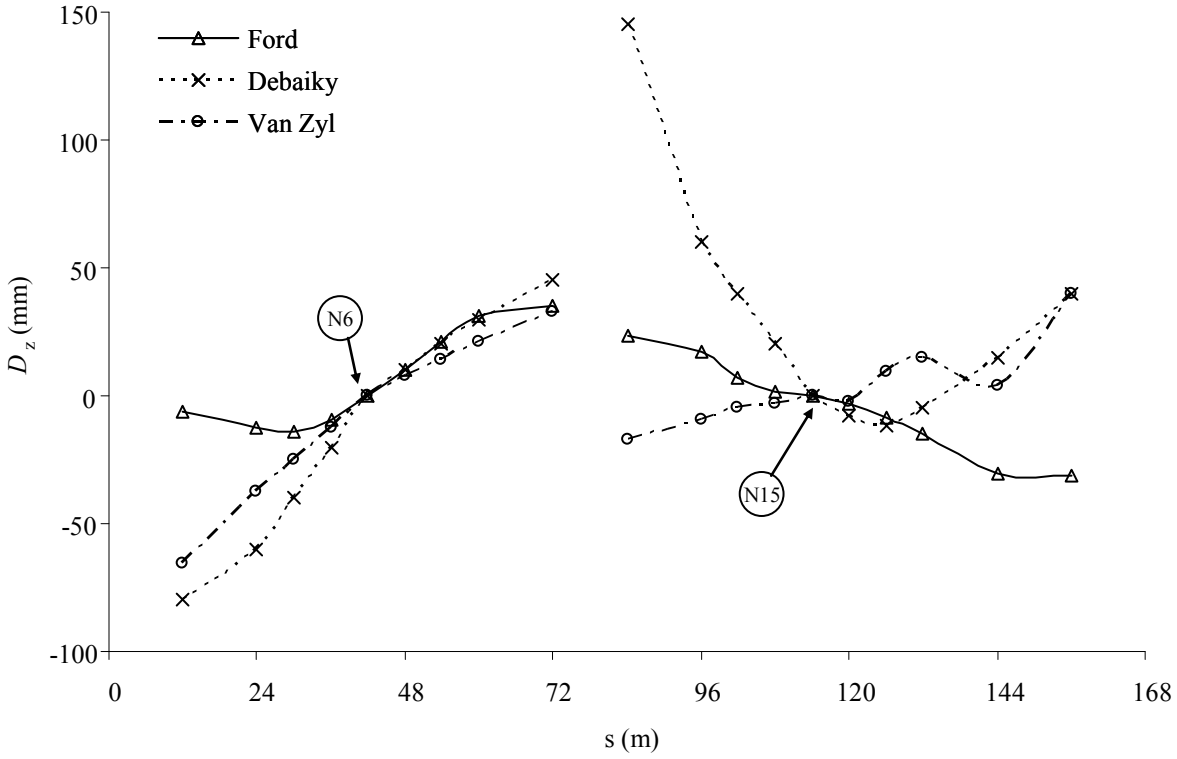

a) Just Prior to Closure (t = 91d, just before Stage 9)

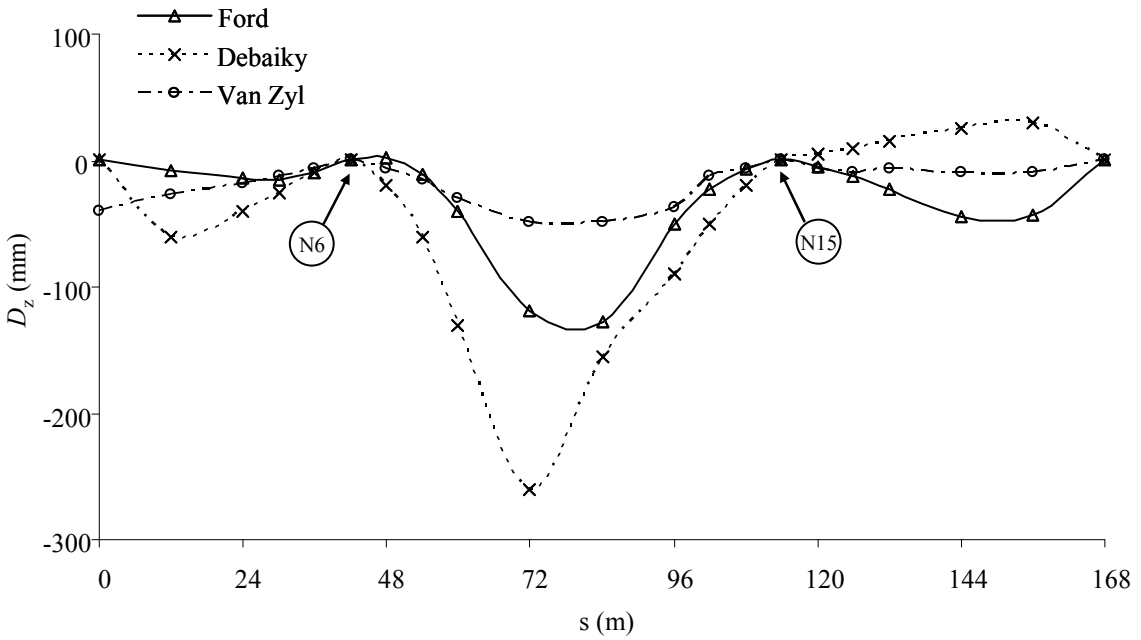

b) at 1000 days

Figure 6.17: Displacements for Van Zyl's Bridge

Debaiky (1997) noted that the 0.0017 radian rotation Van Zyl (1979) required to align nodes 10 and 11 was smaller than actually required. As the figure shows, Debaiky (1997) still had a discrepancy of approximately 100 mm, which would require an additional 0.0033 radians to correct. The projected distance from node 6 to node 10 is 30.2 m.

In the current analysis, the calculations were completed up to stage 8 to determine this requirement. This yielded a displacement of -14 mm at N10 and 36 mm at N11 for a difference of 50 mm. The required rotation at node 6 would be 1.69 mrad for alignment, which complies with the result of Van Zyl (1979). The result of Debaiky (1997) may be higher because of the relative flexibility of the left pier in his analysis.

The final deflected shape of the structure at 1000 d is shown in Figure 6.17b for all three results. There is substantial variance between Van Zyl (1979) and Debaiky (1997), which is not surprising given the difference in boundary conditions. The curvature of the central span means that twist in the member translates to vertical displacement at the tip; since the piers in the analysis by Debaiky (1997) have a finite stiffness, they allow some rotation. Since the out-of-plane offset between nodes 6 and 10 is approximately 3 m, each thousandth of a radian twist at node 6 corresponds to a 3 mm vertical displacement at node 10.

As the figure shows, the deflected shape from the current analysis is comparable with Van Zyl's result. Van Zyl's displacements will be lower because of the higher relative humidity and lower creep. The result of Debaiky (1997) seems higher than a real bridge

would undergo, even given the difference in support conditions. The maximum displacement of 125 mm over a 72 m span is approximately L/600, which is reasonable.

Next the bending moments are compared. Van Zyl did not present the cumulative bending moment diagrams as he was not able to obtain results that supported basic statics. Instead, a comparison with Debaiky (1997) is shown below.

The bending moments correlate well considering the difference in boundary conditions. The midspan moments are nearly a perfect match, but Debaiky (1997) had lower moments at the supports.

One possible source for this error is the datum that the moments are reported on. Since there are large prestressing forces and the primary moments from the prestressing are included, the centroidal moments need to be calculated by subtracting the normal force times its eccentricity. The cross section properties in Debaiky (1997) were different than those of Van Zyl (1979) and as a result the internal forces from the prestressing could vary significantly. Debaiky (1997) also ignored the temporary tendons 5 and 6, which will also result in some discrepancy. Further investigation is required to determine the correct location of the prestressing anchors, as they are not located exactly at the centroid of the section.

Poor correlation was found for the torsion moment diagrams. Some of this results from the change in boundary conditions but in general more investigation is required into the twisting behaviour. The torsional stiffness in the current analysis was calculated using

the simplified method discussed in section 3.8.1. A more accurate approach using membrane analogy would be better.

The shape of the diagram is similar to that shown in Debaiky (1997) but the ordinates are substantially lower.

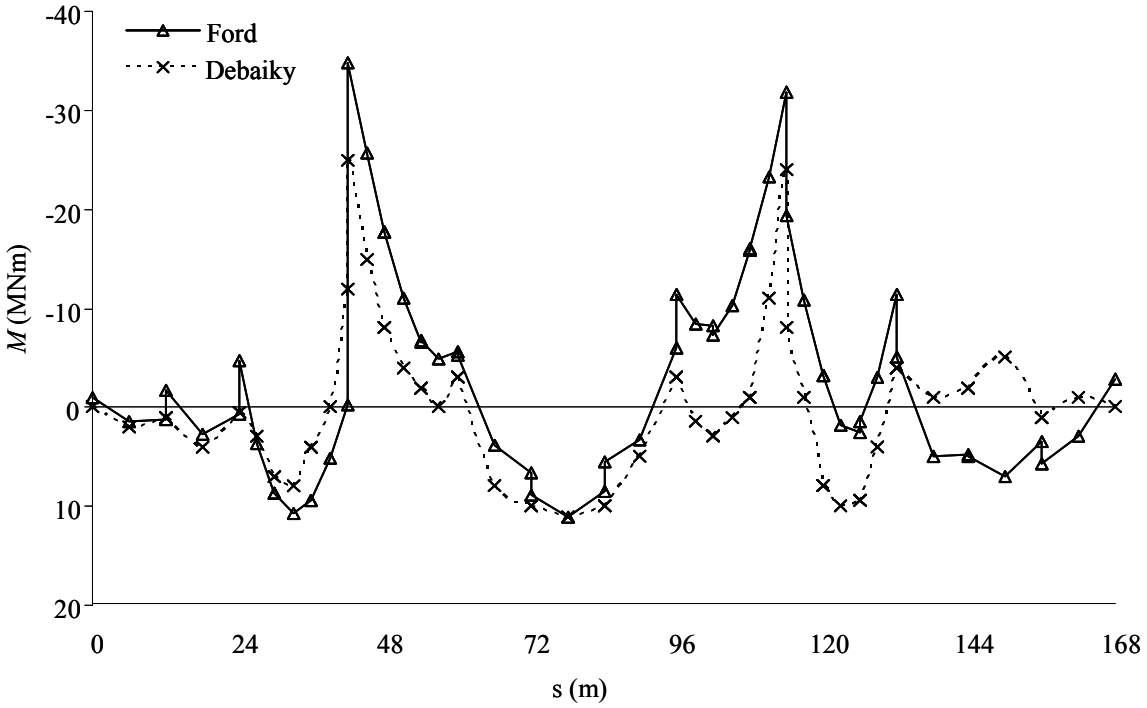

a) Bending Moment Diagram

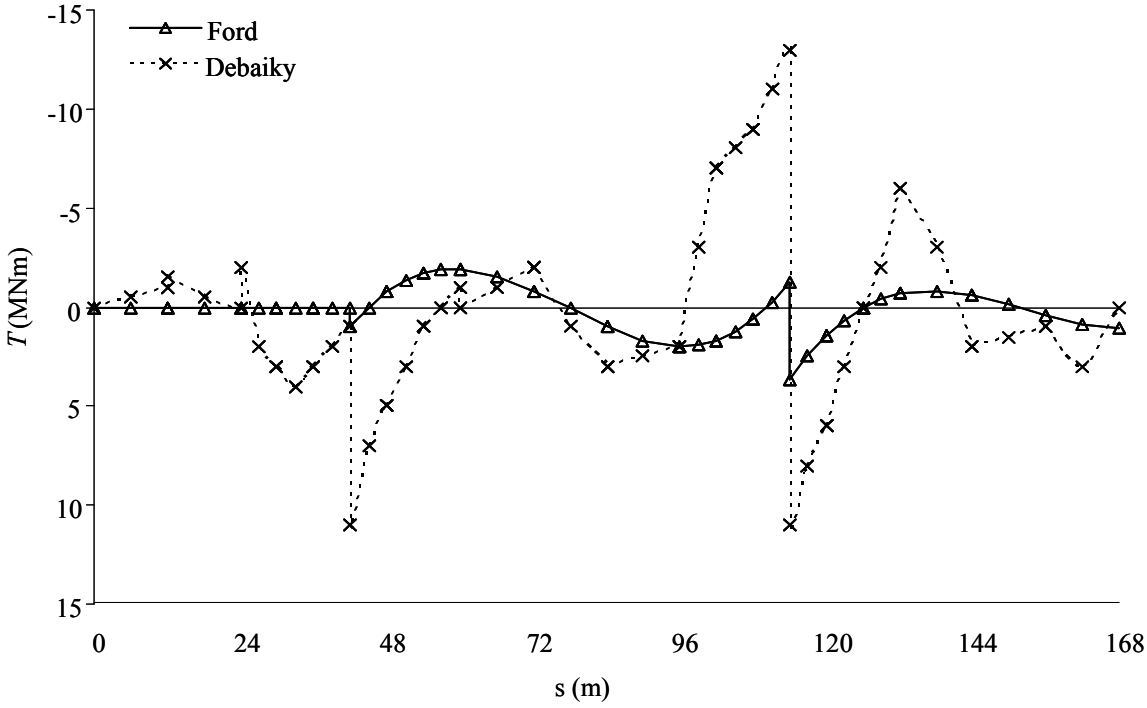

b) Torsion Moment Diagrams

Figure 6.18: Bending and Torsion Moment Diagrams for Van Zyl's Bridge

Lastly, Debaiky (1997) calculated the drop in the force of tendon #9 over time. The results were presented for a section 1.2 m to the right of node 8, which is 31.2 m into the 36 m member length ($\xi = 0.867$) and are shown below.

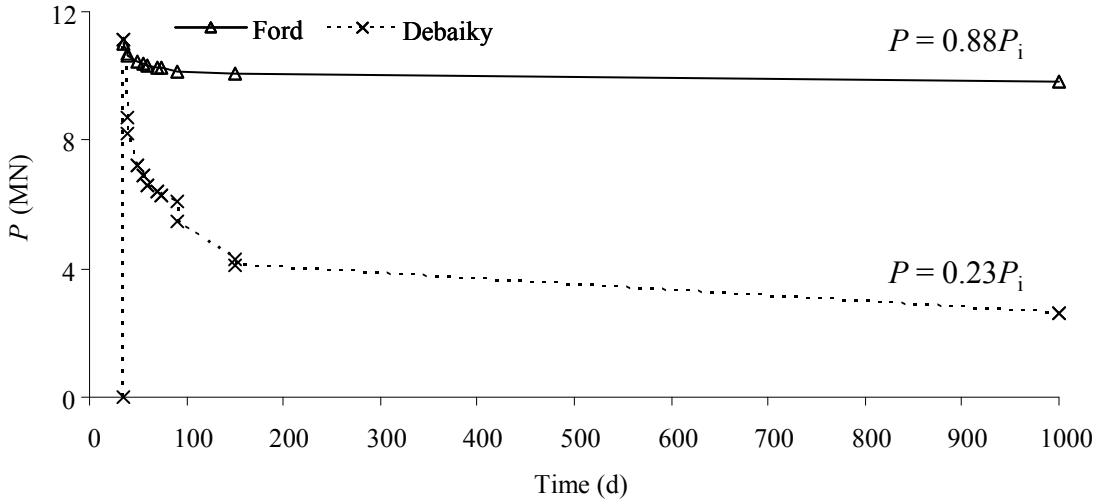

Figure 6.19: Force in Tendon #9

As the figure shows, the prestress loss in Debaiky (1997) is extremely high – especially considering that no intrinsic loss is included in the analysis. The developed model yields a total prestress loss over the first 1000 days as approximately 12%, while Debaiky (1997) gives 77%. This value is very high and indicates problems in the analysis. It is reflected in the high midspan displacements of Debaiky (1997), which are likely incorrect. Some of this difference may be due to the Lagrange model used for the prestress tendons in Debaiky's formulation.

It is important to note that a fundamental assumption in Van Zyl (1979) and Debaiky (1997) is that cracking does not occur. In fact, the centre drop-in span (segment 9)

experiences tensile stresses in the order of 10 MPa before the end of the analysis (due to the excessive prestress loss). In practice, this would result in redesign of the prestressing of the bridge. The next example includes consideration of cracking from the application of live load.

6.2.2 Bow River Bridge

The Bow River Bridge was built in the early 1980s in Calgary, Alberta. It serves as the major thoroughfare into the core of the city from the northeast side and is locally known as the "4th Avenue Flyover".

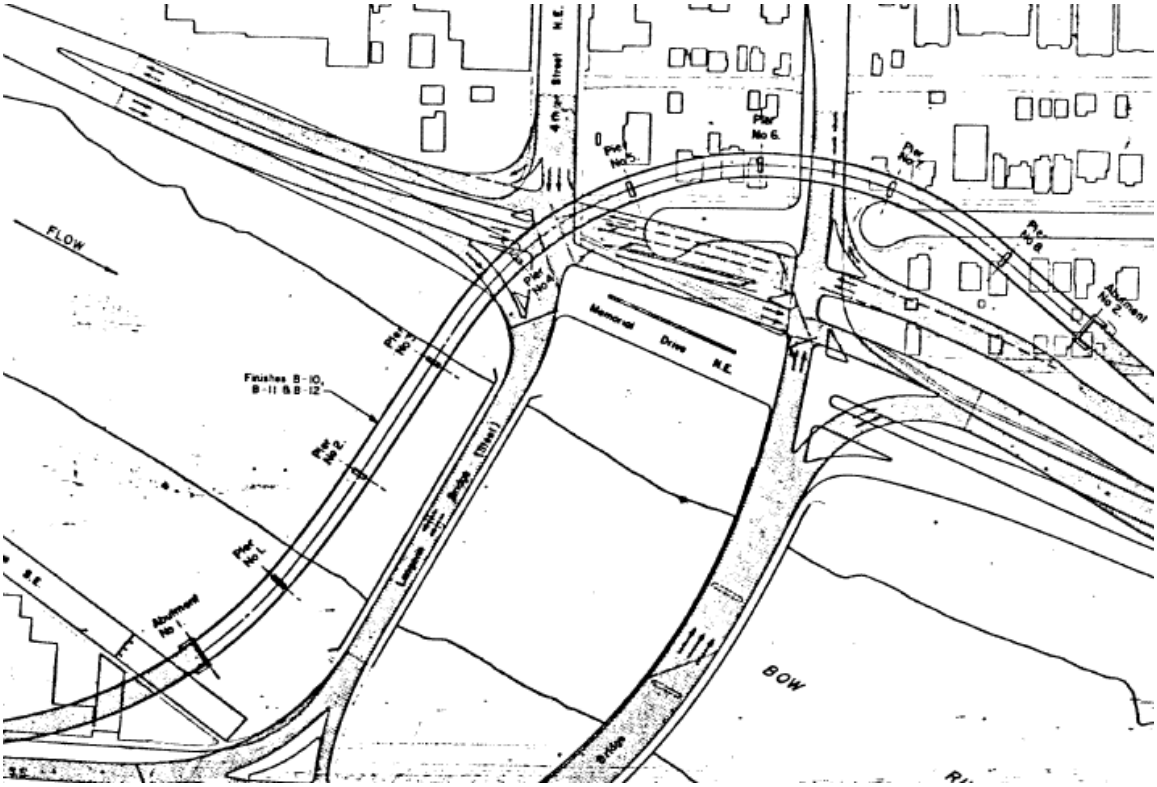

a) plan

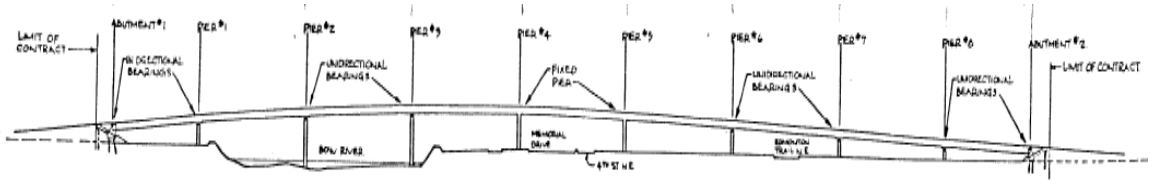

b) profile

Figure 6.20: Bow River Bridge

For demonstration purposes, four of the nine spans were chosen for analysis. Only curved spans were selected. The elevation was flattened. The simplified structure is shown below:

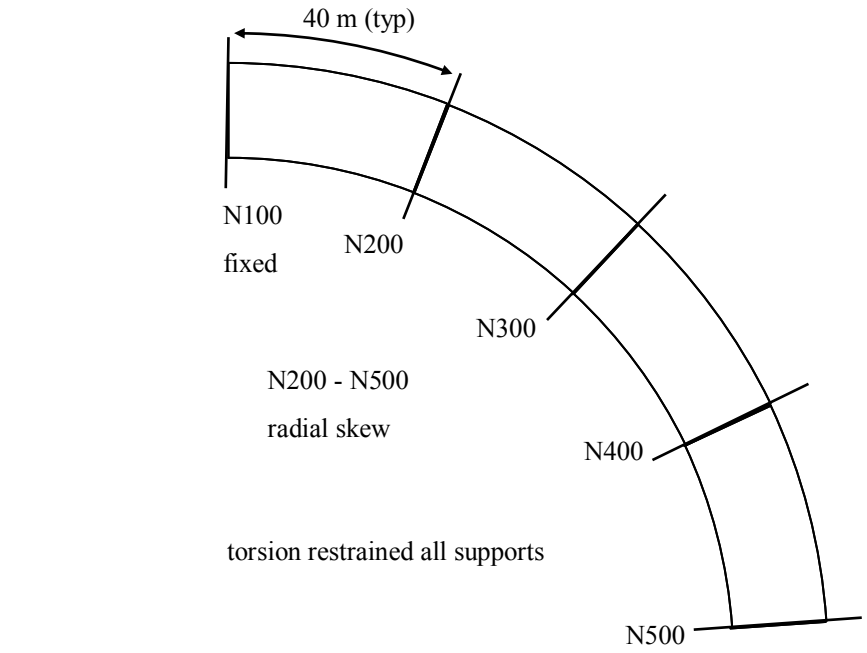

a) plan

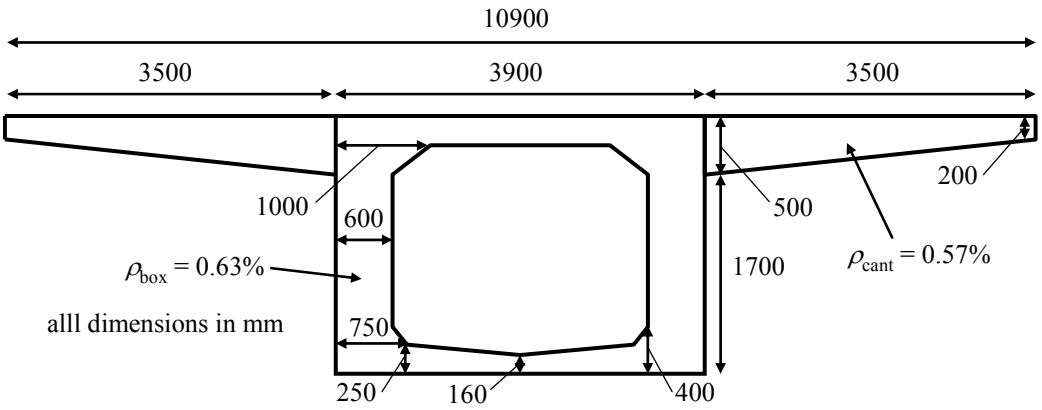

b) section

Figure 6.21: Simplified Bow River Bridge Model

The cross section is composed of a box section and cantilevers. The box is cast and prestressed first, then at a later time the cantilevers are cast and prestressed.

The bridge has 50 m spans. The simplified structure chosen for the model has slightly different boundary conditions and slightly different prestressing. The goal of the analysis is to demonstrate the effect of progressive cracking from live load. To best demonstrate this, the span length was reduced to 40 m. The cross section was kept the same and the radius of the bridge was reduced by 20%. Live load is applied after 50 years to allow all time dependent effects to take place.

Non-prestressed steel was modeled as though it were evenly distributed throughout the cantilever and box sections as shown above. These ratios were determined from the construction drawings for the bridge.

Each span is modeled using 5 members with 3 sections each. The concrete and non-prestressed steel are uniform throughout the bridge. The profile, members, and segments are shown below.

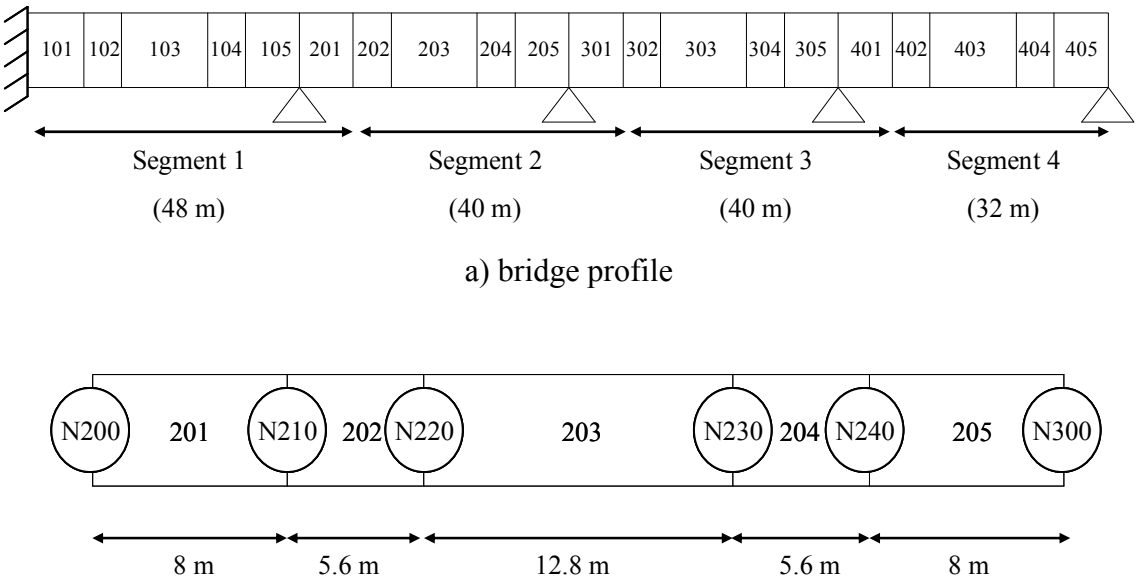

Figure 6.22: Node, Member, and Segment Numbering

Four different prestressing types are used in the bridge:

- Main cables, spanning the entire structure (P_1, 100 series): 4 sets of 19 cables
- Cables in the top of the box over the intermediate supports (P_2, 200 series): 10 sets of 3 cables
- Cables in the bottom of the box in the centre of the spans (P_3, 300 series): 2 overlapping groups of 3 sets of 3 cables
- Cables in the cantilevers (P_4, 400 series)

The construction sequence in the actual bridge used truss supports for the formwork. The concrete was poured and allowed to harden before the prestressing was applied. To

simplify the analysis, the prestressing is assumed to act at the same time as the member is cast. As a result, fewer intervals are required in the analysis (6 vs 12). Creep will be increased slightly as a result since the load acts over a longer time, but over a 50 year analysis this effect will be negligible.

The simplified construction sequence and tendon layouts are shown below. Hatched segments are cast in that stage. Note that the 100 series tendons run through the entire bridge; they are shown separately in Table 6.16 for clarity.

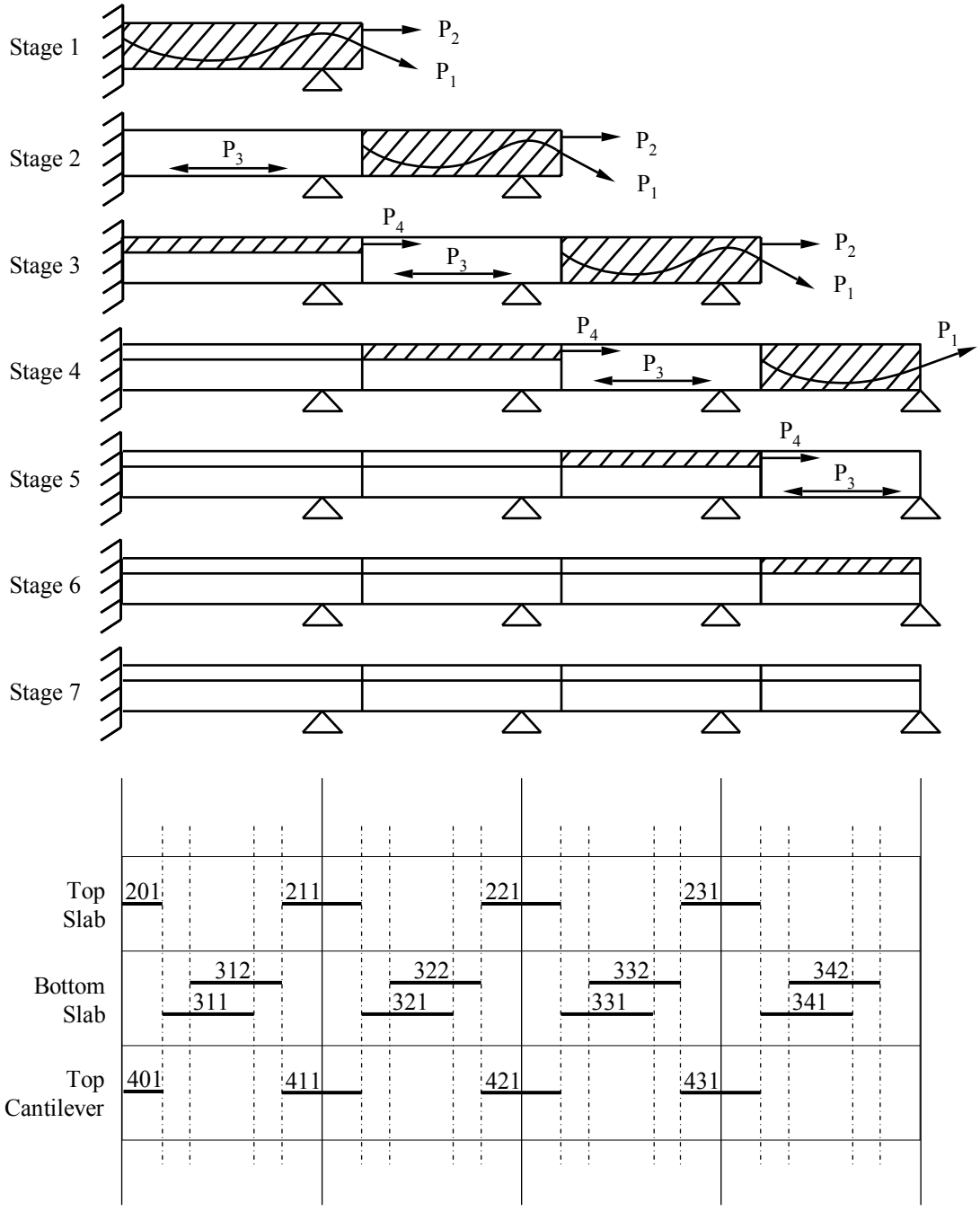

Figure 6.23: Bow River Bridge Prestress Sequence and Layout

A summary of the prestressing tendon properties is shown below:

Table 6.15: Prestressing Geometry Data

Tendon	Stage Added	A_{ps} (mm^2)	A_{duct} (mm^2)	P_i (MN)	z_{ps} (mm)
111-114	1	2660	5027	3.46	See below
121-124	2				
131-134	3				
141-144	4				
201	1	4200	12500	5.47	100
211	1				
221	2				
231	3				
311-312	2	2940	5890	3.83	2050
321-322	3				
331-332	4				
341-342	5				
401	3	9800	19635	12.76	170
411	3				
421	4				
431	5				

The tendon profiles for the 100 series cables are complex and are provided for the sake of completeness below.

Table 6.16: 100 Series Tendon Profiles

Tendon	ξ										
	0	0.1	0.2	0.3	0.4	0.5	0.6	0.7	0.8	0.9	1
111	370	393	1019	1623	1865	1799	1524	1044	430	374	740
112	370	743	1305	1706	1867	1799	1524	1044	430	556	1120
113	535	1116	1632	1918	2032	1964	1689	1209	595	840	1500
114	535	1485	1918	2001	2032	1964	1689	1209	595	1049	1880
121	740	1366	1744	1870	1799	1584	1227	727	370	376	740
122	1120	1536	1786	1870	1799	1584	1227	727	370	649	1120
123	1500	1797	1975	2035	1964	1749	1392	892	535	985	1500
124	1880	1966	2018	2035	1964	1749	1392	892	535	1287	1880
131	740	1366	1744	1870	1799	1584	1227	727	370	386	795
132	1120	1536	1786	1870	1799	1584	1227	727	370	683	1175
133	1500	1797	1975	2035	1964	1749	1392	892	535	1009	1555
134	1880	1966	2018	2035	1964	1749	1392	892	535	1350	1935
141	795	1218	1538	1751	1855	1859	1771	1595	1333	983	546
142	1175	1449	1656	1793	1862	1862	1798	1670	1478	1224	905
143	1555	1744	1887	1982	2029	2028	1978	1877	1727	1526	1275
144	1935	1974	2004	2024	2034	2032	2005	1952	1872	1766	1634

A summary of the construction sequence is shown below.

Table 6.17: Construction Sequence Summary

Stage	Time (d)	Segments Added*	Tendons Stressed	Loads	Boundary Conditions
1	45	1B	111-114 201		100 fixed 200 skew
2	90	2B	121-124 221 311-312		300 skew
3	135	3B, 1C	131-134 231 321-322 401 & 411		400 skew
4	180	4B, 2C	141-144 331-332 421		500 skew
5	225	3C	341-342 431		
6	270	4C			
7	18250			Live load	

* B = Box, C = Cantilever

The bending and torsion moment diagrams after the first stage, the fourth stage when the last box section is completed, and just before the application of live load are shown below.

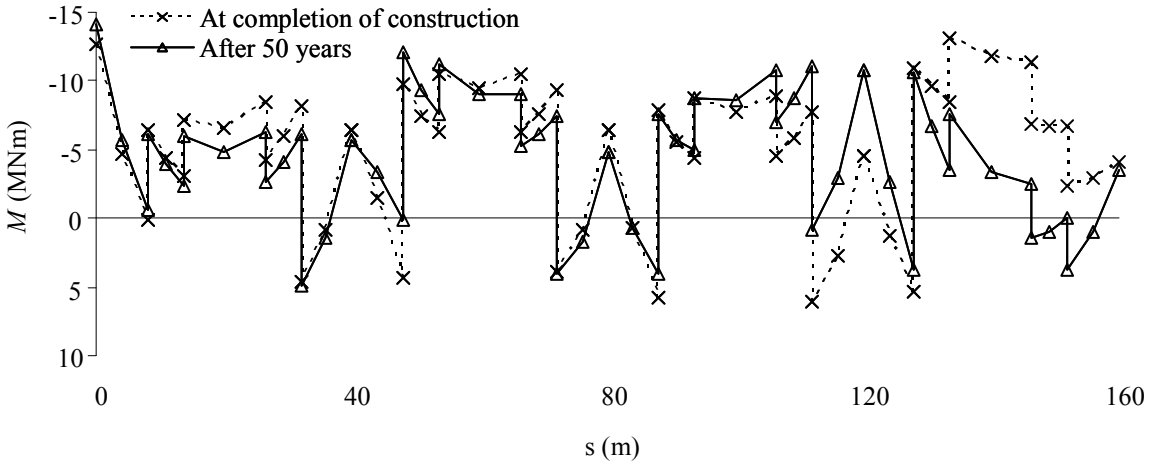

a) Bending

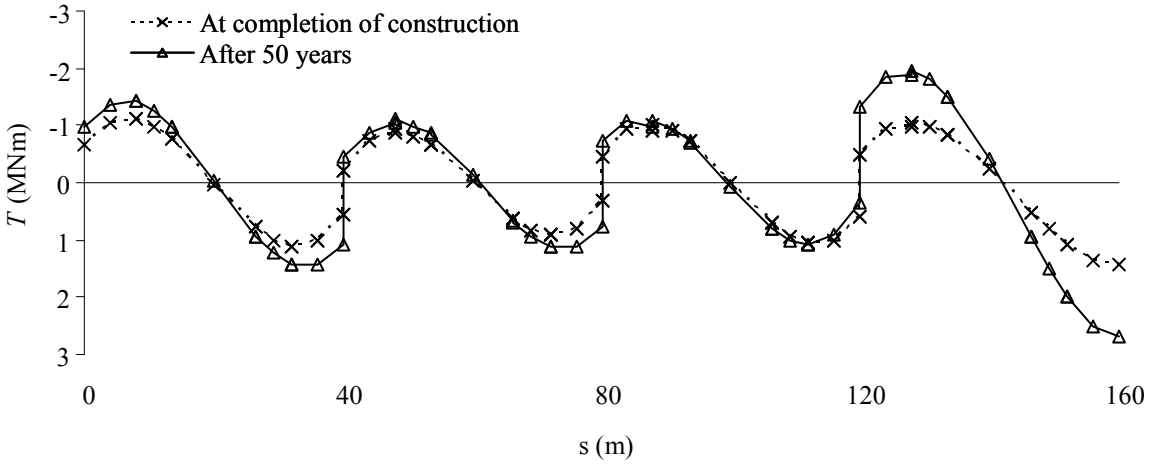

b) Torsion

Figure 6.24: Bending and Torsion Moment Diagrams

To demonstrate the effect of prestressing, the bending and torsion moment diagrams are shown below for a run with no prestressing force as well:

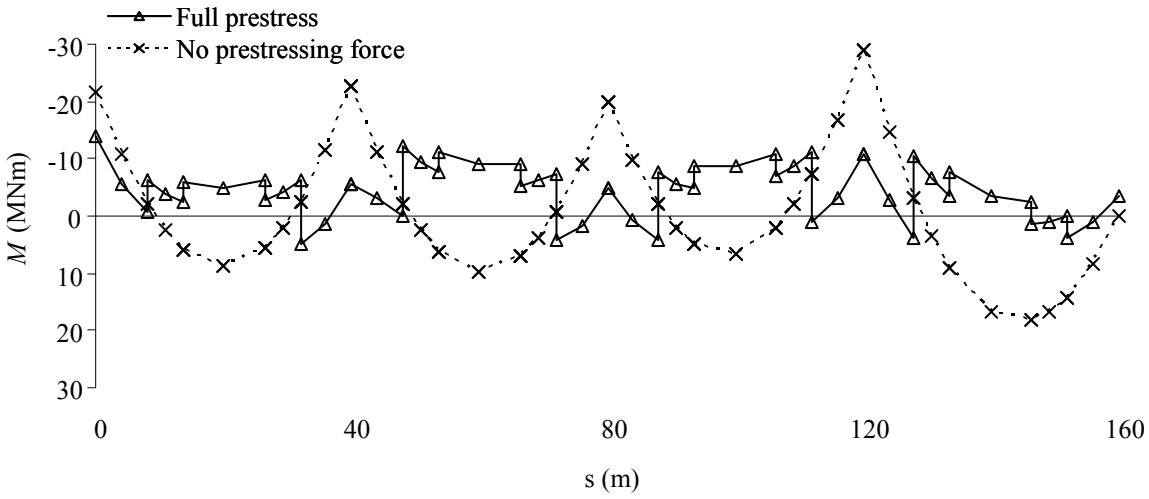

a) Bending

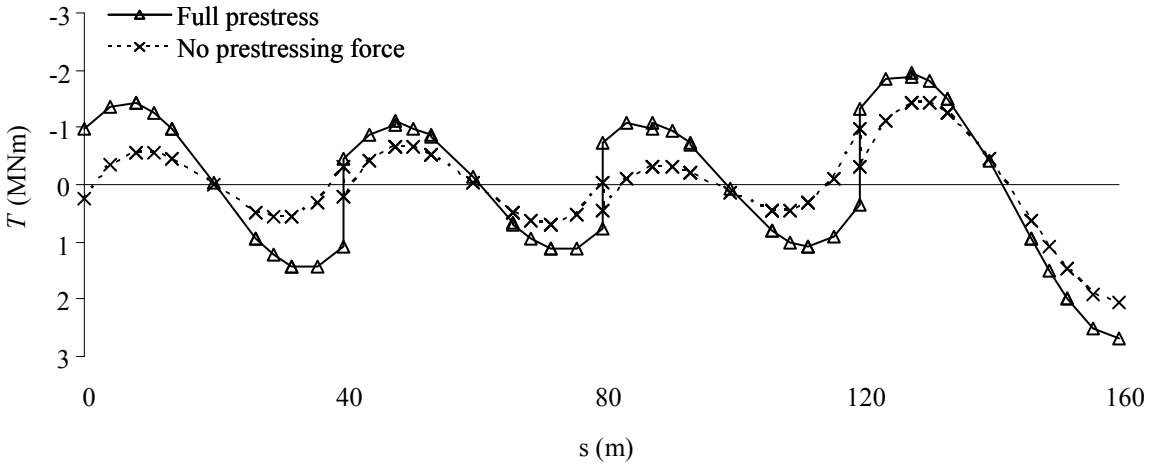

b) Torsion

Figure 6.25: Effect of Prestressing on Bending Moments

As the figure shows, the net prestressing force is eccentric. The majority of the discontinuities in the diagram come from the centre span lower tendons (300 series). Also note that as Maher discussed, the prestressing reduces the bending moments but increases the twisting moments.

As mentioned above, the bridge is being presented to examine the effects of live load. The stress envelopes after 50 years before the application of live load are shown below.

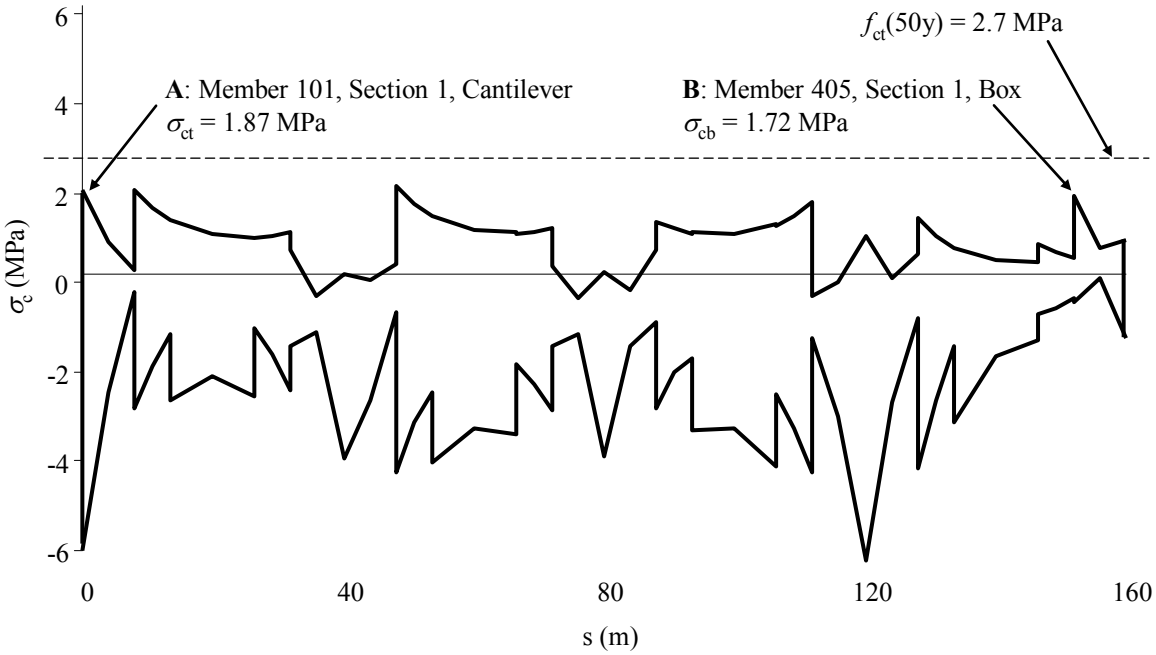

Figure 6.26: Stress Envelope

The maximum tensile stresses occur near the left support and at the outermost edge of the last member, just after the anchorage of tendon 331. They are noted as sections A and B and will be referred to as such going forward. There are high tensile stresses near node 200 as well, but moments are not expected to grow there as load is added. The effect of the age at casting on the tensile capacity is fairly insignificant once 50 years have passed; it is assumed to be 2.7 MPa for all concrete components.

It is not evident from the diagram, but it should be noted that the majority of tensile stresses are occurring in the cantilevers in the negative moment sections. It would be

worthwhile investigating whether additional prestressing in the cantilevers might reduce this effect.

Stress profiles for sections A and B are shown below. Note that these sections are good for study as they are subject to opposite moments.

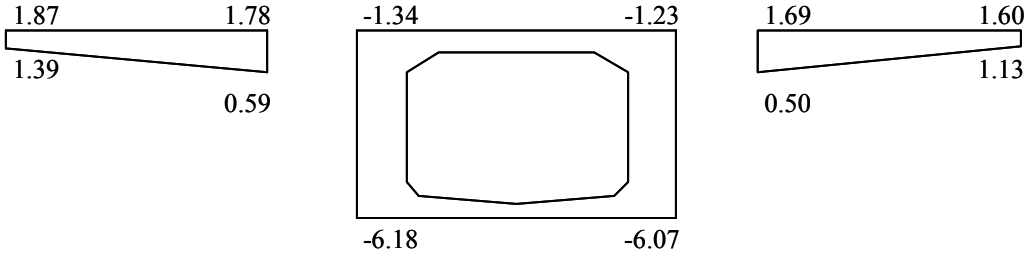

a) Section A (MPa)

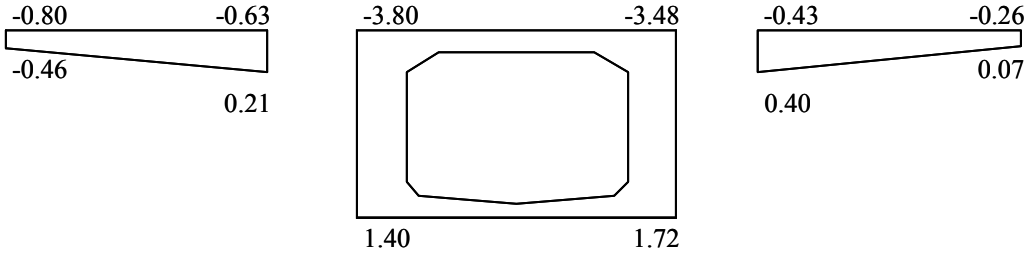

b) Section B (MPa)

Figure 6.27: Cross Section Stresses After 50 years

With the picture before the application of live load now clear, some exercises can be undertaken to demonstrate real world applications. Modern bridge design codes generally require Fatigue Limit State (FLS) analysis in addition to Serviceability Limit State (SLS) and Ultimate Limit State (ULS).

Clauses 8.5.3.1(a) and 8.5.3.2 of the Canadian Highway Bridge Design Code, CSA-S6-10 (2010) requires limiting the stress range from the effects of live load in prestressed and non-prestressed steel to 125 MPa.

Live load requirements are also spelled out in CSA-S6-10 (2010), under section 3.8. The most common choice for live load is a CL-W truck load, which is representative of a series of trucks driving over the bridge. The CL-W schematic from the Canadian code is shown below.

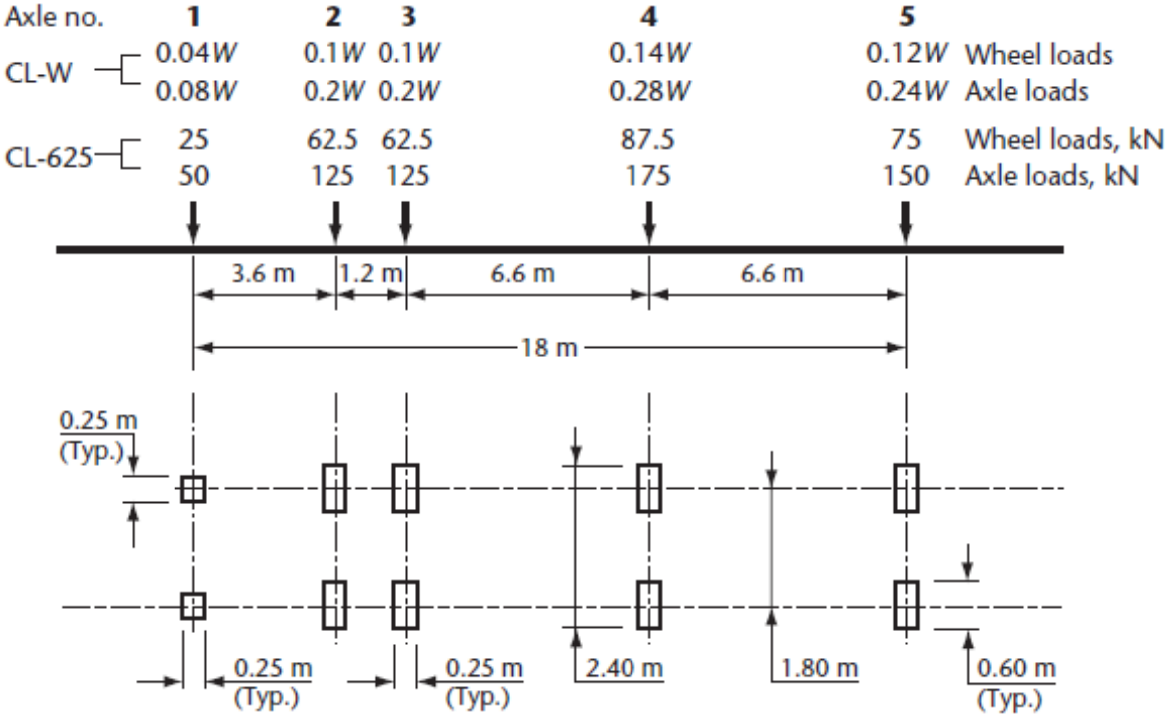

Figure 6.28: CL-W Truck Loading

While the figure and the code call for the CL-625 Truck with a total weight of 625 kN, Alberta Transportation (2012) has a guideline specific to design in Alberta that requires

use of a CL-800 truck. The 800 kN is distributed in the same way as in the figure shown above.

The CHBDC has two cases for loading: the truck itself, and a lane loading case that requires 80% of the loads shown above in addition to a 9 kN/m load distributed to cause maximum effect. According to Clause 3.8.4.1(c), the CL-W truck alone should be checked in any given lane for the FLS check. For SLS checks, the CL-W truck and the lane load cases should both be checked. Note that for this check, the bridge under consideration should be checked for 2 and 3 design lanes per Table 3.4 in the CHBDC.

For illustration purposes here, the FLS will be first examined with the CL-800 load. The stress change in steel and concrete due to live load application will be examined. The CL-800 truck is positioned at 40 different points along the bridge (every 4 m), and refined to 1 m once the critical load positions are determined. For the sake of simplicity, the axle loads will be taken at the indicated spacing and assumed to act 3 m from the centreline of the bridge towards the outside of the radius. The CL-800 loading used in the analysis is shown below, without the twisting moments shown for clarity.

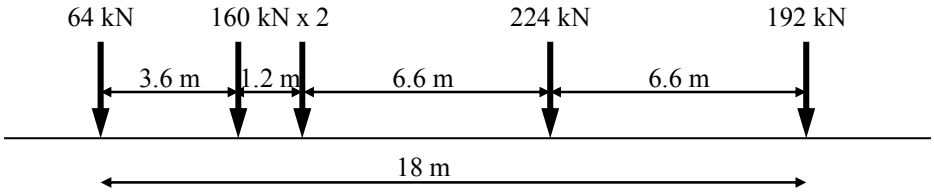

Figure 6.29: CL-800 Truck Axle Loading

For section A, the worst case happens when the leading edge of the 64 kN load is 25 m from the first support. For section B, this occurs when the leading edge of the load is 4 m from the last support. The centroidal internal forces at this section before and after the application of load (and redistribution of forces due to cracking), along with the change in strain and the corresponding increase in steel stress is shown below for each section.

There are 6 points in the non-prestressed steel to check. They are numbered and shown below.

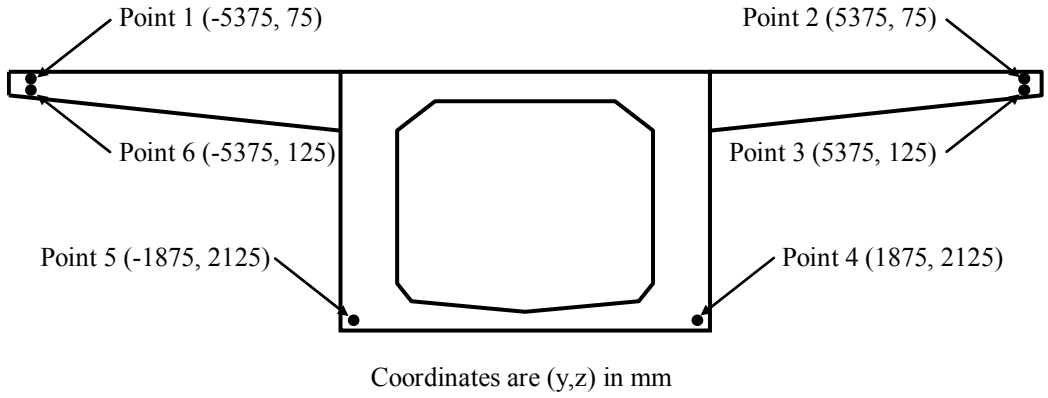

Figure 6.30: Steel Examination Points

Table 6.18: Results at Section A & B

		Section A	Section B
Before CL-800	N (MNm)	-19.1	-10.5
	M_y (MNm)	-11.6	4.0
	M_z (MNm)	0.5	-2.4
After CL-800	N (MNm)	-19.1	-10.5
	M_y (MNm)	-16.3	7.5
	M_z (MNm)	0.4	-2.4
	ζ	0.531	0.623
Change	N (MNm)	0	0
	M_y (MNm)	-4.7	3.5
	M_z (MNm)	-0.1	0
	ε_0 (με)	98.2	-97.0
	ψ_y (με/m)	-76.6	420.8
	ψ_z (με/m)	1.7	-0.4
	$\Delta\sigma_{ns,max}$ (MPa)	20.3	159.6
	at	Point 2	Point 5
	$\Delta\sigma_{ps,max}$ (MPa)	17.2	134.8
	in tendon #	201	144

Despite the increase in moment being larger at section A, the increment in steel stress at section B is significantly higher and in fact exceeds the 125 MPa allowable by design code. To see why this is occurring, examine the cross section at B after cracking:

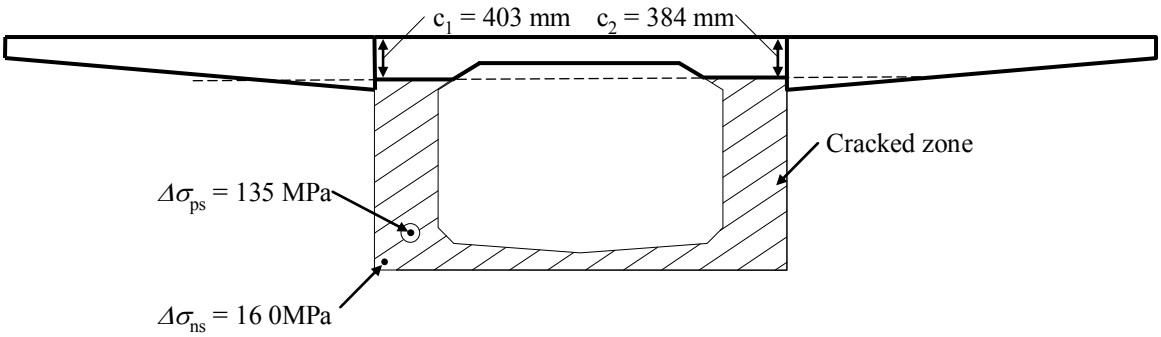

Figure 6.31: Effect of Cracking at Section B

Cracking is extensive. Once the decompression is complete and the full load is applied on the section, nearly 80% of the depth of the box is lost to cracking. Note, as well, that the bottom slab tendons 341 and 342 no longer cover this section; this is why the section directly to the left of B does not suffer from these effects. Due to the segmental nature of the construction, the cracking does not affect the cantilevers.

Given that the bridge in its current design fails the Fatigue Limit State analysis, changes should be made to fix it. The most favourable option is to add prestressing through member 405.

An investigation was done where tendon 342 was simply extended through the member's bottom section, and as expected, the 3.83 MN force it brings tidily fixes the problem. However, it does so by reducing the bending moment to the point where cracking no longer occurs. A better question to ask would be how much prestressing needs to be added into member 405 to reduce the steel stress fluctuation to less than 125 MPa, even if the member still cracks when the load is applied?

A new tendon, 343, was added into member 405 at the same eccentricity as 341 and 342 (150 mm below the bottom of the box). Assuming an initial stressing of $0.7f_{pu}$, the area and jacking force were increased in increments to determine the effect on the steel stress fluctuation. The results are plotted below, showing the resulting change in steel stress and the interpolation coefficient at each increasing prestress value.

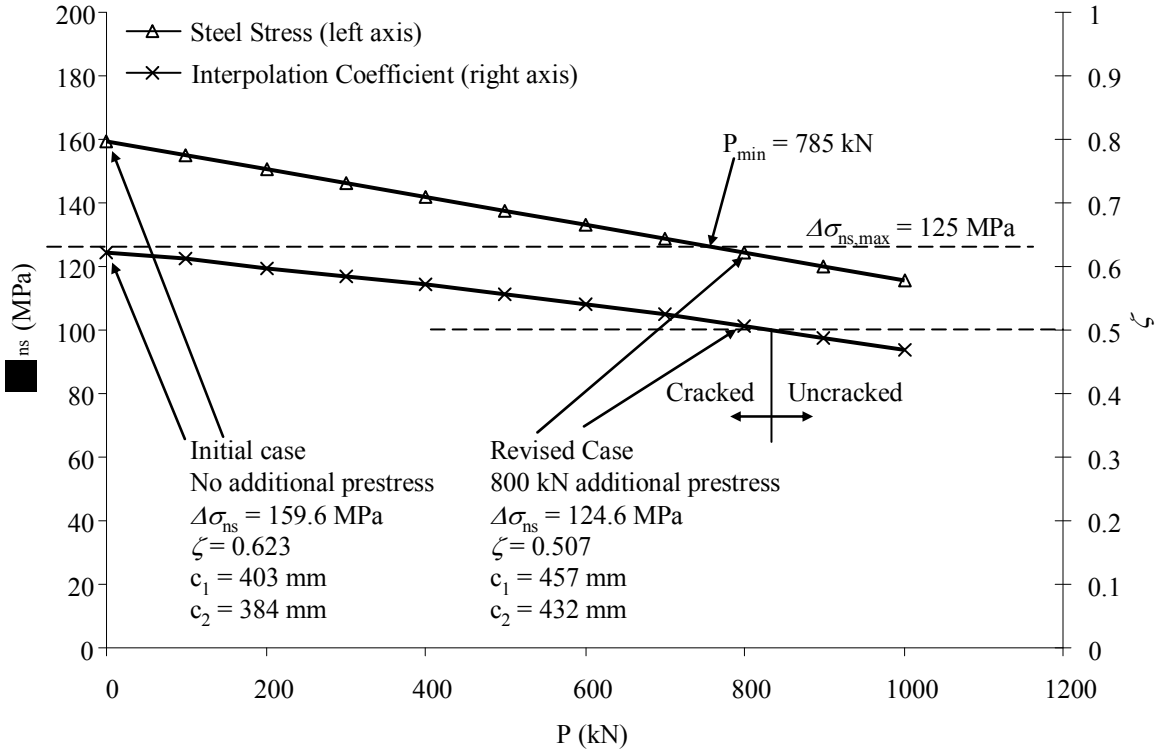

Figure 6.32: Effect of Increased Prestressing

To generate the figure above, cracking was assumed to start at $\beta^{0.5}f_{ct}$. The cracking would truly cease to take place once $\beta < 0.5$, which takes place at roughly 840 kN. However, at 800kN, $\zeta = 0.507$, and the increment in stress is 124 MPa – just below the 125 MPa limit imposed by CSA-S6-10 (2010). To provide 800 kN of prestressing only

takes 430mm^2 of tendon – 4-15mm Freyssinet strands would do it. In fact, as the figure shows, any value between 785 kN and 840 kN would produce allowable stress increments but still allow cracking in the beam.

It is worth noting that the tendon which undergoes the most increase in stress in the new case is in fact the new tendon, which experiences a 113 MPa increase after cracking.

6.3 Summary

The examples above showed how the model can be used on real world problems to check detailed stress levels at individual sections under varying load conditions. The ease of parameterization allows for fluctuations in positions of load, area and jacking force of tendons, reinforcing steel ratios, and almost any other component of the design of a structure.

The model developed and verified here can be applied to very simple and very complex problems and provides fairly accurate results for real world structures. Detailed analysis of stress, strain, force, and displacement is possible at any time throughout the lifespan of a structure. Furthermore, direct correlation to requirements and equations in practical design codes is possible.

Chapter Seven: **SUMMARY, CONCLUSION, AND RECOMMENDATIONS**

7.1 Summary

Reinforced and prestressed concrete forms the backbone of our transportation and infrastructure systems. It is a flexible, adaptable structural system that often proves to be the most cost effective solution to problems facing planners and designers.

While ultimate limit state analysis has always been required, the last 50 years has seen a much greater focus on design for serviceability. This analysis needs to consider the time dependent phenomena of creep and shrinkage in concrete and relaxation of prestressed steel to be accurate. The design codes that govern structural concrete design have been updated to include for their effects, but the simplified methods they present are not able to handle the complexity of real world structures. Segmental construction makes this problem worse.

Previous work by others has resulted in powerful uniaxial elements that can effectively model real world structures using finite element methods. Other work has taken a close look at the behaviour of prestressed, reinforced concrete sections over time, and included the effects of cracking in the analysis. The work presented here combines the two methods, and the result is a simple but thorough formulation that considers the curved nature of many real world structures, time dependent effects, cracking, and segmental construction. Using non-linear techniques, a structure can be analysed through its construction sequence and the result can be used to predict the long term response. The simple formulation provides two significant benefits. First, the intermediate results of

nearly any required stress or strain can be easily obtained. These include both numerical values and the cross section shape after cracking occurs. Second, the input models for time dependent effects can follow the equations recommended in design codes or be changed to any other numerical model.

The developed model is compared to problems in both two and three dimensions, and good correlation is found. Analysis of existing problems that include cracking, prestressed and non-prestressed steel, and variations in section properties are shown to match well. The model is extended to demonstrate capabilities by analysing theoretical and real world structures. Parametric variations are undertaken to consider the changing effects of reinforcing steel and prestress force on cracking and fatigue from live load cycling using modern highway design codes.

7.2 Conclusion

Comparison of the developed model's behaviour to existing studies shows good correlation. This element is suitable for day-to-day use in real structures. The trade-off and balancing required for prestressed concrete design is captured well; the numerical nature of the model allows for very quick analysis with variation of parameters, such as reinforcing ratio or prestress force. The effects of cracking are captured in the analysis, and results match well with other problems where non-linear analysis is required to converge on a solution. Computation time for the examples presented is under 1 minute on a computer with a 1.4GHz processor and 2GB of memory.

It is important to note that at some point the use of existing finite-element models will be superior to any model of this type. While they may not accurately model the non-linearity caused by cracking, even basic FEA packages now include elements with extremely comprehensive capabilities. The developed model makes no attempt to emulate their completeness; rather, it provides a capable, effective tool for the analysis of serviceability of curved prestressed concrete structures. Its inclusion of many procedures in the structural codes (eg: tension stiffening, creep calculation) makes it a valuable tool to the bridge designer. The ease of understanding the output without having to understand the ins and outs of 3D finite element modeling is of real benefit.

The verification and demonstration problems show two important considerations. First, the construction sequence is critical to intermediate structure response. Stresses in the structure can be at their highest well before the full structure is built. Balanced cantilevering, temporary supports, and imposed displacements are sometimes required to offset these effects.

Second, cracking causes very high changes in the stress levels. While stresses, strains, and deflections may be acceptable, the load cycling effect when cracking occurs often exceeds allowable levels for structures where fatigue is a consideration.

7.3 Recommendations for Future Research

The best way to analyze deficiencies and areas for potential improvements in the model is to examine each layer independently.

Since the model is primarily concerned with serviceability analysis, the material interactions and properties are very straightforward and quite simple. As a result, the current scheme is an effective and efficient solution.

The current material models assume a completely linear stress-strain distribution. For serviceability analysis, this is ample. If, however, ultimate state was to be included, material nonlinearity would be required.

Modelling at the section level would benefit the most from future improvements. As discussed in 3.6.3, the shear and twisting geometric properties are very roughly estimated, or must be provided by the user. It would be a very worthwhile addition to include cross-section finite-element analysis; this would also make the calculation of shear stresses in the beam possible, which are critical in ultimate state analysis and reinforcement design. The decompression approach could also be improved on in such a manner, and the location of the shear centre could be properly considered. Most importantly, warping deformations need to be included – their neglect in the current model somewhat limits its applicability for certain sections. Implementation of such an analysis would require a substantial amount of work if done properly, and should include material nonlinearity. Since the member axis can have arbitrary curvature, it might be worthwhile to abandon the idea of the reference point and simply use the centroid and the principal axes (which, of course, can change throughout the analysis). This would dramatically simplify the calculations at this level, and would allow proper consideration

of twisting and shear (and possibly warping). Taking the analysis through to ultimate state would make it more powerful.

At the member level, external and unbonded prestressing would be useful for several situations. While the model does allow internal tendons to be unbonded, it enforces strain compatibility at each section. There are some problems for which tendon slippage needs to be considered. The inclusion of the formation of plastic hinges in the analysis would add value.

Geometric nonlinearity should be included to allow for the analysis of structures such as cable stayed bridges, where deflection affects stiffness. The stiffness and member force calculations would need to be adapted, but the central non-linear analysis component of the program is sufficient.

Detailed investigation into correlation between the developed model's results and those of an actual curved bridge would be beneficial. Such research should include comparison to established finite element models for prestressed concrete.

Finally, cases where nonlinear convergence is not rapid could potentially be mitigated by adapting a different solution approach. Additional research into why certain configurations result in non-convergence would be beneficial.

LIST OF REFERENCES

Alberta Transportation (2012), "Bridge Structures Design Criteria Version 7.0", Government of Alberta, Edmonton, Alberta, Canada, 2012.

American Concrete Institute (ACI) Committee 209, (1992), "Prediction of Creep, Shrinkage, and Temperature Effects in Concrete Structures (209R-92)", ACI, Detroit, Michigan

Bathe, K. J., (2003), "Finite Element Procedures", Prentice Hall, New Jersey, 7th Edition

Bazant, Z. P., (1972), "Prediction of concrete creep effects using age-adjusted effective modulus method", ACI Journal, 69(4), 212-217.

Bazant, Z. P., and Wu, S. T., (1973), "Dirichlet series creep function for aging concrete", Journal of Engineering Mechanics, 99(em2).

Cheney, W., and Kincaid, D., (1999), "Numerical Mathematics and Computing", Brooks/Cole, Pacific Grove, USA, 4th Edition.

Comite Euro-International du Beton (CEB) – Federation Internationale de la Precontrainte (FIP), (1990), "Model Code for Concrete Structures (MC-90)", Thomas Telford, London, 1993.

CSA Standard A23.3-04, (2004), "Code for the Design of Concrete Structures for Buildings", Canadian Standards Association, 2004

CSA Standard CAN/CSA-S6-10 (2010), Canadian Highway Bridge Design Code (CHBDC), Canadian Standard Association, Rexdale, Ontario, Canada, 2010.

Debaiky, A., (1997), "Analysis of Time-Dependent Effects on Segmental Prestressed Concrete Curved Box-Girder Bridges", M. Sc. Thesis, Department of Civil Engineering, the University of Calgary, Calgary, Alberta, Canada, November, 1997, 190 pp.

El-Badry, M. M., (1988), "Serviceability of Reinforced Concrete Structures", Ph. D. Thesis, Department of Civil Engineering, the University of Calgary, Calgary, Alberta, Canada, November, 1988, 295 pp.

El-Badry, M. M. and Ghali, A., (1989), "Serviceability Design of Continuous Prestressed Concrete Structures", Prestressed Concrete Institute, PCI Journal, Vol. 34, No. 1, pp. 54-91

El-Badry, M. M. and Ghali, A., (1990), "Users Manual and Computer Program CPF: Cracked Plane Frames in Prestressed Concrete", Research Report No, CE85-2, Department of Civil Engineering, The University of Calgary, Calgary, Alberta, Canada, January 1985 (Revised March 1989).

El-Badry, M. M. and Debaiky, A., (2004), "Time-Dependent Analysis of Segmentally Erected Curved Concrete Box-Girder Bridges. I – Formulation", unpublished manuscript.

El-Badry, M. M., (2005), "Time-Dependent Analysis of Segmentally Erected Curved Concrete Box-Girder Bridges. II – Verification and Applications", unpublished manuscript.

Espion, B. and Halleux, P., (1988), "Moment Curvature Relationship of Reinforced Concrete Sections under Combined Bending and Normal Force", Materials and Structures, Vol. 21, No. 5, pp. 341-351

Ghali, A., Neville, A. M., and Brown, T. G., (2009), "Structural Analysis: A Unified Classical and Matrix Approach", Spon Press, London, 6th Edition, 833 pp.

Ghali, A., Favre, R., and El-Badry, M. M., (2011), "Concrete Structures: Stresses and Deformations – Analysis and Design for Serviceability", Spon Press, London, 4th Edition, 638 pp.

Hassoun, M. N. and Al-Manaseer, A., (2008), "Structural Concrete: Theory and Design", 4th Edition, John Wiley & Sons, New Jersey, 901 pp.

Jirousek, J. and Bouberguig, A., (1979), "A Macro Element Analysis of Prestressed Curved Box-Girder Bridges", Computers and Structures, Vol. 10, No. 3, pp. 467-482

Jirousek, J., (1981), "A Family of Variable Section Curved Beam and Thick-Shell or Membrane-Stiffening Isoparametric Elements", International Journal of Numerical Methods in Engineering, Vol 17, pp. 171-186

Kabir, A. F., (1976), "Nonlinear Analysis of Reinforced Concrete Panels, Slabs and Shells for Time dependent Effects," Ph.D. Dissertation . Civil Engineering, University of California, Berkeley, USA.

Kawakami, M. and Ghali, A., (1996), “Cracking, Ultimate Strength and Deformations of Prestressed Concrete Sections of General Shape”, Prestressed Concrete Institute, PCI Journal, Vol. 41, No. 4, July-August 1996, pp. 114-122

Kawakami, M. and Ghali, A., (1996), “Time-Dependent Stresses in Prestressed Concrete Sections of General Shape”, Prestressed Concrete Institute, PCI Journal, Vol. 41, No. 3, May-June 1996, pp. 96-105

Ketchum, M. A., (1986), “Redistribution of Stresses in Segmentally Erected Prestressed Concrete Bridges”, Report No. UCB/SESM-86/07, Division of Structural Engineering and Structural Mechanics, University of California at Berkeley, Berkeley, California, May 1986

Khalil, M. S., (1979), “Time Dependent Non-Linear Analysis of Prestressed Concrete Cable-Stayed Girders and Other Concrete Structures”, Ph. D. Thesis, University of Calgary, Calgary, Alberta, Canada, April 1979, 246 pp.

Maher, P., (1985), “Torsion in Curved Prestressed Bridges”, M. Sc. Thesis, Department of Civil Engineering, the University of Calgary, Calgary, Alberta, Canada, November, 1985, 185 pp.

Neville, A. M., (1997), “Properties of Concrete”, Wiley, New York, 4th Edition

Oden, J. T., and Ripperger, E. A., (1980), “Mechanics of Elastic Structures”, McGraw Hill, New York, 2nd Edition

Shangchow, C., (1984), “A Partial Boundary Element Approach to the Elastic Torsion Problem of a Prismatic Beam with Cracked Rectangular Cross Section”, International Journal of Numerical Methods in Engineering, Vol. 20, No. 9, September 1984, pp. 1745-1749

Stanley Associates Engineering Ltd, (1980), Design Drawings for Bow River Bridge

Surana, K. S., (1979), “Isoparametric Elements for Cross Sectional Properties and Stress Analysis of Beams”, International Journal of Numerical Methods in Engineering, Vol. 14, No. 4, 1979, pp. 475-497

Timoshenko, S. P., and Gere, J. M., (1961). "Theory of Elastic Stability, McGraw-Hill, New York

Trost, H., & Marsh, J. G. (1967)., “The consequences of the principle of superposition on creep and relaxation problems in concrete and pre-stressed concrete”, Beton und Stahlbetonbau, pp 230-238.

Van Zyl, S. F., (1978), “Analysis of Segmentally Erected Prestressed Concrete Box Girder Bridges”, College of Engineering, University of California, U.S.A.

Van Zyl, S. F., (1979), “Analysis of Curved Prestressed Segmental Bridges”, Journal of the Structural Division, ASCE, Vol. 105, No. ST11, 1979, pp. 2399-2417.